Tectonic Geomorphology and Paleoseismology of the Lees Valley Fault Zone, South Island, New Zealand

---

A thesis submitted in partial fulfilment of

the requirements for the degree of

Master of Science in Geology

at the

University of Canterbury

by

Ellyse Sonja Gore

December 2015

Abstract

Oblique-convergent plate collision between the Pacific and Australian plates across the South Island has resulted in shallow, upper crustal earthquake activity and ground surface deformation. In particular the Porters Pass - Amberley Fault Zone displays a complex hybrid zone of anastomosing dextral strike-slip and thrust/reverse faulting which includes the thrust/reverse Lees Valley Fault Zone and associated basin deformation. There is a knowledge gap with respect to the paleoseismicity of many of the faults in this region including the Lees Valley Fault Zone.

This study aimed to investigate the earthquake history of the fault at a selected location and the structural and geomorphic development of the Lees Valley Fault Zone and eastern rangefront. This was investigated through extensive structural and geomorphic mapping, GPS field surveying, vertical aerial photo interpretation, analysis of Digital Elevation Models, paleoseismic trenching and optically stimulated luminescence dating.

This thesis used a published model for tectonic geomorphology development of mountain rangefronts to understand the development of Lees Valley. Rangefront geomorphology is investigated through analysis of features such as rangefront sinuosity and faceted spurs and indicates the recently active and episodic nature of the uplifted rangefront. Analysis of fault discontinuity, fault splays, distribution of displacement, fault deformation zone and limited exposure of bedrock provided insight into the complex structure of the fault zone. These observations revealed preserved, earlier rangefronts, abandoned and uplifted within the eastern ranges, indicating a basinward shift in focus of faulting and an imbricate thrust wedge development propagating into the footwall of the fault zone and along the eastern ranges of Lees Valley.

Fault scarp deformation analysis indicated multiple events have produced the deformation present preserved by the active fault trace in the northern valley. Vertical deformation along this scarp varied with a maximum of 11.5 m and an average of 5 m. Field mapping revealed fan surfaces of various ages have been offset and deformed, likely during the Holocene, based on expected relative surface ages. Geomorphic and structural mapping highlighted the effect of cross-cutting and inherited structures on the Lees Valley Fault, resulting in a step-over development in the centre of the eastern range-bounding trace.

Paleoseismic trenching provided evidence of at least two earthquakes, which were constrained to post 21.6 ± 2.3 ka by optically stimulated luminescence dating. Single event displacements (1.48 ± 0.08 m), surface rupture earthquake magnitudes (Mw 6.7 ± 0.1, with potential to produce ≥ 7.0), and a minimum recurrence interval (3.6 ± 0.3 ka) indicated the Lees Valley Fault is an active structure capable of producing significant earthquake events.

Results from this study indicate that the Lees Valley Fault Zone accommodates an important component of the Porters Pass - Amberley Fault Zone deformation and confirms the fault as a source of potentially damaging, peak ground accelerations in the Canterbury region. Remnants of previous rangefronts indicate a thrust wedge development of the Lees Valley Fault Zone and associated ranges that can potentially be used as a model of development for other thrust-fault bounded basins.

Acknowledgements

Throughout my Masters, the New Zealand Earthquake Commission and the New Zealand Federation of Graduate Women have supported both me and my research, for which I am very grateful.

First and foremost, I must thank my supervisors Jarg Pettinga and Mark Quigley. Mark, thank you for sparking in me the desire to learn about active tectonics, guiding me into my research topic, teaching me valuable field techniques and always challenging me to do better. Jarg, thank you for your knowledgeable input, guidance when needed, constructive feedback and engaging discussions, your support has been much appreciated and it has been a pleasure to work with you.

The technical and secretarial staff at UC have been very helpful. Pat Roberts, Rebekah Hunt, Janet Warburton, and Cathy Higgins thank you for helping my project run smoothly. Special thanks to Sacha Baldwin-Cunningham and Rob Spiers. Sacha, for your support and especially your dedication in attempting to contact me while I was unreachable in the wilderness and Rob, for happily fulfilling my somewhat difficult and last minute field equipment requests. I would also like to thank Anekant Wandres for your help in GPS processing. An extra special thank you to Matthew Cockcroft who braved the weather with me to do Geophysics, I am glad the temperatures managed to reach above negative that day.

Others who deserve my thanks for their crucial support include Narges Khajavi, David Jacobson and Tim vanWoerden. Narges, thank you for your most helpful discussions and friendly talks. David, your never ending enthusiasm to help in the field was much appreciated as were our talks. Tim vanWoerden, thank you so much for your support in the field and your monumental task of aiding me with ArcGIS and CorelDRAW. Of course thanks also goes to my great office mates Kieran Grace and Romy Ridl, our chats have kept me sane throughout the year and I've enjoyed spending the time with you both. Also thanks to Richard Mellis, our philosophical lunch time debates have been a highlight.

The various landowners in Lees Valley have been great. I thank them for their interest and enthusiasm for my project, and for granting me access to their properties. I thank the Dalzells for allowing me to visit whenever I wanted and to dig a trench on their land with no restrictions. Brandon, you and your family I thank for welcoming me so warmly and

providing me with accommodation, and even great food. Also to all the other farm workers there at the time, thanks for the friendly and entertaining conversations, you all made my time out in the field memorable.

Last but certainly not least I thank my family up in the North Island, friends and flatmates, you have provided love, great moral support and good reality grounding when needed. And of course a special thanks to my partner Tim, you have been my sanity balancer and strength provider, thank you for your unwavering support and constant belief in me, I wouldn't have achieved this without you.

Contents

List of Figures

List of Tables

Introduction

1.1 Background and Relevance of Study

New Zealand's location within an active plate boundary collision zone results in earthquake activity and active earth deformation. Tectonic geomorphic and paleoseismic studies of active faults are essential to build our understanding of the active earth deformation and geological hazard in New Zealand. The contrasting styles of structural deformation in different regions can be complex, while studies of individual active faults and folds not only characterize and quantify seismic hazard but are also important in understanding linking relationships between individual active structures and the upper crustal active earth deformation driver across wider regions.

The South Island's major tectonic features include the Marlborough Fault System in the north which amalgamates into the Alpine Fault to the south-west (Yetton, 2000), with associated uplift forming the Southern Alps and ranges in the northeast South Island. The Alpine Fault accommodates ~70% of the strain in the central sector of the South Island (Norris and Cooper, 2000). While the remaining ~30% of deformation strain is distributed across the wider plate boundary, accommodated to the east of the Southern Alps on a complex array of faults and folds extending to beyond the east coast (Wallace et al., 2007; Norris and Cooper, 2000). The numerous active faults are seismically important as they are part of the ongoing tectonic deformation in the South Island, accompanied by large magnitude earthquakes, such as the 2010 M_w 7.1 Darfield earthquake. Deformation in the Canterbury region in eastern South Island is dominated by a hybrid interaction of reverse and dextral strike-slip faulting (Campbell et al., 2012). Some of these structures, such as the Porters Pass–Amberley Fault zone, Esk Fault and Culverden Basin fault system have previously been intensively studied, including determining their slip rates, recurrence intervals, co-seismic displacements and earthquake magnitudes (eg. Cowan, 1992; Howard et al., 2005; Noble, 2011). However, many other contractional structures in the Canterbury region remain poorly documented in terms of their structural geometries and earthquake potential. The focus in this project is one such fault zone, the Lees Valley Fault.

The Lees Valley Fault is a predominantly southeast-dipping oblique reverse/thrust fault (Garlick, 1992). It is part of the North Canterbury deformation zone south of the Marlborough Fault System and links into the Porters Pass Fault further to the south (Pettinga

et al., 2001). The Lees Valley Fault is important because of its connection with the Porters Pass-Amberley Fault Zone, its relatively close proximity to the township of Oxford and also the rural community in Lees Valley (Figure 1.1). Furthermore, previous reconnaissance mapping indicates there have been multiple co-seismic uplift events along the Lees Valley Fault surface trace with likely activity in the Holocene (Garlick, 1992; Cowan et.al, 1996). A recurrence interval has been crudely estimated at 3,000 – 5,000 years, based on documented faulting and uplift subsequent to loess accumulation (10,000 – 20,000 years) and an estimated minimum of four uplift events and earthquake magnitude ~ 6.7, based on segment length and estimated slip rates (Garlick, 1992; Pettinga et al., 2001). These previous studies have based estimates on limited field information and standard published fault-scaling relationships. Accordingly, gathering further detailed field mapping and quantitative data from paleoseismic investigations of the fault may provide more accurate data on the fault rupture history and recurrence intervals.

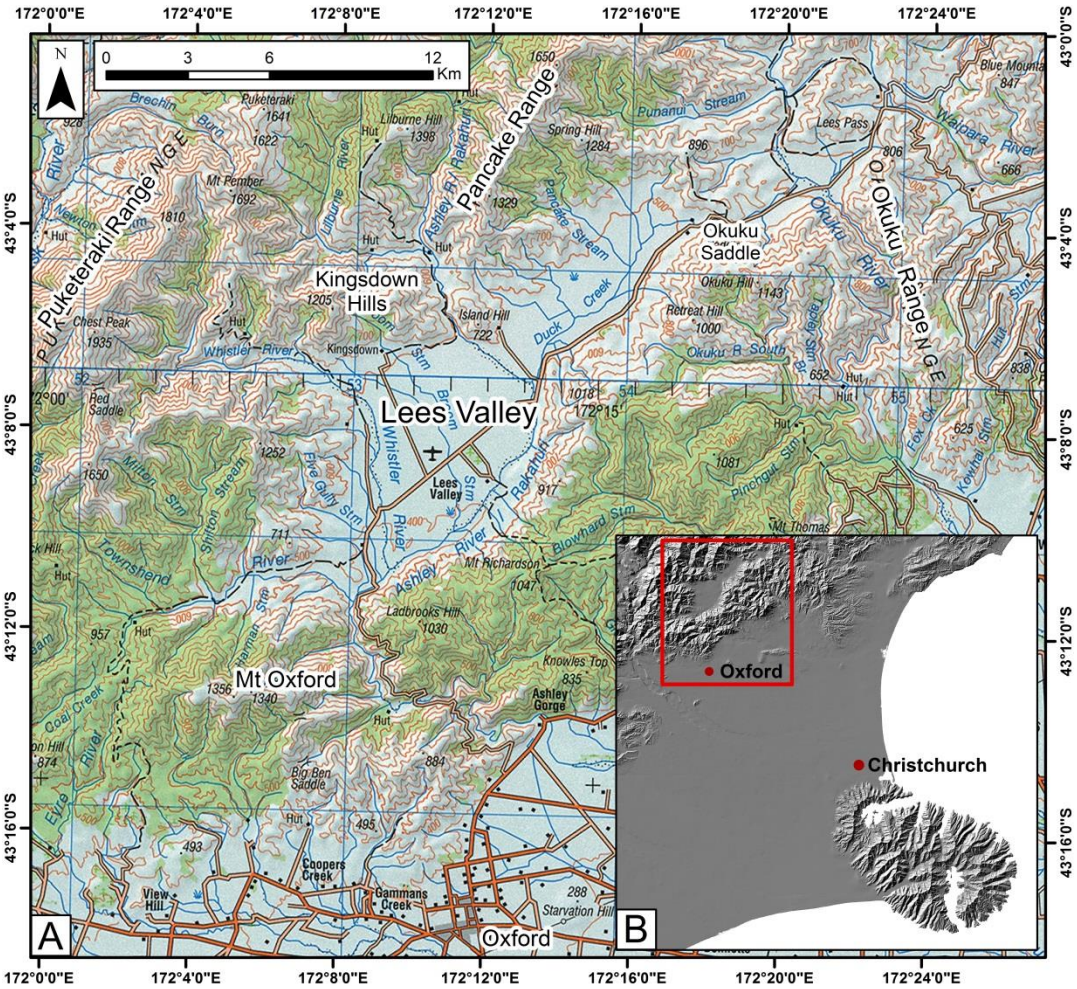

Figure 1.1: *A) Map of field area location in relation to Christchurch and Oxford, Modified from Forsyth et al. (2008). B) Field area and topographic features of importance, modified from Land Information New Zealand (2014).*

Since September the 4, 2010 through to September 2015, Christchurch and the wider Canterbury region have experienced ~3,900 earthquakes $M_L \geq 3$ (GeoNet, 2015) (Figure 1.2). The M_w 7.1 Darfield earthquake of September 4, 2010 and the M_w 6.2 Christchurch Earthquake of February 22, 2011 which claimed 185 lives (Bannister & Gledhill, 2012; Quigley et al., 2010; Quigley et al., 2012), acutely raised awareness of the regional earthquake hazard and associated risks throughout the region. The 2010-2012 Canterbury Earthquake Sequence (CES) has highlighted the importance of understanding the tectonic setting and activity across the region.

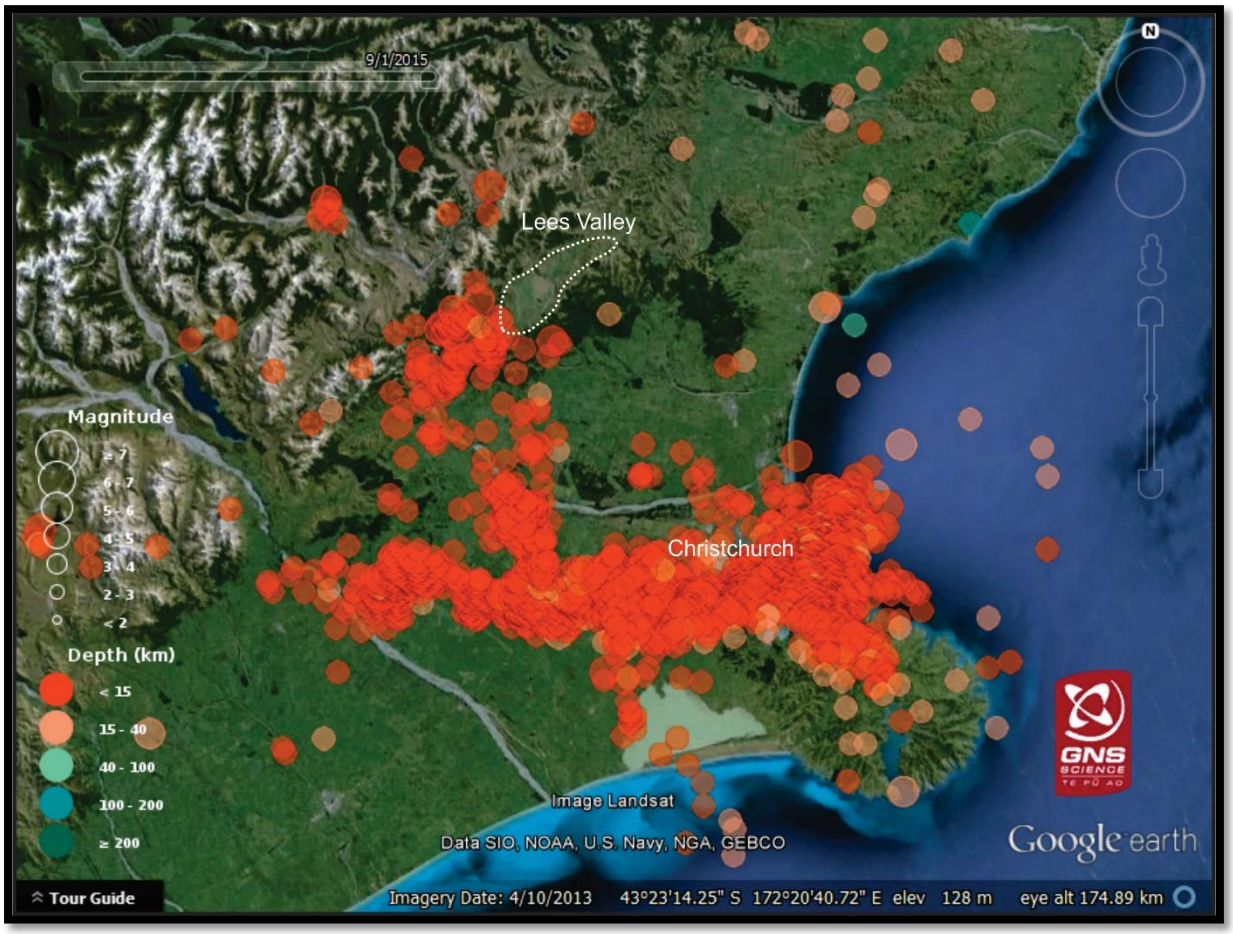

Figure 1.2: *Earthquake distribution $M_L \geq 3$ from 4th September 2010 through to September 2015. The Lees Valley study location is indicated in relation to Christchurch. From GeoNet (2015) and Google earth (2013).*

Of particular interest following the Canterbury Earthquake Sequence are the positive regional stress changes observed by Steacy et al. (2014) (Figure 1.3). Results from analysis of the slip models and stress fields indicate that aftershock locations in the CES were influenced by Coulomb stress changes. In particular all $M \geq 5.5$ events subsequent to the Darfield event were located in areas of positive stress change within modelled stress maps (Figure 1.3). This

indicates faults exposed to positive increased stress changes in Canterbury have the potential to rupture earlier than expected from current recurrence intervals, although this is magnitude dependent and limited to optimally oriented faults within the regional stress regime. Some studies have suggested this correlation has insufficient evidence to support it. For example Bebbington et al. (2015) found through application of static triggering modelling that during the CES the majority of faults that failed were already under high stress conditions, higher than failure strength, before rupture. They state that while the stress conditions affected the rupture sequence in severity of aftershocks there is not adequate evidence to indicate that static stress changes cause triggering of fault failure. While is it uncertain whether positive stress changes trigger faulting it is important to note it has an effect on fault behaviour. It is also important to note positive stress changes have been observed in many areas of the Canterbury region, including in the southern section of the Lees Valley basin.

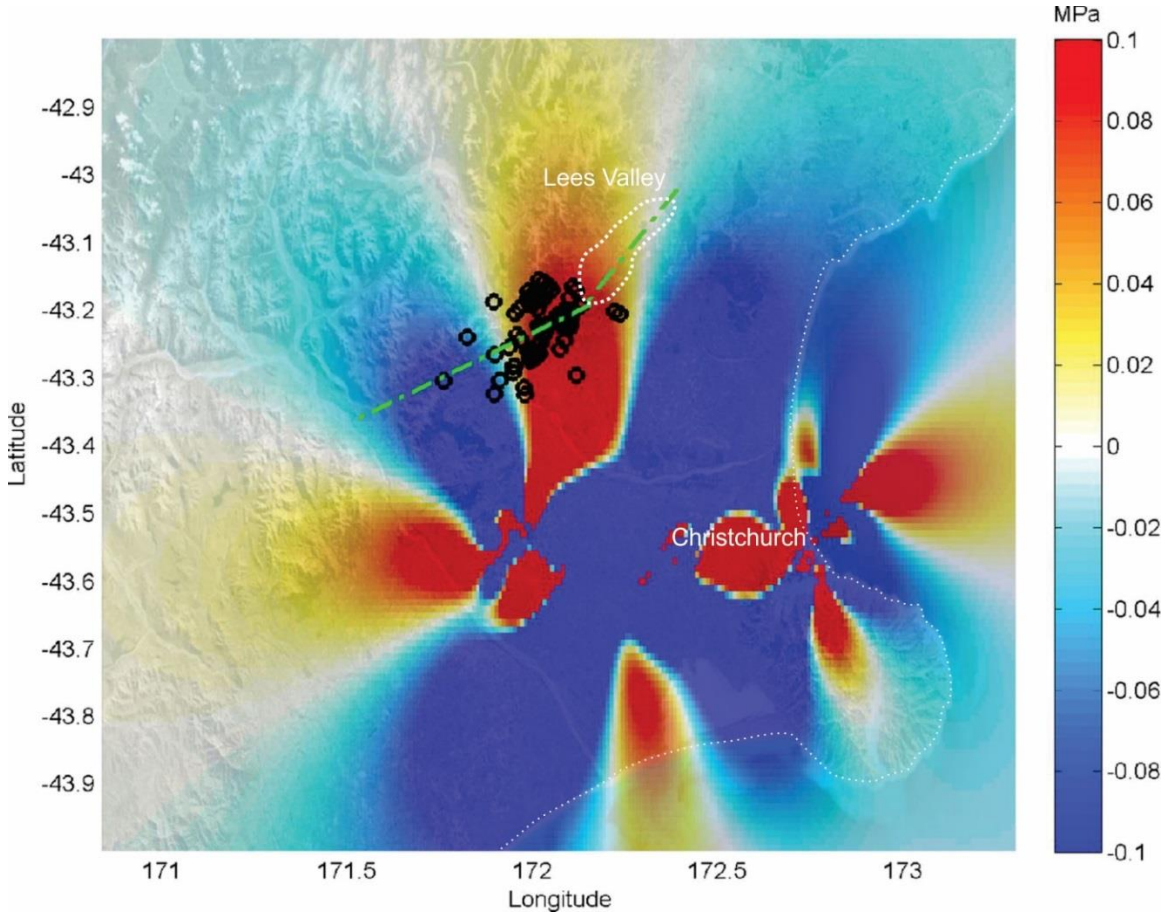

Figure 1.3: *Figure showing stress changes from the main Canterbury earthquakes; the Mw 7.1 Darfield event, the Mw 6.2 Christchurch earthquake, Mw 6.0 event in June 2011, and two earthquakes Mw 5.8 and 5.9 in December 2011. The Lees Valley Fault indicated (green line oriented NE) also shown is the Porters Pass Fault (green line oriented ENE). Open circles specify events M ≥ 3 within 10 km of the fault zone, following the 2010 Mw 7.1 Darfield Earthquake through to September 2012. Figure modified from Steacy et al. (2014).*

Moderate to severe co-seismic ground shaking in Oxford, Rangiora and Christchurch are likely in the event of rupture of the Lees Valley Fault. Gaining further understanding of the structural and paleoseismic characteristics of the Lees Valley Fault is of considerable importance.

1.2 Aims and Methodology

This study contributes to our understanding of the structural geomorphology of the Lees Valley Fault and paleoseismic history of its northern segment. Furthermore it describes controls on the evolution of the Lees Valley basin and adjacent ranges. Specific aims of this study include:

1. The development of a structural and geomorphic model for the Lees Valley Fault Zone and eastern rangefront.
2. Investigation of the paleoseismic history of the Lees Valley Fault at a selected location.

Previous studies focused on the Lees Valley Fault have provided no paleoseismic information, hence there are no reliable age constraints for any of the displaced surfaces or fault rupture events. A key aim of this thesis is to better constrain paleoseismic ground rupture event(s). This in turn is complemented by detailed structural and geomorphic mapping to assess the evolution of the Lees Valley Fault Zone and eastern rangefront. A structural and geomorphic evolution model for the fault system and rangefront is also presented to document the spatial and temporal rangefront development, which in turn may provide new insights into how active faulting drives mountain range development.

This study will provide new information on the structural setting of the Lees Valley Fault, its segmentation, geometry, co-seismic development, seismic history, large earthquake magnitude potential and constrain its contribution to the regional seismic hazard. The resultant information will help in understanding the structural complexity of Lees Valley Fault Zone and its structural connections with the Porters Pass – Amberley Fault Zone.

Kinematics of the fault and associated geomorphology were investigated through extensive geological and geomorphological mapping of the fault zone and associated surface rupture traces. Additional data include vertical aerial photo interpretation, analysis of Digital Elevation Models (DEMs) and Global Positioning System (GPS) field survey data.

Geomorphic fault expression was analysed through field surveying using hand held GPS. Paleoseismic investigation involved a paleoseismic trench, acquisition and analysis of detailed trench logs and associated geochronology through optically stimulated luminescence (OSL) dating for ages of material and event horizon(s) identified within the trench.

1.3 Location and Characteristics of Study Area

Lees Valley is located approximately 55 km northwest of Christchurch and 20km north of Oxford (refer to Figure 1.1). Accessed is via a narrow, winding gravel road through Ashley Gorge, linking to the southern end of Lees Valley. Current land use is predominantly focused on sheep, cattle and deer farming.

Lees Valley is an elongate structural basin 18 km in length and trending northeast-southwest. The valley is bounded by its eastern ranges, to the southeast by Mount Oxford (el. ~1364 m) and to the west by the Kingsdown Hills and Pancake Range (refer to Figure 1.1). Further west the ranges increases in elevation with the ranges bounding the basin reaching up to 1950 m (Garlick, 1992). The ranges bounding the valley vary in average topographic slope angles. The eastern ranges are characterized by steeper slopes coupled to the valley floor while along the western margin of the valley the topographic slopes are much shallower in slope angle. Here wider slopes are decoupled from the valley floor by extensive alluvial fans.

In map view the valley can be divided into two sub-basins each with distinct geomorphic character (Figure 1.4). The northern basin is narrower (~3 km wide by 8 km long) and pinches out at the northern end as the ranges to the east and west coalesce. The southern basin is wider (~6.5 km wide by 10 km long). Three major rivers drain into the valley; the Ashley, Whistler and Townsend Rivers. These all flow towards the base of the eastern ranges eroding the lower rangefront slopes in the southern valley. The rivers coalesce and form the Ashley River flowing south, exiting the valley through the geomorphically spectacular antecedent Ashley Gorge. The northern valley contains no major river systems, smaller streams and creeks flow into the southern valley and join the major Ashley River system. The floor of the northern basin is not flat displaying a relationship of overlapping alluvial fan deposits and many swamps located between fan surfaces indicating impeded drainage. The valley floor is also tilted significantly to the south controlling overall drainage toward the southern valley basin.

There is very little forest cover in the region, providing good exposure of tectonic and geomorphic features that are preserved in the ranges and basin floor. The basin infill is mostly fluvial braided river and stream deposits, alluvial fan deposits and areas of impeded drainage characterised by swamps. The general structural features of Lees Valley are indicated in Figure 1.4 and the outline of the area investigated in this study, with the northern and southern valley sub-basins indicated.

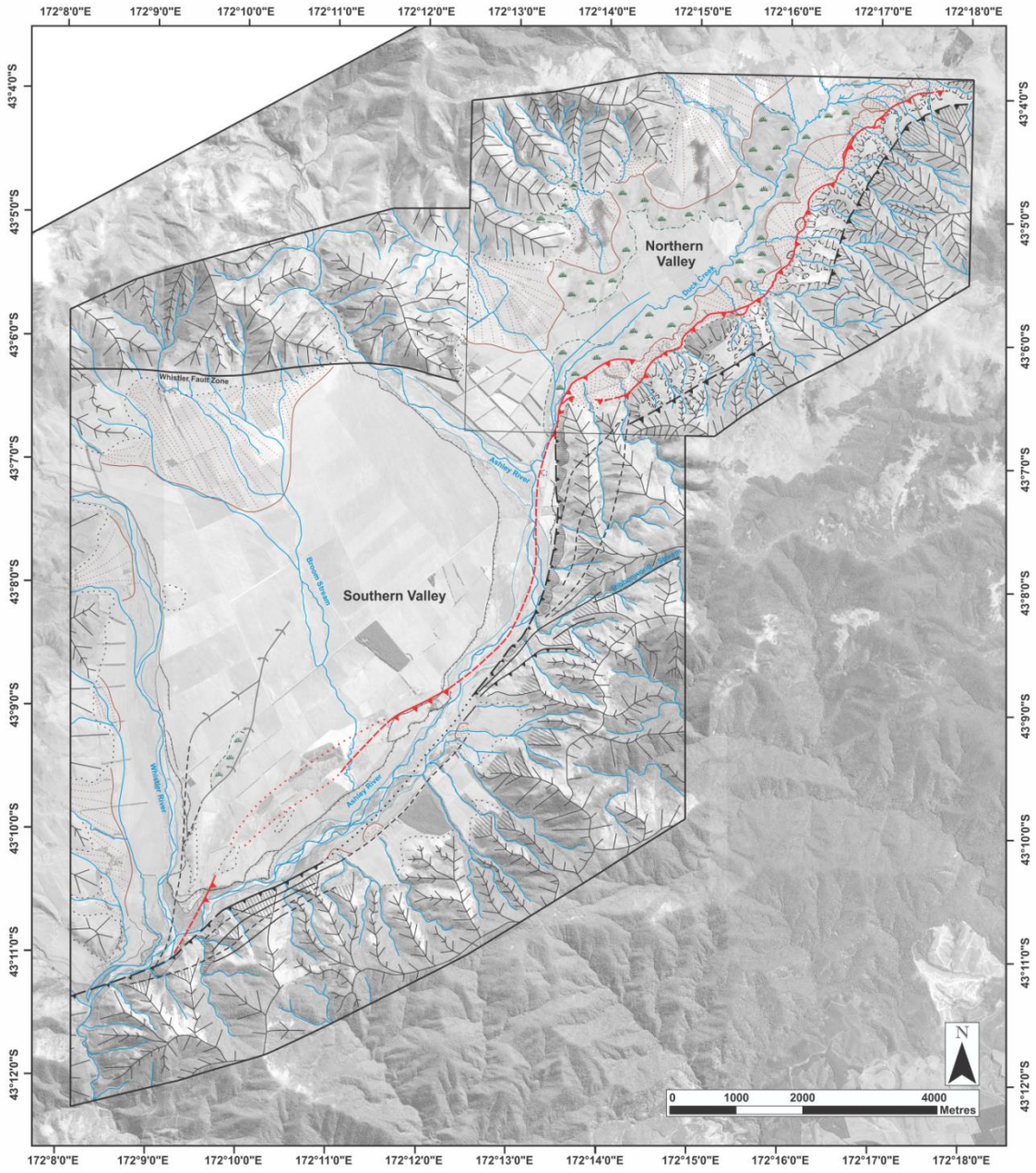

Figure 1.4: *Geomorphological and structural map of field site with an outline of the northern and southern Lees Valley sub-basins, incorporating Cowan (1992a) and Barrell and Begg (2013). (refer to Figure 2.5 for legend)*

1.4 Geological setting

1.4.1 Plate Boundary Tectonics

New Zealand is a geomorphologically and tectonically diverse country due to its location straddling the boundary between the Pacific and Australian plates. The obliquely-convergent plate collision across the South Island has resulted in a high rate of strain, expressed through shallow, upper crustal earthquake activity and ground surface deformation. Active faulting, folding and continuing strain gives rise to features such as the Southern Alps and eastern foothills. Variation in the orientation of plate collision beneath New Zealand results in varying convergence rates along the length of New Zealand with the highest rates of ~ 47 mm/year across the North Island margin, decreasing to ~ 39 mm/year near the top of the South Island (De Mets et al., 1994; Norris and Cooper, 2000; Wallace et al., 2007; DeMets et al., 2010) (Figure 1.5).

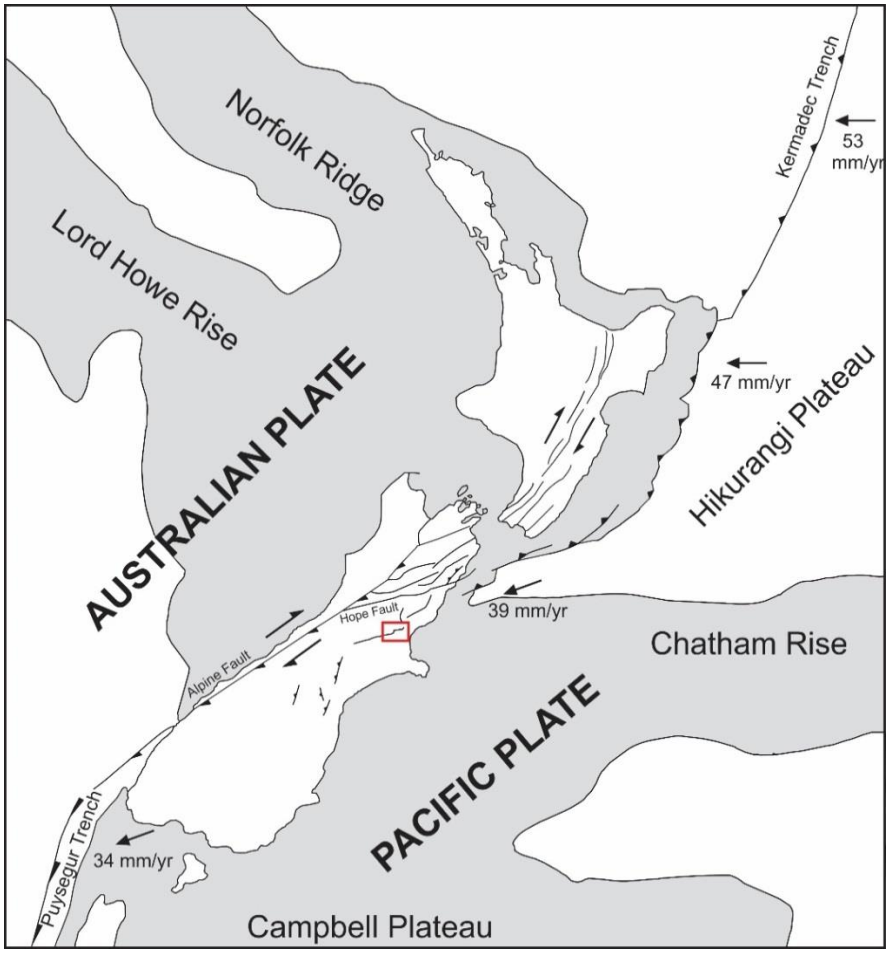

Figure 1.5: *Map of New Zealand Tectonic setting. The major active structural features, Alpine Fault and Hope Fault, are indicated with the area of focus for this study indicated (red box). Numbered arrows show relative plate motions from DeMets et al. (1990). Figure is modified from Pettinga et al. (2001).*

Similarly, across the Canterbury region the amount of deformation reduces from northwest to southeast, due to the oblique plate motion in the South Island (Pettinga et al., 2001). The change in plate motion is reflected in the structures present, the plate motion is transferred across northern South Island by the Marlborough Fault System, linking the Hikurangi Subduction margin to the Alpine Fault (Walcott, 1998) (Figure 1.5). The Marlborough Fault System in the northern South Island accommodates primarily dextral strike-slip on northeast striking faults. There are four main faults within the Marlborough Fault System (MFS); the Wairau, Awatere, Clarence and Hope Faults, of which the Hope Fault is the most active (Eusden et al., 2000; Armstrong, 2000). Each fault within the MFS splays off the Alpine Fault and is aligned subparallel to the plate motion vector. The Hope Fault experiences high slip rates (eg. ~ 8 – 13 mm/yr (Hurunui segment), 23 ± 4 mm/yr (Conway segment), and ~10 – 18mm/yr (Hope River segment)) and has generated co-seismic ground rupture events with significant movement in the past, including the estimated M 7.1 – 7.3 earthquake in 1888 (Cowan, 1989; Pettinga et al, 2001; Langridge, 2003, Khajavi et al., 2014). The Hope Fault also separates contrasting structural domains to the north-west and south-east across the fault. Distinct regions of faulting across Canterbury have been classified into eight main structural domains, each with distinctive styles of deformation (Figure 1.6) (Pettinga et al., 2001). These are:

1. The Marlborough Fault Zone
2. The West Culverden Fault Zone
3. The Porters Pass-Amberley Fault Zone
4. The North Canterbury Fold and Thrust Belt
5. The Mt Hutt – Mt Peel Fault Zone
6. The South Canterbury Zone
7. The Canterbury Plains Zone and
8. The Southern Alps Zone

This study is focused on the Lees Valley Fault located south of the Hope Fault within structural domain 3 the Porters Pass - Amberley Fault Zone (Figure 1.6).

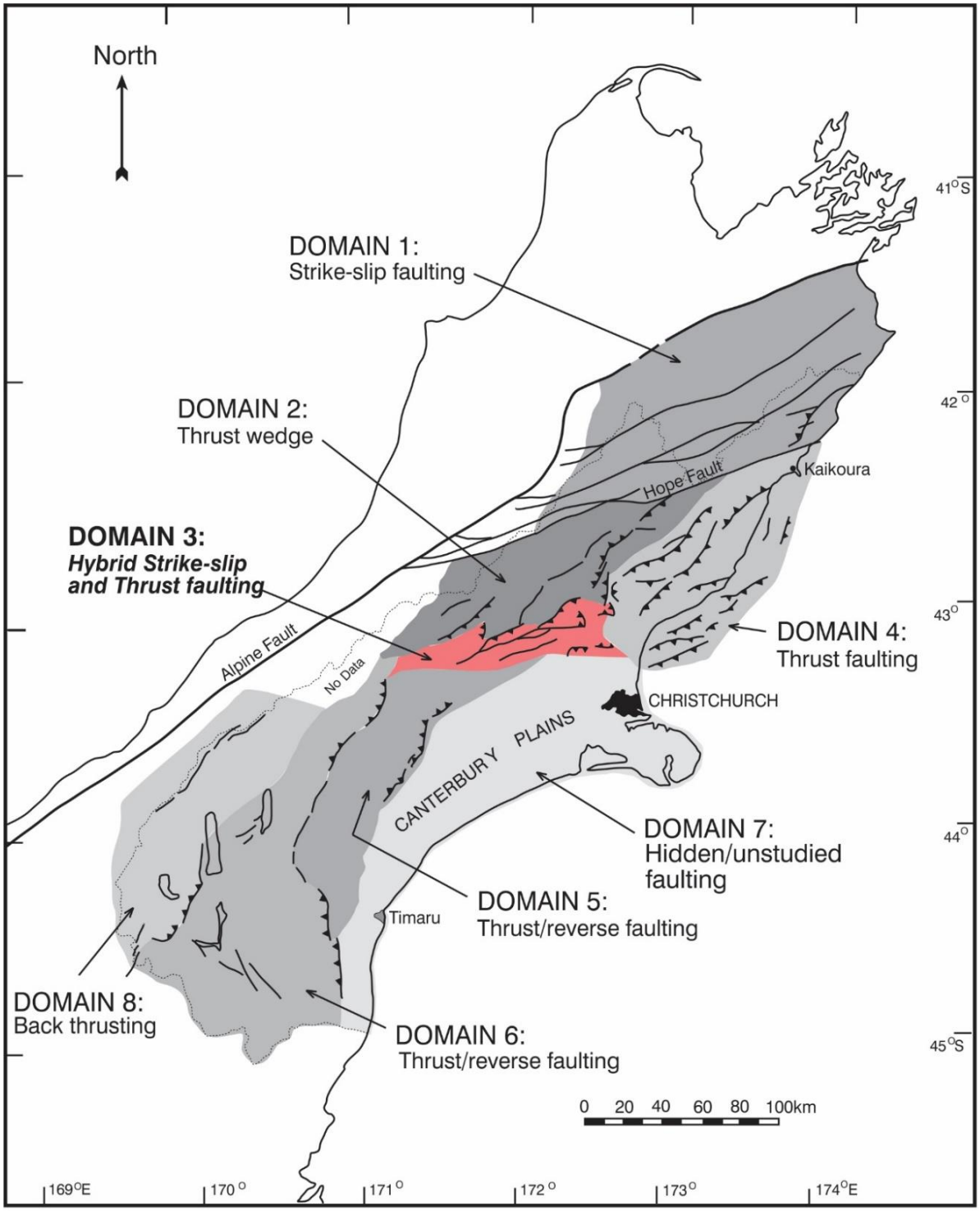

Figure 1.6: *Map of the South Island indicating the structural domains of the Marlborough/ Canterbury Region. Active faults are shown in black. Domain 3, the Porters Pass-Amberley Fault Zone, is highlighted in red as the domain of focus containing the Lees Valley Fault. The Alpine Fault and Hope Fault are indicated. Modified from Pettinga et al. (2001).*

1.4.2 Local Faulting

The Porters Pass - Amberley Fault Zone (PPAFZ), a complex hybrid zone of anastomosing dextral strike-slip and thrust/reverse faulting is located in the wider Canterbury Deformation Zone (Pettinga et al., 2001) (Figure 1.7). Much of the deformation in the Canterbury foothills of the Southern Alps is caused by the various northeast oriented faults in the region including strike-slip, oblique-thrust and reverse faults. Limited paleoseismic data indicate faults within the PPAFZ have a return period between 1300-500 years and a slip rate of ~ 3-4mm/year for single event displacements of 4-8 m (Cowan et al., 1996; Howard et al., 2005).

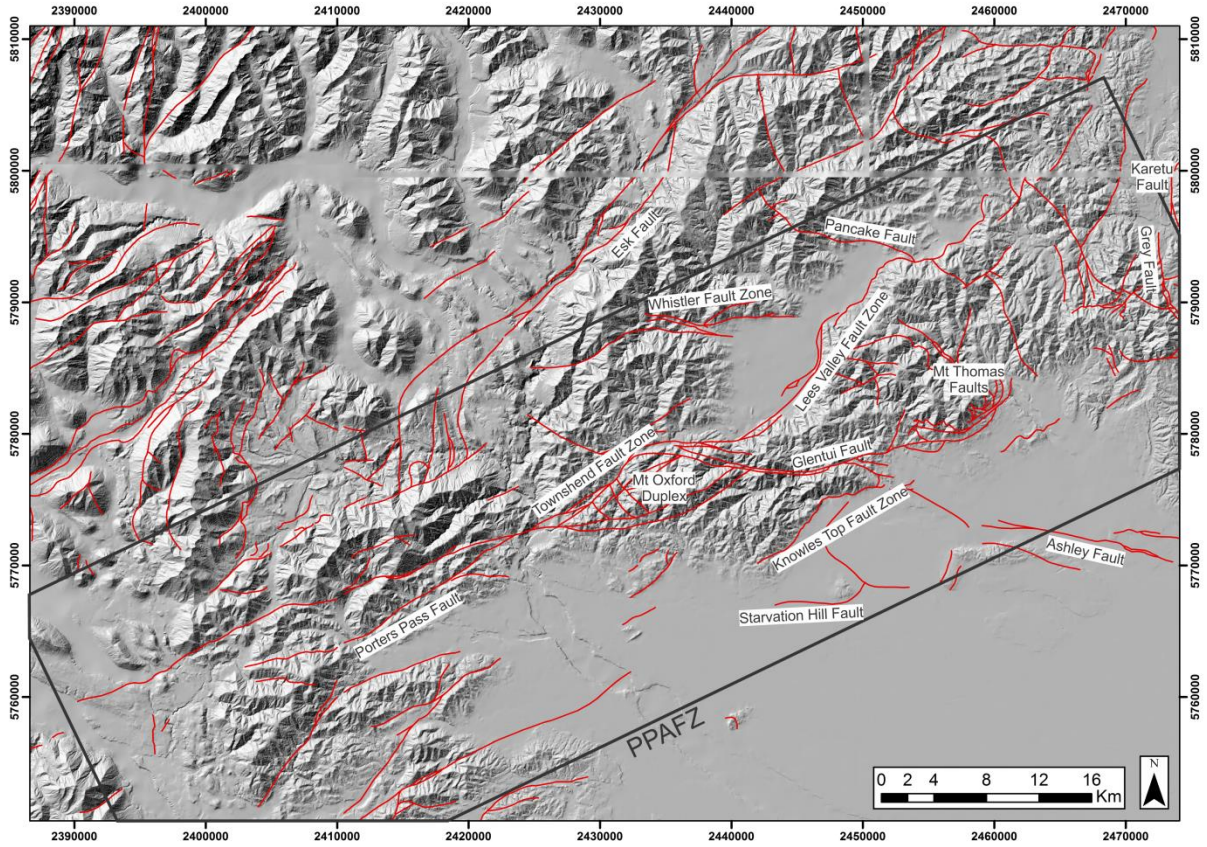

Figure 1.7: *Map of faults in the North Canterbury region. PPAFZ is indicated (black box within which the Lees Valley Fault and other important faults are labelled. Modified from Nathan et al. (2002), Rattenbury et al. (2006), Cox and Barrell (2007) and Forsyth et al. (2008).*

A number of individual faults within the PPAFZ have been the subject of structural and paleoseismic research. The fault zone can be separated into two sub-domains, with predominantly strike-slip in the southwest and a hybrid thrust and strike-slip in a northeast domain. The dextral strike-slip Porters Pass Fault to the south has been investigated in detail (Cowan, 1992; Cowan, et al. 1996; Howard, 2001; Pettinga et al., 2001; Howard et al. 2003;

Howard et al., 2005; Nicol et al., 2012) due to its clear geomorphic expression and potential for large magnitude earthquakes in close proximity to Christchurch. The Porters Pass Fault has a recurrence interval between ~2000 - 2500 years, slip rates of 0.3 – 0.9 mm/yr in the west and 2.5 – 3.7 mm/yr in the east and the potential to produce major events of up to 7.7 M (Pettinga 2001; Howard et al. 2003; Howard et al., 2005). Evidence of faulting during the Holocene indicate possibly 4 – 5 earthquake events, however, there remains considerable uncertainty with respect to paleoseismic history because of the complex segmentation and structural geometry of the PPAFZ.

Other important seismogenic faults within the PPAFZ domain include the: Mt Oxford Duplex (Townshend Fault Zone, Cooper-Creek Fault Zone, Cross faults), Glentui Fault Zone and the Whistler Fault Zone (Barrell & Begg, 2013; Pettinga et al., 2001; Cowan, 1992) (Figure 1.7). Limited paleoseismic data and structural complexity with respect to these structures make it too difficult to estimate their individual slip rate or large earthquake recurrence intervals. Parameters that have been determined and/or estimated in previous studies are presented in Table 1.1. The northern PPAFZ domain includes such faults as the Lees Valley Fault, the Mt Thomas Fault and the Mt Karetu – Mt Grey Fault Zone.

Other faults outside of the PPAFZ but in relatively close proximity to the Lees Valley Fault (the focus for this study) have also been the subject of structural and paleoseismic research in the area. The Torlesse, Cheeseman, Springbank and Craigieburn Faults again are characterized by limited data (Cowan, 1992; Pettinga, 2001; Forsyth, 2008) while the Esk Fault has been more extensively investigated by Noble (Noble, 2011). Their known and/or estimated fault and paleoseismic parameters are summarised in Table 1.2. These structures are all reverse/thrust faults and estimated capable of producing seismic events $M_W \geq 6.5$ (Table 1.2). These faults mostly define the rangefronts to ranges and topographic highs in the surrounding region with respect to the Lees Valley Fault.

The Lees Valley Fault is a south-eastward dipping active splay of the PPAFZ, and is located along the eastern range, bounding Lees Valley (Figure 1.4, 1.7 & 1.8). It is a complexly splayed hybrid oblique strike-slip dextral thrust/reverse fault zone (Garlick, 1992; Cowan, 1992; Pettinga et al., 2001). The thrust-bound Lees Valley basin has evolved through basement warping and faulting in response to regional compression. Research on surrounding structures demonstrates the region is highly active, the Lees Valley Fault along with the Knowles Top Fault Zone, the Starvation Hill Fault and the Ashley Fault Zone (Figure 1.7),

are the most active features in the Waimakariri District (Barrell & Begg, 2013). Lees Valley Fault also has a complex connection to the surrounding faults within the PPAFZ much of which remains poorly known. This study will shed new light on the structural style of deformation, fault zone geometry and associated rangefront evolution of the Lees Valley Fault. This in turn may provide insight and constraints on the tectonic development and paleoseismic history of the PPAFZ as a whole.

Table 1.1: *Fault parameters for PPAFZ from Pettinga et al. (2001) and Howard et al. (2005). Modified after Garlick (1992), Cowan (1992).*

Fault Name	Fault Type(*)	Interpreted Dip Angle (deg)	Length (km)	Average Displacement / event (m)	Slip Rates (mm/year)	Last Rupture(s) (years)	Recurrence Intervals (years)	Magnitude (Mw) (estimated)
Mt Grey Fault	Rev/SS	30 – 80 NW	15	2 – 4	0.5 – 1.8	300 - 450[(1)] 2300 – 2400[(1)]	1300 - 2000	6.9
Mt Thomas Fault	Rev/SS	30 – 80 NW	16	-	-	-	2000 – 5000[(2)]	6.5
Lees Valley Fault	Rev/SS	30 – 80 SE	25	1 - 3	2.5 – 5	-	(2000 – 5000)	6.7
Townshend Fault	SS/Rev	40 – 90 S	14 – 16	-	-	-	-	-
Glentui Fault	SS	60 – 90	10 – 12	-	-	-	-	-
Coopers Creek Fault	SS/Rev	60 – 90 N	14 – 16	-	-	2000 – 2500	-	-
Porters Pass Fault	SS	60 – 90 N	35 – 40	5 - 7	2.7 – 5.0	500 – 700[(1)] 2000 - 2500[(1)]	7500 – 11700 1500	7.1 – 7.4
Ashley Fault/Cust Fault	Rev	20 – 50 NW	72	0.5 – 4.0	-	-	2000	7.2

(*): Based on Paleoseismic and/or slip rate data.
([1]): C^{14} dates expressed as years B.P. are given prior to 1950, and are only approximate to calendar years. The relationship is not constant through time.
([2]): Based on recurrence interval of neighbouring faults.
Rev: Reverse Fault
SS: Strike-Slip

Table 1.2: *Fault parameters for faults outside of PPAFZ but within same region from Pettinga et al (2001), Forsyth et al. (2008) and Noble (2011).*

Fault Name	Fault Type(*)	Interpreted Dip Angle (deg)	Length (km)	Average Displacement / event (m)	Slip Rates (mm/year)	Last Rupture(s) (years)	Recurrence Intervals (years)	Magnitude (Mw) (estimated)
Torlesse Fault	Rev	50 – 80 SE	31	-	-	-	2000 – 4000	6.7
Cheeseman Fault Zone	Rev	20 – 70 W	23	-	0.25 – 1.0	-	2000 – 5000	7.0
Springbank Fault	Rev	20 – 70 NW	68	-	-	-	5000	7.1
Esk Fault	Rev/SS	50 – 80 W	71	-	0.31±0.06(1) 0.82±0.06(2)	12800 – 9500 6324 – 716	5, 612±445	7.0 – 7.5
Craigieburn Fault	-	-	32	-	-	-	-	-
West Culverden Fault Zone	Rev	30 – 70 W	24	-	1	1495 – 1925	5000 – 10000	6.9

(*): Based on Paleoseismic and/or slip rate data
(1): Vertical
(2): Lateral
Rev: Reverse
SS: Strike-Slip

1.4.3 Geological Setting of Lees Valley

The Torlesse composite terrane, the stratigraphic basement within North Canterbury, is comprised of quartzofeldspathic sedimentary rocks, primarily sandstone and argillites and ranges in age from Late Carboniferous to Early Cretaceous (Forsyth et al., 2008). There are two distinct terranes within the basement rock that vary in characteristics, the Rakaia Terrane to the South and the Pahau Terrane to the North (Figure 1.8). These are separated by the Esk Head Mélange (Bradshaw, 1973; Botsford, 1983), a zone approximately 12 km wide that has undergone intense deformation in the Early Cretaceous. The younger "cover" sequence ranges in age from late Cretaceous to early Quaternary. It is predominantly a marine succession with localised interbedded mafic igneous rocks (Forsyth, et.al, 2008). The cover succession is preserved within and around the margins of the structural basins developed between the Torlesse cored ranges formed by uplift associated with active faulting and folding in the region. During the Quaternary extensive non-marine fluvial deposits were laid down covering much of the Cretaceous-Tertiary sequence and are primarily preserved.

Lees Valley is positioned close to the boundary between the Rakaia and Pahau Terranes, the Rakaia Terrane dominates in the region and outcrops of the Esk Head Mélange are found in the northern end of the valley (Figure 1.8). The majority of the basin has filled with aggradational Quaternary alluvial fan deposits that rest unconformably above the Torlesse and Tertiary sedimentary rocks (Garlick 1992). Late Cretaceous and Tertiary deposits are present in outcrop in the Ashley River, on the eastern side of the southern valley. At the southern end of the lower valley some small exposures of extrusive volcanics are present.

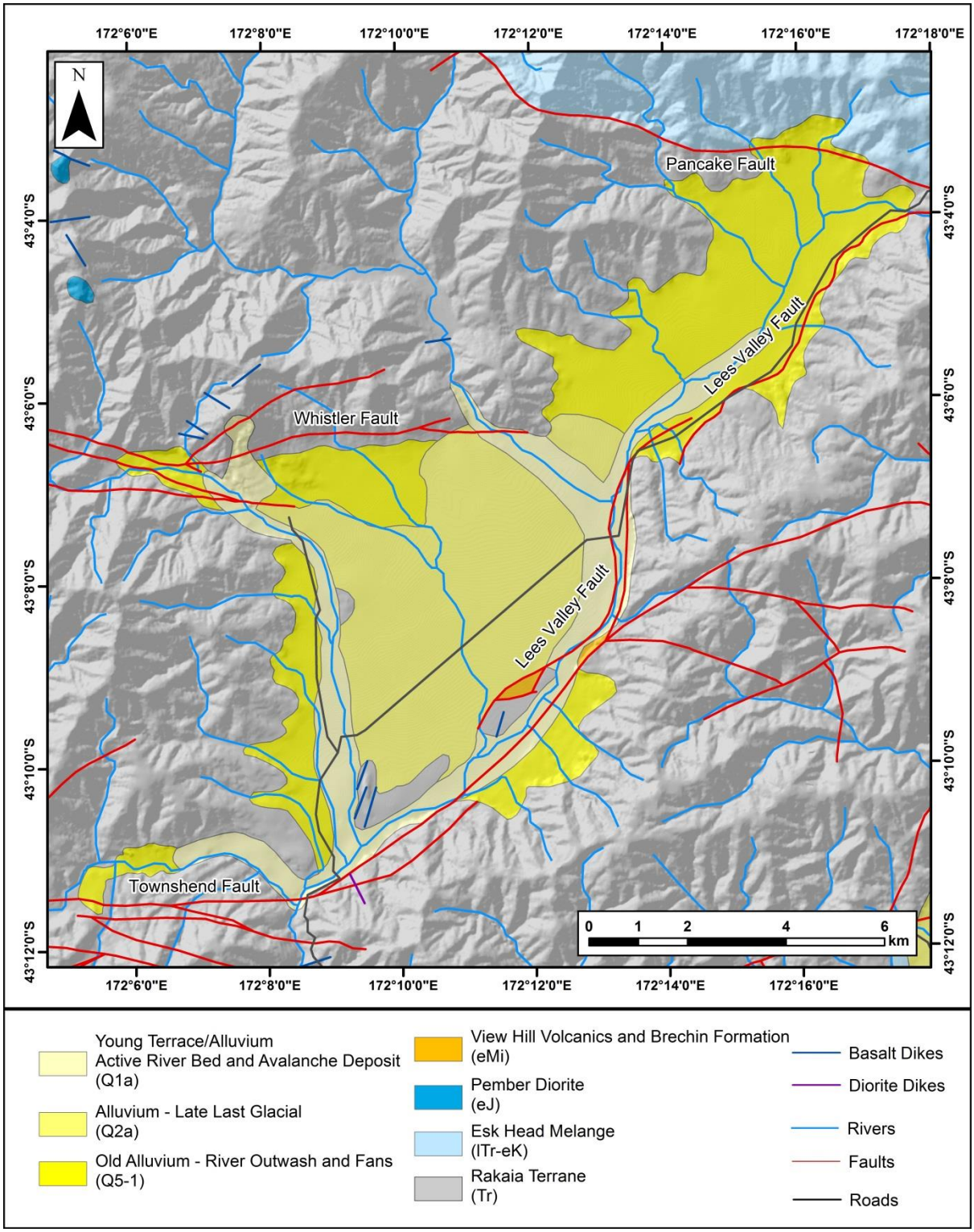

Figure 1.8: *A simplified geological map of Lees Valley and the surrounding area. Modified from Forsyth et al. (2008) and Jongens et al. (2009).*

1.4.4 Historic Seismicity

Over the last 53 years (since records started for the area in 1962) ~300 earthquakes have occurred in and around Lees Valley (Figure 1.9). They ranged from magnitude 1.7 to 5.2 and 75% were shallow, occurring at depths of ≤ 15 km. Most of the earthquakes were clustered at the southern end of the Lees Valley Fault (Figure 1.9), where it links with the surface trace of the Townshend Fault (Figure 1.7 & 1.8). Of these earthquakes ~ 52% occurred since September the 4th 2010.

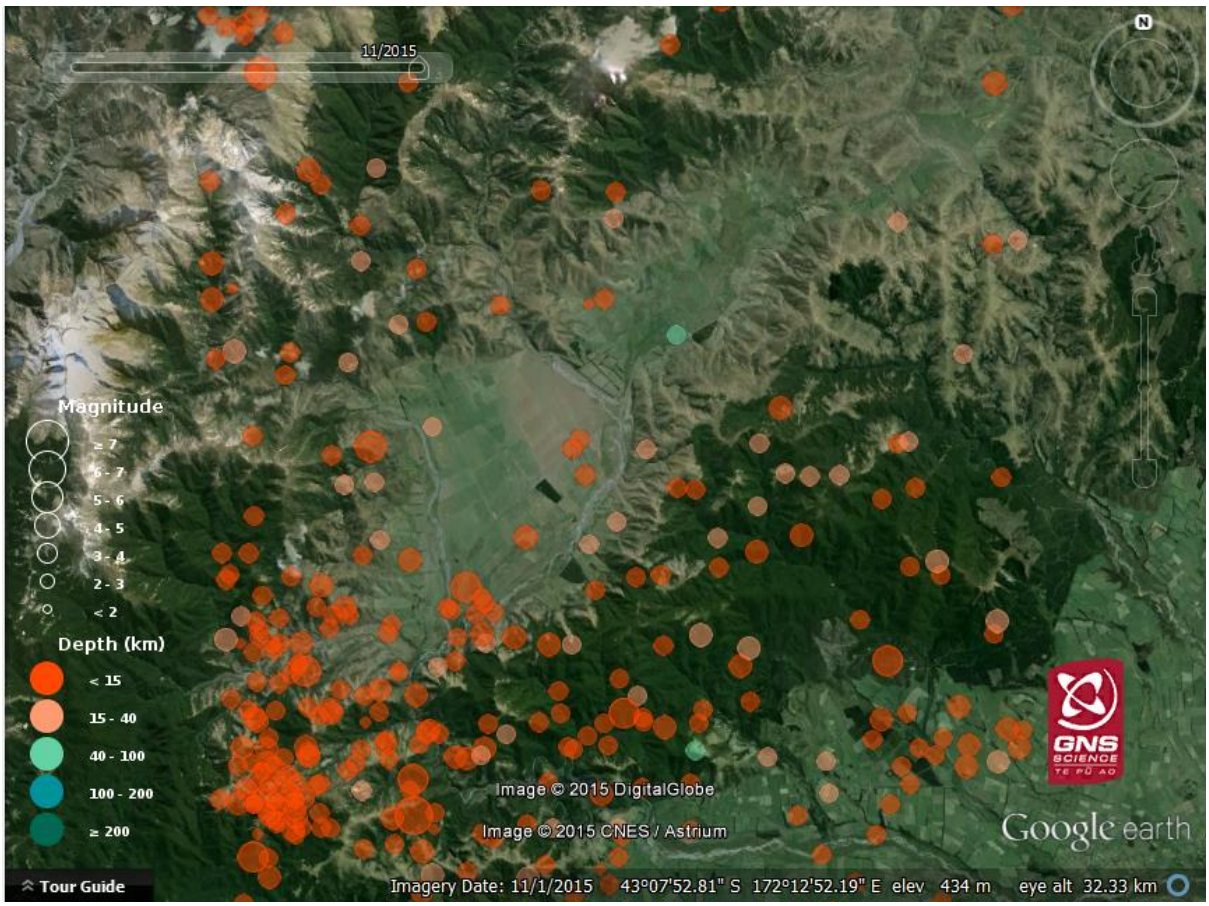

Figure 1.9: *Earthquake distribution from 1962 till present in and around Lees Valley. Modified from Geonet (2015) and Google Earth (2015).*

1.5 Previous Studies

Structural elements within Canterbury such as the PPAFZ were studied as early as 1872 by Julius Von Haast when he surveyed the geology of North Canterbury (cited in Noble, 2011). Early investigations on Lees Valley were limited, but provided important observations on its geology, geomorphology and structural characteristics. This earlier work is well summarised by Garlick (1992), and includes studies on the valleys geomorphology, faulting, drainage

patterns and Tertiary sediments by Speight (1926), age of Tertiary sediments and locations of fossils in unpublished records held by GNS Science and Department of Geological Sciences at University of Canterbury, mapping of the basin and fault trace (Gregg, 1964), mapping and descriptions of the Esk Head Mélange (Botsford, 1983), and descriptions of Tertiary sediments and faulting by Field and Brown (1989).

More recent studies were completed by Cowan (1992) and Garlick (1992). Cowan focused on the PPAFZ, mapping an extensive area along the eastern foothills of the Southern Alps to Amberley. The structure, seismicity and tectonics of the PPAFZ were described in detail in Cowan (1992) and includes regional mapping of the southern and eastern margins of Lees Valley and its structural elements. Cowan also provided a short description of the Lees Valley Fault, how it connects to the wider regional tectonics and its expression throughout the valley, and noted the concealed nature of the fault through much of the valley beneath the southeast floodplain margin and active Ashley River bed and extensive basin margin Quaternary alluvial fan deposits. The fault is exposed in the lower slopes of the eastern rangefront where crushed Torlesse basement is described as thrusting over Lower Tertiary marine strata and Quaternary fan gravel deposits (Cowan, 1992). The fault was noted to have a dip to the south – southeast at ~ 15˚-50º. Surface fault rupture traces in the upper valley are recorded as having scarp heights of up to ~ 6 m and displacing many of the Holocene alluvial fan surfaces. Cowan further inferred that the surface fault ruptures were active in the Holocene due to their clear geomorphic expression, including sharp steep scarp risers, sharp crests, and associated ground warping. Other splays off the main Lees Valley Fault into the eastern ranges are indicated by saddles and topographic lineaments in the ranges and have steep-to-vertical dips, no crushed zones were observed at the surface by Cowan.

The most focused research on the Lees Valley Fault was completed by Garlick (1992). In this study the structure, geomorphology and active tectonics of the Lees Valley Fault Zone are documented. Contractional deformation recorded in Garlick (1992) was classified into four main types of faulting (Table 1.3). All of the faults bounding the eastern side of the valley display an orientation of NNE-SSW and are classified by Garlick as range-bounding, internal thrust/reverse faults. Garlick indicates the most recent visible active fault trace offsets alluvial fan deposits in the northern sector of the valley and represents the most westward propagation of the rangefront uplift and faulting.

Table 1.3: *Styles of faulting observed in Lees Valley, after Garlick (1992).*

1	Widespread bedding parallel shears which preferentially deform mudstone beds.
2	Minor faulting which cross cuts and offsets bedding.
3	Concentrations of small faults, predominantly in sandstone, with quartz mineralisation displaying stepped striations.
4	Zones of intense shearing, cataclasis and gouge formation, associated with large active faults. The shear fabric anastomoses around lozenges of mostly intact rock.

Garlick concluded that it was likely the fault scarps observed in the upper valley were formed by multiple co-seismic fault rupture events and that the difference in scarp height laterally along the fault zone resulted from the offset of different age topographic surfaces. Based on clear geomorphic evidence, Garlick (1992) proposed most recent co-seismic movement occurred in the Holocene. Garlick also noted that the fault continuation north of Lees Valley is difficult to define, with multiple splays resulting in a wider zone of deformation, with displacement transfer and strain partitioning. Garlick (1992) proposed a model for the development of the rangefront involving a fault-bounded wedge of uplifted basement, requiring the multiple splays along the valley margin to converge at depth.

Cowan (1992) included a study on seismicity of the newly formed PPAFZ and this included the Lees Valley area. In a later extension of this work, Cowan et.al. (1996) compared the seismicity rate of the newly formed (juvenile) PPAFZ to the more evolved Hope Fault in North Canterbury. This research utilised inferred paleoseismic dates of surface ruptures and landslides in order to show the importance of structural maturity of the fault zones in comparison with seismicity rates. The combined landslide volume in Lees Valley from several discrete landslides is indicated to be 10^7 m^3 and have an age of 580 ± 90 years before A.D. 1950. Data gathered using the weathering rind method, showed 62 rinds measured in 1991 A.D. gave an age in calendar years of A.D. 1320-1500.

Following the detailed studies of Cowan (1992) and Garlick (1992) no further studies on the Lees Valley Fault have been completed although the location has been mentioned in reports with a regional scope. These have focused on the active landscape in the Canterbury region and indicate the importance of the Lees Valley Fault in the wider regional development. Nicol (1991) mentions the NNE trend of the Lees Valley Fault as part of PPAFZ in his PhD thesis defining structural styles and kinematics of deformation in the Waipara region. Barrell & Begg (2013) describe the characteristics of the faulting and folding in Lees Valley,

mentioning the morphology and features of note in the valley as part of the identification of general distribution and characteristics of active faults and folds in the Waimakariri District. Due to being an inland basin Barrell and Begg describe that the confinement of rivers to narrower paths forming paleo-deposits which record the occurrence of Late Quaternary faulting, including in the Lees Valley. One main feature noted is the monoclinal flexure in the southern valley, and is associated with active faulting beneath the valley floor. Here warping affects the ~ 18,000 year old alluvial (paleo) surface, formed by river channels, over a width of approximately 150 m with a cumulative vertical deformation across the structure of ~ 5 m. Barrell and Begg (2013) also support conclusions in Garlick (1992) and Cowan (1992) by noting the variability in fault expression throughout the basin and note there are "definite", "likely" and "possible" fault traces. Also noted is the East-West trending Whistler Fault Zone which enters the valley on the western margin from the Puketeraki Range, and extends across toward the toe of the eastern range defining the transition from the northern and southern Lees Valley (Cowan, 1992; Barrell & Begg, 2013).

In summary, Barrell & Begg (2013) estimate, using field observations and reinterpretation of supporting evidence from Garlick (1992) and Cowan (1992), that the Lees Valley fault last ruptured ~18,000 years ago, this in contrast with the earlier studies proposing Holocene timing. Based on a maximum scarp height of 8 m vertical deformation and a calculated average vertical-dip-slip rate of 0.4 mm/year, the implied long term average recurrence interval is given as 4,500 years (assuming 2 m vertical deformation per event). The mismatch between the estimated recurrence interval and timing of last rupture indicates an amount of error in one or both estimates. It is unclear from existing research how many events have formed the current structural features, it may have been multiple smaller events or one large event which can significantly alter expected recurrence intervals. Barrell and Begg (2013) estimated their recurrence interval from vertical displacement along a monocline feature offsetting a fluvial river plain estimated to be ~18,000 years old, based off provisional age estimates from regional geological knowledge. The age of the surface is not well constrained with dated material from the site and the number of rupture events on the feature is not known, contributing to error included in their estimate. Significant uncertainty is expected due to the poor definition on slip rate for the fault zone which is difficult to constrain as it is also estimated from the age of offset surface and amount of vertical offset hence the same uncertainty will apply. Offset measured by Barrell and Begg (2013) was limited to vertical deformation height of the scarp therefore a level of uncertainty will remain due to the lack of

evidence for the actual slip offset. Furthermore the Lees Valley Fault Zone contains multiple fault traces that have the potential to have diverse individual fault rupture histories. The Barrell and Begg estimates are based off features than run through the basin floor and at a different orientation than the eastern range-bounding faults. It is not likely that these features have the same behaviour characteristics, therefore estimates by Barrell and Begg cannot confidently be attributed to the main structural features of the Lees Valley Fault Zone that bound the eastern range.

Several findings have been accumulated and reviewed by Pettinga et al. (2001) characterising the Lees Valley Fault with a recurrence interval between 2000 – 5000 years based on a slip rate of 2.5 – 5.0 mm per year. The range in values highlights the uncertainty in defining these parameters of the fault given the current data. Pettinga et al. (2001) also described the fault as having a 30 – 80º SE interpreted dip angle, an average 1 – 3 m displacement per event and an estimated magnitude of 6.7 Mw.

1.6 Thesis Organisation

Chapter 2: Structure and Geomorphology

This chapter begins by reviewing Bull's (2007) model for the tectonic geomorphology development of mountain rangefronts, selecting particular structural and geomorphic features to assess. The model is subsequently compared to Lees Valley and supported by extensive mapping and GPS surveying, to investigate the valleys structural and geomorphic development. The valley is divided into two sections, northern and southern valleys, based on changes in expression of the fault and the structure and geomorphology is described for each. Characteristics such as sinuosity and faceted spurs are used to analyse and discuss the tectonic activity class of the rangefront. Analysis of fault discontinuity, fault splays and the distribution of vertical displacement along the fault is discussed to provide further understanding of fault behaviour. Limited exposure of the thrust plane is described to indicate the complexity of faulting and a summary of the important findings from the chapter is provided.

Chapter 3: Paleoseismology

This chapter provides the paleoseismology results from the trench and aims to constrain the timing of Late Quaternary surface rupturing events. The Lees Valley Fault is one of the most active features in the Waimakariri district and prior to this study no paleoseismic studies had

been undertaken on the fault. The aim of this chapter was to build on this knowledge gap by analysing data to provide estimates on fault characteristics such as potential slip rate, slip per event, recurrence interval and potential magnitude. The data was gathered from the paleoseismic trench and supported by mapping and surveying. A brief description of potential seismic hazard from the Lees Valley Fault is also given.

Chapter 4: Discussion

Chapter 4 discusses the analyses from the previous chapters and gives interpretations of their findings in terms of the Lees Valley development and episodic behaviour of the fault system. It also reviews the Lees Valley Fault link to the regional structures, comparing slip rates and discussing fault segmentation and structural links. A model for evolution of the valley and fault system is provided in relation to the wider structural picture.

Chapter 5: Conclusions

This chapter summarises the results of the structural, geomorphic and paleoseismic analyses and the discussion on their implications for the development of the fault zone. It provides the main conclusions from the study about the behaviour of the fault and development of the fault zone and associated ranges. Suggestions for possible future work in the area are also discussed.

Appendices

Attached appendices and digital appendices are included to provide additional information on methods used and results.

2. Structure and Geomorphology

2.1 Introduction

The Lees Valley Fault is a complex reverse-rangefront fault zone that extends along the east margin of an intermontane basin with distinct geomorphology. Furthering understanding of this fault zone required detailed structural and geomorphic analysis, including detailed field mapping and interpretation, and detailed fault scarp profiles. Previous work by Garlick (1992) and Cowan (1992) indicated the wide range of structural and geomorphic features within the valley that could aid in interpretation and development of a rangefront evolution model. Cowan (1992) mapped sections of the fault zone in the southern sector of the Lees Valley, while Garlick (1992) worked towards understanding the suite of traces and activity in the northern sector of the valley. This study aims to combine recent data with previous studies to build towards a more coherent picture of the basin and fault zone development.

The key aims addressed in this chapter include:

1. Map full extent of fault trace and associated features within Lees Valley.
2. Describe selected basin surface and structural characteristics.
3. Investigate the Activity Class of the eastern rangefront based on geomorphic features.
4. Investigate deformation expression of the Lees Valley Fault along strike.
5. Investigate structures that may be affecting basin development.
6. Discuss Lees Valley structural and geomorphic development.

The following section (2.2) provides a review of the currently widely accepted model for the general development of faulted rangefronts and their classification in terms of tectonic class, through analysis of such features as fault scarps and alluvial fans (Bull, 2007). Using new data from this study and previously identified rangefront structural and geomorphic features within the Lees Valley basin a new rangefront development model will be established. Analysis of the fault zone surface expression through field mapping and GPS surveying has aided in understanding fault characteristics such as deformation, fault dip and sense of motion. Large scale (1:20,000 and 1:40,000) maps have been produced for each section of the valley. Features of interest such as fault splays and fault transition/step-over zones within the valley have been mapped in more detail. Variation in surface fault expression, deformation, and basin development differs significantly in the northern and southern sections of Lees

Valley, consequently these will be considered separately within some sections of this study and compared for discussion (refer to Figure 1.7).

2.2 Review of Published Model for Tectonic Geomorphology Development of Mountain Rangefronts

Mountain front descriptions and tectonically induced geomorphology have been described in detail by Bull (2007) and Burbank & Anderson (2012). This section will outline some of their important observations and models to be referred to within this chapter. It is important to note that the majority of work these models are based on was performed in North American field areas which are often defined by normal (extensional) faulting in arid environments, the opposite of this field study area. Regardless, many of the processes and relationships discussed in these models remains applicable to aid in understanding the development in this study area, although slight variations in results may be expected.

2.2.1 Describing Mountain Fronts

Mountain fronts are a result of long-term interactions of uplift and denudation mostly from fluvial processes initiated by the first uplift movement. This interaction and influence on the evolution of a fault generated mountainous escarpment was elegantly modelled by Wallace (1977) (Figure 2.1).

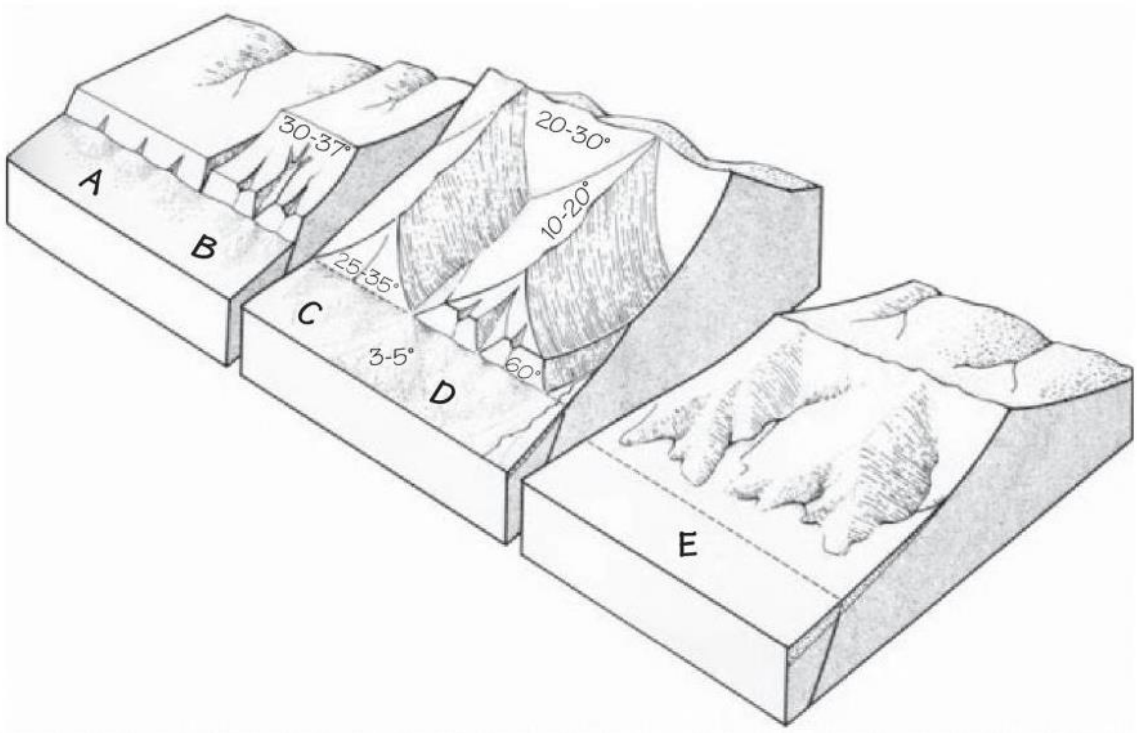

Figure 2.1: *Schematic diagram of sequential development of mountain fronts along a fault generated escarpment. A) Linear scarp of initial faulting. B) Migration of scarp crest from rising range boundary to form range crest. C) Formation of valleys and faceted spurs in rising block; valley floor locations indicate induced stream downcutting by rapid tectonic activity. Spur ridge crests indicates slow tectonically induced degradation. D) A steep, straight mountain-piedmont junction results from episodic displacement along a range-bounding fault. Uplift of main and spur ridge divides is faster than degradation. E) A sinuous mountain-piedmont junction forms alongside widening of valley floors when uplift ceases. Degradation lowers ridge crests and rangefront relief lessens. Figure from Wallace (1977) modified by Bull (2007).*

In actively deforming mountainous landscapes a range of distinct tectonic landforms may be created. These include faceted spurs, mountain-piedmont junctions and piedmont forelands (Bull, 2007). Faceted spurs are triangular facets that result from fault planes being modified by erosion and base-level fall (stream/river incision). Uplift increases a facet height while valleys become deeper through fluvial incision, resulting in faceted spurs in a tectonic environment becoming higher and progressively dissected over time, sometimes forming nesting of younger facets within higher older facets. Bull has provided 6 stages of erosional dissection of faceted spurs (Table 2.1)

Table 2.1: *Triangular facet dissection stages from Bull (2007).*

Facet Class	Erosional landforms
1	Planar surface with only rills. Includes scarps that have yet to be carved into facets by streams flowing across the scarp.
2	Planar surface with shallow valleys extending a short distance into the facet.
3	Valleys extend more than 0.7 the horizontal distance between the base and top of the facet.
4	Deep valleys extend more than 0.7 the horizontal distance.
5	Greatly dissected but the general form is still obvious.
6	So dissected that the general form of a facet is not obvious.
7	Triangular facets are not present because they have been removed by erosion, or they never existed.

A mountain-piedmont junction is the distinct geomorphic change from rangefront escarpment to basin floor (Bull, 2007) and is a result of the interplay between uplift and fluvial erosion. Analysis of junction sinuosity is useful in the investigation of the relationship between rangefronts and active range-bounding faults. A more linear junction with low sinuosity indicates recent uplift while a highly sinuous junction indicates less active uplift during a period of tectonic quiescence, where erosion has degraded the junction. Influences on the expression of these junctions include: lithology, joints, foliations, bedding planes and the width of the drainage basin. The larger the drainage basin or the weaker the lithology, the more sinuous the junction is due to increased rates of erosion. Climatic setting is also important due to its impact on the relationship between uplift and fluvial degradation.

Piedmont forelands form by fluvial debris deposition at the base of mountains but can be shifted up a mountain range when uplifted by active range-bounding faults (Bull, 2007) (Figure 2.2). As a thrust fault system propagates into a basin new thrust escarpments are created in the fault zone footwall and earlier faults are abandoned. These then form "internal" mountain fronts that are less active or become inactive as tectonic deformation is transferred to the new outermost fault splay (Bull, 2007; McCalpin, 2009). The morphology will display ruptures, folding and tilting as a result of deformation. Older piedmont surfaces undergo the fluvial erosional processes of the rangefront they have been incorporated into, altering its appearance whereby the top surface becomes rounded as erosion degrades the crests and drainage channels erode and incise into the slopes.

Tectonic driven ground surface deformation such as fault ruptures, folding and tilting also influence the flow path of streams over active thrust faults. Investigation into stream responses to tectonic deformation can often aid in locating active structures. Furthermore

uplift causes these streams to downcut leaving strath terraces which can indicate base level drop related to episodes of uplift. Analysis and recognition of piedmont landform elements along a rangefront bounded by active faults helps define the tectonic structure.

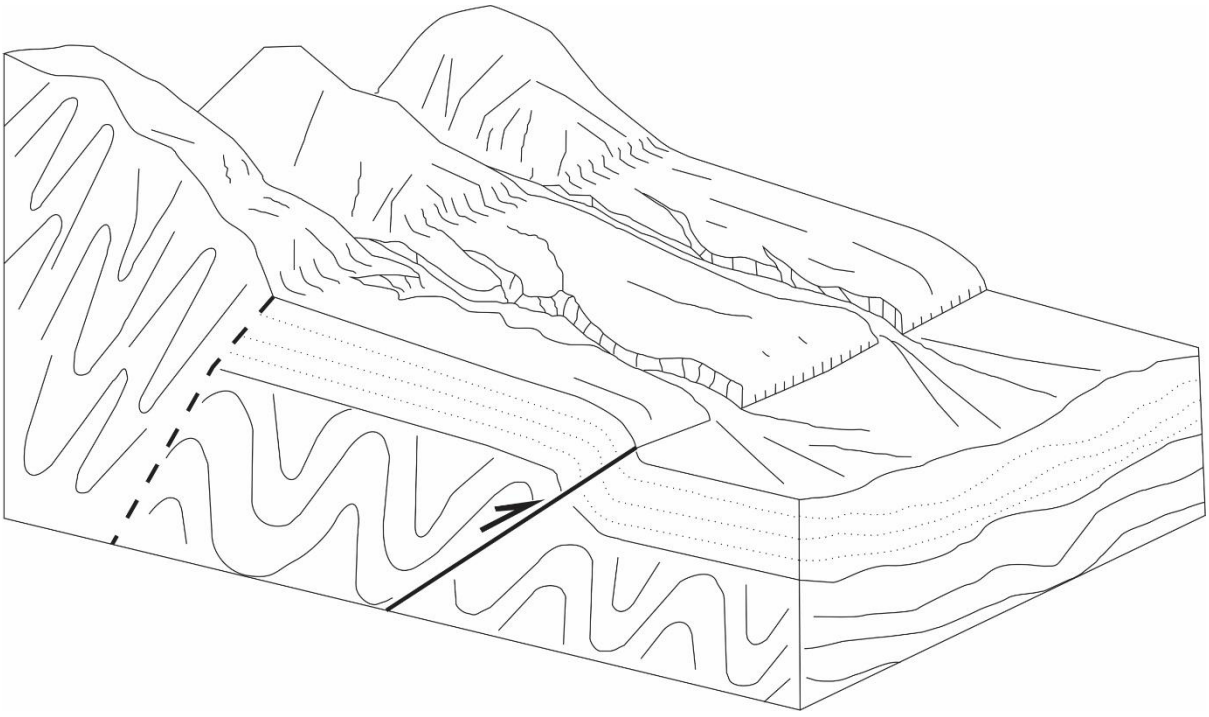

Figure 2.2: *Schematic diagram of the migration of active faulting, shifting outward of the range, forming a new rangefront boundary. Old abandoned faults and associated shear fabrics remain within the hanging wall of the uplifting mountain range alongside the uplifted and dissected fans. Modified from Bull (2007).*

Reverse fault systems often occur as an accumulation of different fault splays with varying structural, lithologic and topographic characteristics. For these reasons faults do not always rupture along the entire length of their identified fault zone (Bull, 2007). Consequently when considering the constraints on estimation of earthquake size they can be broken up into segments to investigate the individual styles of surface rupture, magnitude and timing. However, identification of these fault segment boundaries is not easily done and a level of uncertainty will apply. Methods such as identifying topographic, lithologic and geophysical changes, structural branching, and intersections with other faults provide low reliability. Changes in fault style, slip rate, recurrence interval and change in fault orientation (bends and step overs) are even less reliable. While topographic changes are often used to distinguish sections it cannot be ruled out that it is possible for a fault zone to display various types of behaviour.

2.2.2 Tectonic Activity Classes

Analysis of landforms along a rangefront can be used to provide estimates of relative tectonic activity. Relative uplift rates can be inferred by investigating features such as mountain front sinuosity, widths of valleys and triangular spur facets.

The sinuosity of a mountain front directly indicates the amount of erosional modification and infers the degree of tectonic activity by defining the tectonic class of the rangefront. The piedmont junction, as identified by Bull (2007), is the sharp transition from escarpment to basin floor. Generally the relationship of this junction is straight if an active fault along the mountain front is controlling the uplift of the ranges. In practice a low sinuosity of the junction indicates the rangefront has been recently active with appreciable slip-rate. A higher sinuosity indicates there has been a slow slip-rate, one where erosion has become a dominant factor with transportation and re-deposition of material causing the junction to become more irregular.

The sinuosity is given as a ratio (J) and measured as follows:

$$J = \frac{Lj}{Ls}$$

Where Lj is the planimetric length of the topographic junction between mountains and the adjacent piedmont and Ls is the length of the range-bounding geologic structure or straight line length of the mountain front segment Bull (2007). J has a minimum value of 1, increase in J indicates an increase in fluvial processes degrading the junction and decreased uplift rates. Values of 3 – 10 describe an inactive mountain front, while values of 1.5 – 3 describe moderately active uplift with values nearer to 1 and within 1 – 1.5 indicate highly active uplift.

The valley floor width to height ratio is another landform relationship that can be used to analyse recent uplift. Cessation of faulting decreases uplift while erosion continues causing lessening of landform relief. This decreases valley height while valleys increase in width through fluvial degradation and aggradation processes. This ratio is influenced by strength of lithology to withstand erosion. Consequently sites chosen for analysis must be within the same lithology type and also the same basin-position coordinate for a suite of similar size drainage basins along a given mountain front. Furthermore there is a limitation in the size of drainage basin that provides accurate ratios due to the changes in stream discharge. Due to

the difficulty of obtaining accurate ratios this method has not been investigated quantitatively in this study.

Triangular facets are very useful in identifying areas of tectonic activity and providing relative tectonic classes based on their height and stages of dissection Bull (2007). The base of such features often resemble an active fault trace and will have a high triangular facet or have become a degraded fault plane with highly dissected facets. The appearances of the facet state reflects the rates and magnitudes of uplift, such classes are outlined in Table 2.2.

Four base level processes control mountain front morphology, these are; channel down-cutting (cd), aggradation (pa), degradation (pd) and uplift (u) (Bull, 2007). The unique combination of these processes builds distinctive landforms that can be used to identify relative tectonic activity. Rapid uplift encourages sustained channel down-cutting and deposition on the piedmont fan. Consequently an active basin landscape without significant alluvial basin fill can be defined using these three processes:

$$\frac{\Delta u}{\Delta t} < \frac{\Delta cd}{\Delta t} > \frac{\Delta pd}{\Delta t}$$

Active landscapes are generally defined as Class 1. They have straight mountain fronts due to range-bounding faults, triangular facets with minimal dissection of basal sections and V-shaped valleys. An outline of these classes is provided in Table 2.2 as examples of some landscape responses to uplift.

Table 2.2: *Geomorphic classes of Quaternary relative tectonic activity of mountain fronts from Bull (2007).*

Class of Relative Tectonic Activity	**Relative Uplift rate**[1]	**Typical Landforms**	
		Piedmont[2]	**Mountain**[3]
Active			
Class 1A – maximal	$\Delta u/\Delta t \geq \Delta cd/\Delta t + \Delta pa/\Delta t$	Unentrenched alluvial fan [0.6-0.9]	V-shaped valley profile in hard rock [1.1-1.4]
Class 1B – maximal	$\Delta u/\Delta t \geq \Delta cd/\Delta t + \Delta pa/\Delta t$	Unentrenched alluvial fan [0.6-0.9]	U-shaped profile in soft rock [1.0-1.3]
Class 2 – rapid	$\Delta u/\Delta t < \Delta cd/\Delta t > \Delta pa/\Delta t$	Entrenched alluvial fan [1-1.1]	V-shaped valley [1.1-1.3]
Class 3 – slow	$\Delta u/\Delta t < \Delta cd/\Delta t > \Delta pa/\Delta t$	Entrenched alluvial fan [1.1]	U-shaped valley [1.0-1.1]
Class 4 – minimal	$\Delta u/\Delta t < \Delta cd/\Delta t > \Delta pa/\Delta t$	Entrenched alluvial fan [1.1]	Embayed front [1.0-1.1]
Inactive			
Class 5A	$\Delta u/\Delta t << \Delta cd/\Delta t > \Delta pa/\Delta t$	Dissected pediment [1.1]	Dissected pediment embayment [1.0-1.1]
Class 5B	$\Delta u/\Delta t << \Delta cd/\Delta t = \Delta pa/\Delta t$	Undissected pediment [1.0]	Disssected pediment embayment [1.0]
Class 5C	$\Delta u/\Delta t << \Delta cd/\Delta t < \Delta pa/\Delta t$	Undissected pediment [1.1]	May be like class 1 landscapes.

[1] (cd) = Channel downcutting, (pa) = aggradation, (pd) = degradation, (u) = uplift.

[2] Unentrenched = entire fanhead deposited recently, or only Holocene fan surfaces are entrenched. Entrenched = alluvial fanhead surfaces with Pleistocene soils are entrenched.

[3] Stream power / Resisting power ratios in [ ] suggest departure from equilibrium value of 1.0.

Although not all landscapes will progress through all of these stages Table 2.2 provides a good outline for interpreting landscape morphology. It is important to keep in mind a landscape can revert back to Class 1 upon fault reactivation or even display a combination of classes when there are both active and inactive faults present.

2.2.3 Fault Scarps

Range-bounding faults scarps can be difficult to analyse due to uncertainty in separating uplift increments, a diversity of lithology and structure, and multiple ruptures creating steep and irregular slopes. However, they are important to discuss for the insight they give on the latest surface ruptures and the stage of fault propagation the system is in. Climate and lithology both have strong influence on scarp expression and interpretation of scarp models.

The elements that make up a fault scarp are outlined in Figure 2.3. Multiple fault splays can produce complex scarps which are difficult to model, due to the accumulated effects of both degradation and aggradation, and will display different stages of each of the elements outlined in Figure 2.3. Fault scarp parameters must be analysed with care as scarp height is often larger than throw in a sloping alluvial environment. Under such circumstances the apparent throw is the net separation of each topographic surface in the profile. The apparent throw adjusted for land surface and fault plane dip provides the true dip.

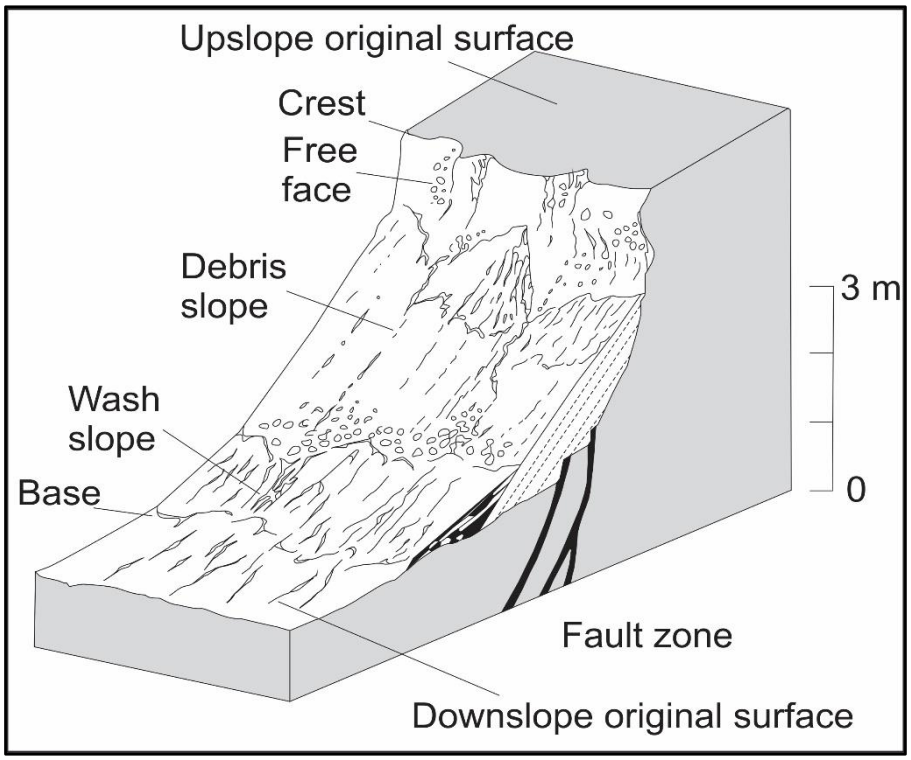

Figure 2.3: *Topographic elements of a diagrammatic single-rupture (normal) fault scarp. Modified from Wallace (1977).*

In contrast to rangefront normal fault zones, range-bounding thrust fault zones repeatedly form new mountain fronts each time a new fault splay propagates basinward into the footwall. Following uplift on a fault antecedent streams will downcut rapidly and small consequent streams will erode into the newly formed scarp. This builds a new suite of fan

deposits initiated from the new scarp. Newly formed fault scarps in alluvium will go through several stages of erosion resulting in sequential changes in profile appearance. The slope of the fault scarp, the convexity of the crest, and the concavity of the base will decrease over time as the scarp progresses through being fault, gravity, debris and then wash controlled. Taking into account this degradation sequence, the length and height of historic fault scarps can give an indication of earthquake size, although the true vertical displacement cannot be directly taken from scarp height. Scarp height can vary as a result of change in dip of the fault, migration of scarp base and crest. Surface extrapolation is often used to estimate for true vertical displacement, however, limitations for surface extrapolation include; reactivation of faults that change slope, block rotation altering pre-faulted surface slope angle and uplift along multiple faults. Accounting for these limitations it is possible to get an indication of rupture frequency and cumulative displacement by analysing the tectonic deformation expressed as scarp morphology.

Climate can vary both spatially and temporally and have substantial effects on landscape morphology. Climate variation within basins depends on prevailing weather conditions and differing climate conditions outside the bounding ranges, altering seasonally or through less frequent major regional shifts. Lithology has just as significant a control on fault scarp expression as climate. Differences in lithology cause variation in mass strength and resistance to erosion. Sandy piedmont gravels are a particularly difficult material in which to model scarp degradation due to its non-uniform, non-cohesive characteristics. Inclusions of clay and variation in the abundance of, and size of, boulders can vary cohesiveness spatially. This can affect the geometry of faulting through the material and patterns of fluvial erosion that produce the final scarp appearance.

The scarp crest sinuosity can also be a measure of erosion of a normal of strike-slip fault scarp. The more sinuous the fault scarp the more fluvial degradation has occurred indicating a longer time since rupture. Directly following rupture, the ratio of the sinuous scarp crest to the straight line scarp length is low, any increase from 1 indicates time since rupture during which erosion has increased. Reverse faulting often results in collapse of the fault scarp and formation of colluvial wedges which inhibits the use of the scarp crest sinuosity as a measure of erosion over time since rupture.

2.2.4 Alluvial Fans

Alluvial fans within an actively deforming landscape associated with a range-bounding fault show complex relationships. Uplift causes shifts in location of deposition resulting in fan surfaces overlapping, onlapping and downlapping when younger sediments overlie earlier deposits (Burbank and Anderson, 2012). Consequently fan surfaces become segmented and/or nested with sharp changes in slope.

Steady tectonic uplift and increase in water discharge results in entrenchment of upper fan, and a shift in deposition centre down fan (Burbank and Anderson, 2012) (Figure 2.4). Accelerating uplift causes deposition to focus at the head of a fan as there is creation of accommodation space that traps sediments from streams (Figure 2.4 A). This creates a relatively steep fan head and a sharp transition at the lower fan surface as the gradient lowers. Alternatively slow rates of uplift decreases the rate of accommodation space formation, causing streams to entrench the fan head and deposit sediment at the lower reaches of the fan Figure 2.4 B).

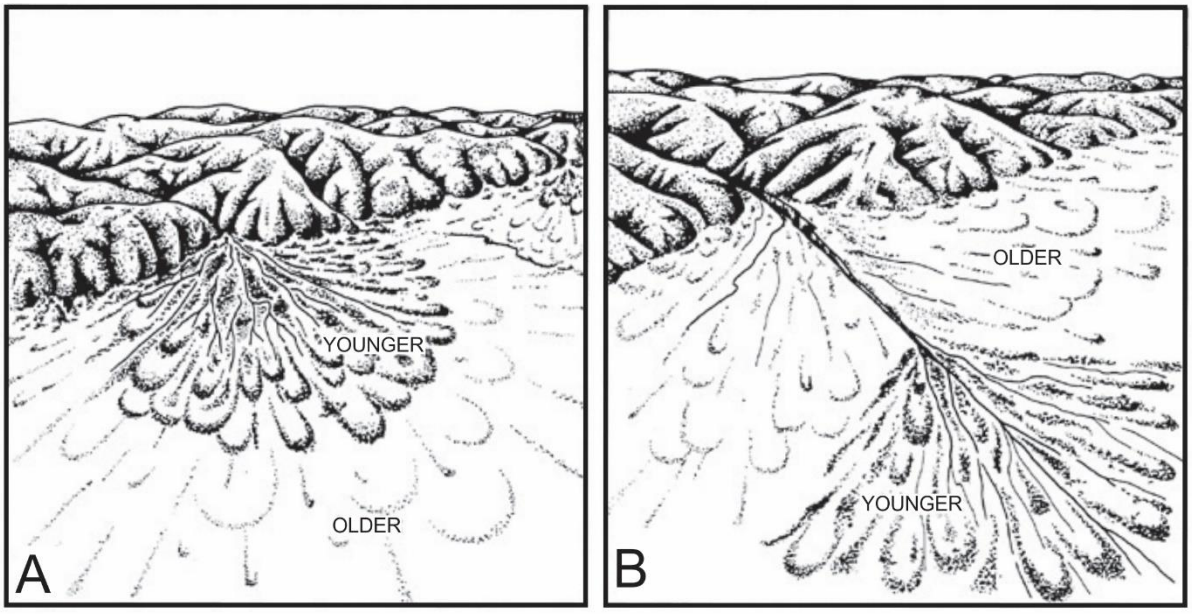

Figure 2.4: *A schematic example of alluvial fan morphology. A) Fan deposition directly adjacent to the mountain front. B) Fan head entrenchment has shifted the deposition downfan. Figure from Keller (1986).*

Dating of different fan surfaces can provide timing of shifts in deposition, possibly indicating timing of uplift events, although it can sometimes be difficult to distinguish between climatic and tectonic causation (Burbank and Anderson, 2012). However, within a basin or small study location it can be possible to assume similar climatic conditions. Therefore, if the

pattern and timing of fan segmentation is similar, it is likely a result of climatic variation in deposition. While a difference in fan segmentation patterns and timing of segmentation, with local coherence, can be attributed to tectonic control.

Tectonic uplift can also cause tilting of fan surfaces, resulting in elongation of the fan in direction of tilt. It is possible to quantify this tilt by measuring the major and minor axes on contour ellipses of fan deposits (Burbank and Anderson, 2012). The slope can be measured and an estimation of tilt (β) can be obtained, although tilt must be relatively rapid in order to have a discernible effect. Furthermore, time since tilt is important as active deposition anneals the fan restoring concentric un-tilted conical geometry. This method is best used for intervals post-dating the last major aggradational episode (late glacial or post glacial ~ 20 ka).

2.3 Project Methodology

2.3.1 Geomorphic and Structural Mapping

The majority of field mapping was undertaken on enlarged A3 sized vertical aerial photos with overlay at a scale of (1:1,000, 1:4,000 and 1:1,500). In general the basin investigation was divided into two sections; the southern valley and the northern valley (refer to Figure 1.7). The main reason for division is a notable change in fault expression and geomorphology, these differences will be discussed throughout this chapter. Caution was taken in only noting down features that were of tectonic origin and where appropriate tectonic geomorphic and fault zone features translated to the maps, such as fault scarps, were given appropriate symbols in regards to being definite, inferred or projected. A legend of the symbols used in the maps is provided in Figure 2.5. Field maps were all compiled and further analysis and comparisons were made with vertical aerial photographic imagery and Digital Elevation Models (DEMs) to produce final structural and geomorphic maps.

Vertical aerial photo imagery attained through a DigitalGlobe Foundation imagery grant was used during field mapping to help identify areas of interest for detailed mapping. Once field mapping was completed it also aided in comparison and identifying features not visible on the ground. Stitched overlapping aerial photo imagery obtained from Dr. A. Nicol (Department of Geological Sciences, University of Canterbury) were used to create a 5 m and 1 m DEM by Dr. C. Gomez (Department of Geography, University of Canterbury). Further analysis also enabled by the DEMs included contouring, height profiles and slope angle analysis.

The total mapped length of the Lees Valley fault within this study is approximately 25 km, similar to previous lengths reported for the fault (Garlick, 1992; Cowan, 1992; Pettinga, 2001). Geomorphic mapping was undertaken throughout the entire valley while structural and geomorphic mapping was focused along the eastern side of the valley due to the presence of the Lees Valley Fault Zone bounding the eastern ranges. There was also more of a focus in the northern valley section due to the more evident fault expression and analysis potential.

Once features were confirmed all of the evidence was compiled onto digitised maps. Maps of 1:20,000 and 1:40,000 scale were compiled for both the northern valley and the southern valley respectively (Figure 2.7 & 2.8) and then maps of 1:1,500, 1:2,500 and 1:6,000 scale were produced for areas with features of note. The observed features include:

Tectonic features:

1. Fault Discontinuity/Step-overs
2. Topographic flexure
3. Change in number of faults at surface
4. Old Fault traces (Inactive/ Less active)
5. Fault Transition (Apparent en-echelon)

Geomorphic features:

1. Tilted Block
2. Monocline
3. Faceted Spurs
4. Ridge steps
5. Fan deposit suites

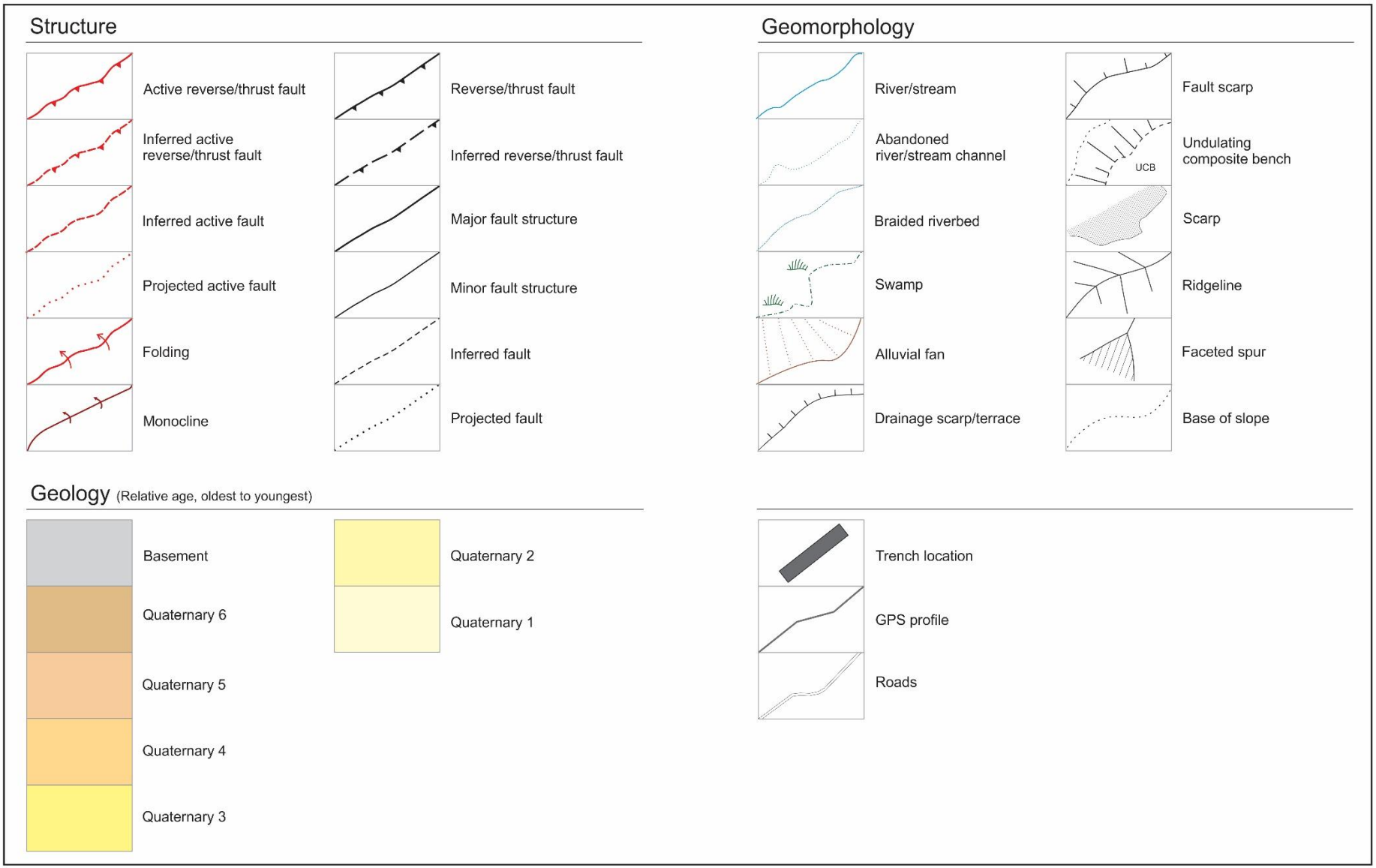

Figure 2.5: *Legend for structural and geomorphic maps (Figures 2.7, 2.8, 2.15, 2.16, 2.17, 2.20).*

2.3.2 GPS Surveying

Numerous survey lines were obtained in the northern valley, using a handheld GPS unit, to analyse profiles of the fault scarp and collect height data for associated locations (Figure 2.6). During surveying the dGPS was held at a consistent height around 1.4 m and points were collected at intervals of about 1 m. In some locations where there was ease of movement a 1 second interval was chosen, however, due to the change in pace from walking along flat fan surfaces and steep scarps using a time interval for sampling would have resulted in an unbalance of points along a survey. In some locations vegetation as well as steep topography significantly slowed the surveying. For this reason distance intervals of 1 m were chosen for most surveys to remain consistent and remove error of having several data points for one location. The surveys were run in lines perpendicular to the fault scarp in order to give the best representation of the fault scarp and its parameters such as height, width and total deformation. In total, 227 survey lines were conducted over the 7.6 km length of the northern valley scarp.

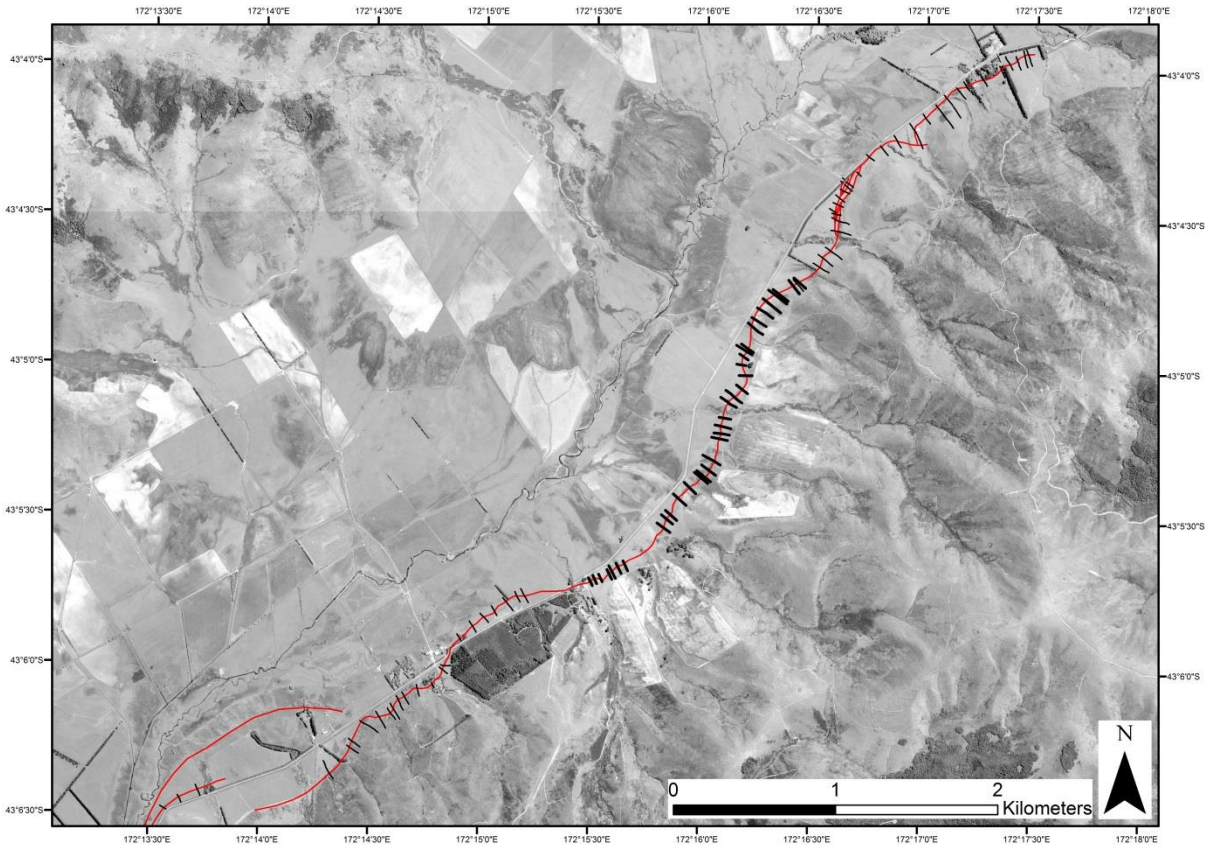

Figure 2.6: *Map showing location of selected GPS survey lines in the northern valley, 1 – 73 from north to south.*

Following surveying, data files were imported into ArcGIS and point profiles of each survey line were created and analysed for scarp parameters using methodology from Xiaodong et al. (2015). These included scarp height, scarp width, surface dip and projections of total vertical offset.

The width of deformation zone was very difficult to determine here due to the presence of significant topography directly behind (upslope) of much of the fault trace. Even in those locations with little significant topography upslope of the scarp it is still difficult to determine any back-tilting or folding deformation in the hanging wall, due to the ruptured ground surface being a fan deposit with initial depositional tilt and irregularities on the surface due to past fluvial channels.

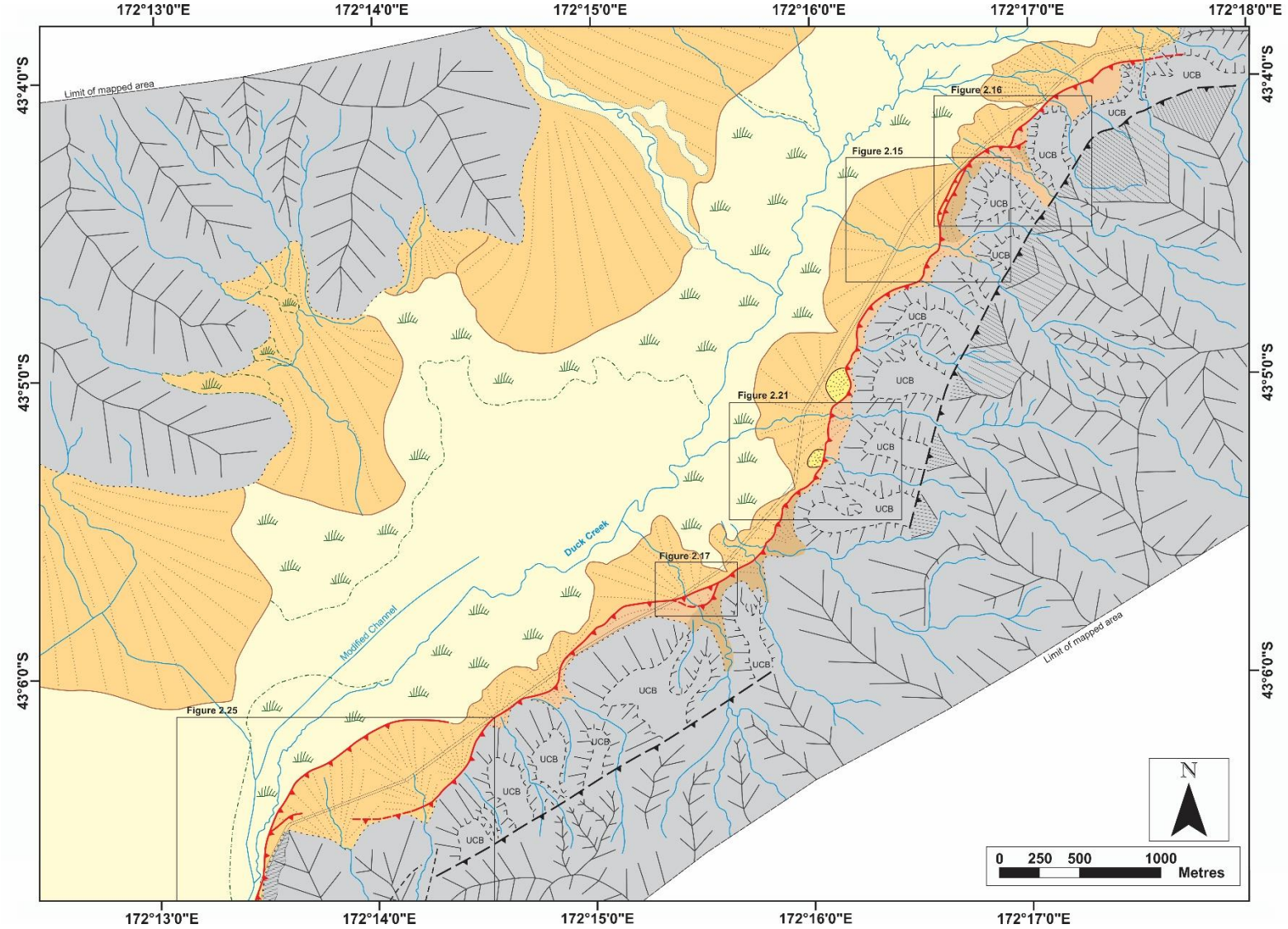

Figure 2.7 A): *Structural and geomorphic map of the tectonic, geomorphic and structural features in the Northern Valley. Boxes indicate location of detailed maps.*

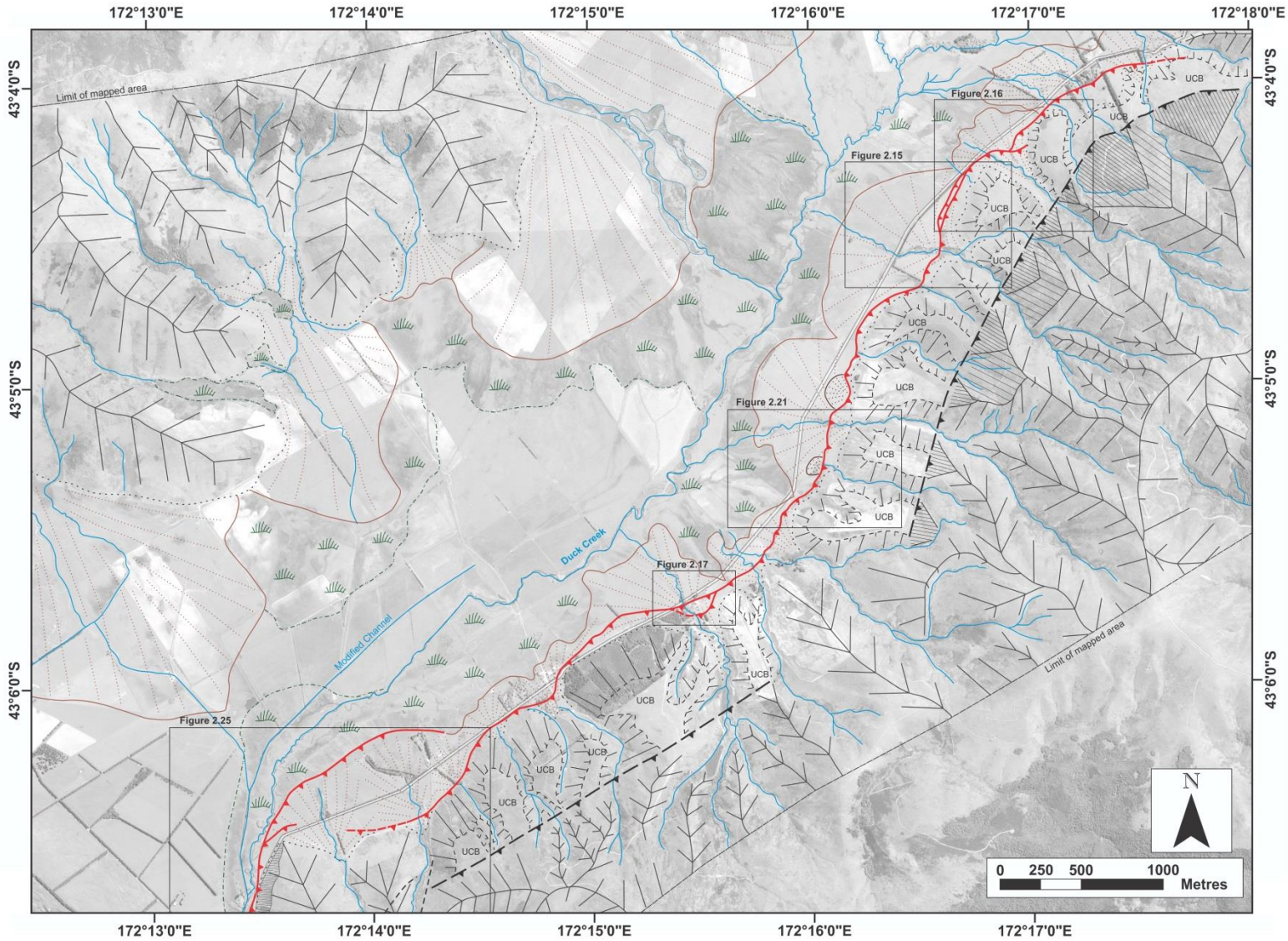

Figure 2.7 B): *Vertical aerial photo map of the tectonic, geomorphic and structural features in the Northern Valley. Boxes indicate location of detailed maps.*

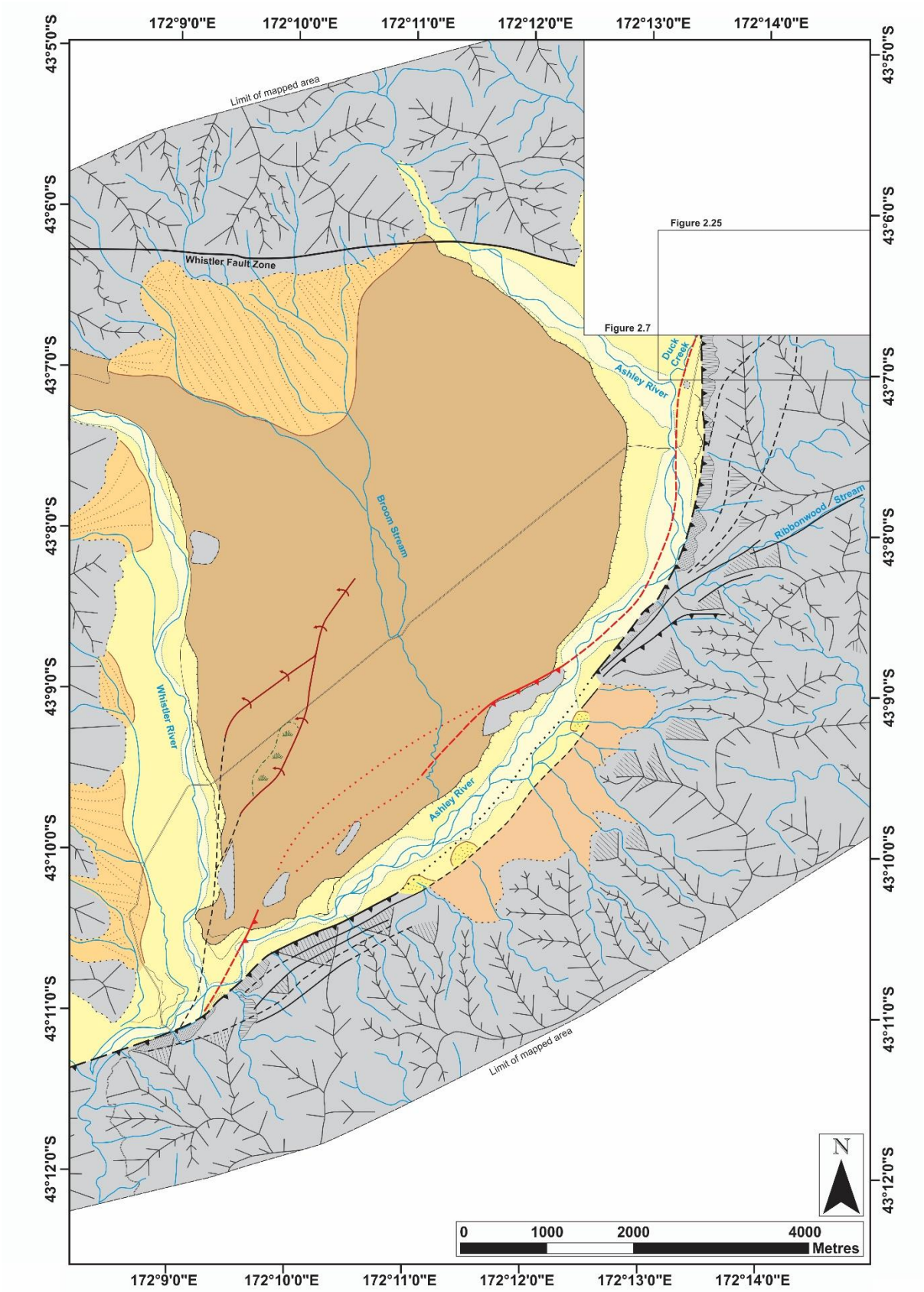

Figure 2.8 A: *Structural and geomorphic map of the tectonic, geomorphic and structural features in the Southern Valley. Boxes indicate location of detailed maps. Incorporating Cowan (1992a) and Barrell and Begg (2013).*

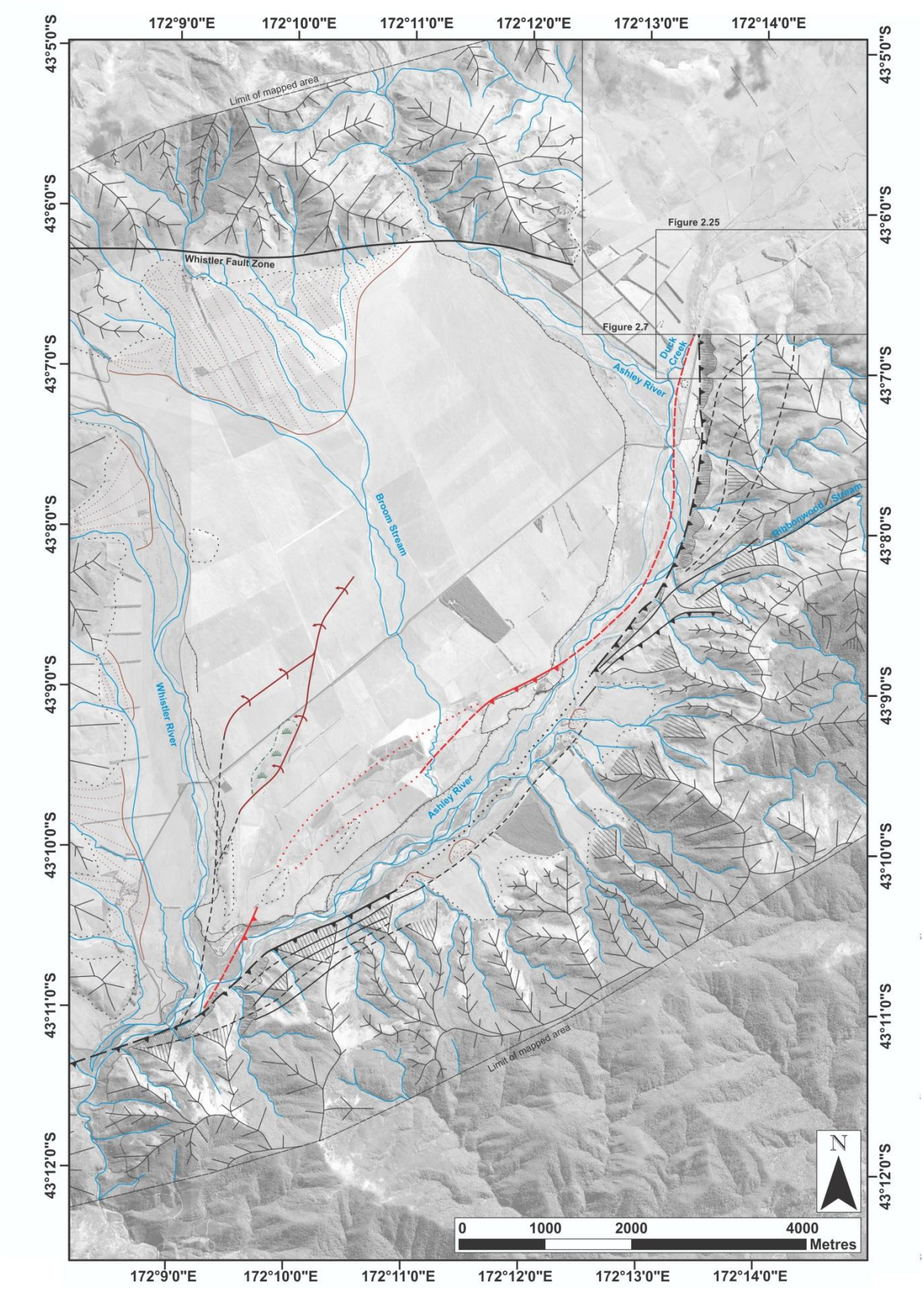

Figure 2.8 B: *Vertical aerial photo map of the tectonic, geomorphic and structural features in the Northern Valley. Boxes indicate location of detailed maps. Incorporating Cowan (1992a) and Barrell and Begg (2013).*

2.4 Findings

2.4.1 Basin and Rangefront Geomorphology

Analysis of basin floor and rangefront structural, geomorphic and topographic detail and the active surface processes provides understanding of the tectonic geomorphic evolution along the faulted eastern rangefront of the Lees Valley. The northern valley is approximately 8.5 km long and 2.5 km wide while the southern valley is larger in areal extent, with a length of approximately 10.5 km long and a width of 7 km at its widest point.

No Quaternary valley glaciers have been recorded to have reached into the Lees Valley basin although there has been glacier activity documented in the nearby Puketeraki Ranges, located approximately 9.5 km east of the head of the Whistler River in the Lees Valley (Rother, 2006). Consequently no glacial ice flow related geomorphic features are present in the valley.

There are three main river systems draining into the valley; the Ashley River, the Whistler River in the southern basin and Duck Creek in the northern basin (Figure 2.7 & 2.8). In addition, smaller minor fluvial features include Broom Stream in the southern valley and Pancake Stream present in the northern valley (Figure 2.7 & 2.8). Okuku River lies just north of the upper reaches of the basin. Ashley, Whistler and Okuku Rivers predominantly flow east with some diversions to the south or southwest in the basin (and ranges for Okuku River). Duck Creek, however, flows southwest along its entire length into the southern basin.

Climate influences the rate of fluvial erosion and the degradation (or aggradation) of geomorphic features. Today, Lees Valley has a moderate to cool climate, receiving an average of 1023 mm of rain annually based on readings from the Wharfedale weather station within the valley from 1951 – 2000 (CliFlo, NIWA). Although due to the limitation of only one reading station it does not pick up the slight variations within the valley. The precipitation mostly comes from the SW; the prevailing wind direction, which funnels though the ranges. Lees Valley has a moderate climate with typical temperature ranges of -6˚ to 33ºC, however, has received extreme frosts down to -11ºC (Bartram, 1958). Under these conditions it is expected the exposed bedrock will weather at a moderate to slow rate.

The dominant processes forming geomorphic features in the basin are tectonic uplift along the eastern range-bounding fault and fluvial erosion through the extensive drainage systems. The main geomorphic features in the valley are; i) extensive fan deposits, ii) fluvial plains, and iii) active braided river channels.

Northern Valley Section

The northern valley floor tilts significantly to the southwest causing a variation in elevation from 500 m in the north to 460 m to the south. Consequently all the streams from the ranges drain into the basin floor join Duck Creek, and then flow southwest into the southern basin (Figure 2.7). Interaction of the fan deposits and numerous streams from opposing ranges has impeded drainage, and led to development of extensive swamp development on the northern valley floor, with the fan apexes forming the irregular ground surface, resulting locally in higher dry areas. Furthermore, farm development modification of the ground surface and drainage systems has created a dry section in the centre of the northern valley which extends to the southern valley.

Extensive fan deposits have formed extending from each mountain rangefront, the fans build out and interact on the basin floor which is dominated by swampland (Figure 2.7). The fans on the western rangefront are few in number, large and extend significantly out onto the basin floor, in contrast the fans on the eastern rangefront are numerous, smaller, with their extent into the basin more limited and nested within each other in a suite of fan deposits. This is the result of the range-bounding fault on the eastern rangefront repeatedly uplifting the fan deposits leading to incision. Uplift of the hanging wall focuses deposition near the head of fan deposits on the footwall and results in fans that do not extend very far (Section 2.2.4). Formation of a new rangefront at the fault scarp shifts fan deposition centres and also creates new smaller fans. The older rangefront becomes abandoned as it is uplifted into ranges (Figure 2.9)

The active range-bounding fault zone also controls other geomorphic features observed in the northern valley which will be discussed individually further in the chapter these include; the mountain–piedmont junction sinuosity (Section 2.4.3), ridge steps and faceted spurs (Section 2.4.4).

Figure 2.9: *Photo view of the eastern rangefront in the northern valley displaying the active fault (red dashed line) of the current rangefront and the uplifted and abandoned earlier rangefront indicated by a fault trace (Dashed white line), faceted spur and uplifted fan deposits. Grid reference: 245209 579278.*

Southern Valley Section

The basin floor has a slight tilt to the southeast ranging in elevation from 500 m a.s.l. in the west to 405 m a.s.l. in the east as the larger fans build out from the west ranges into the basin. The floor also tilts to the southwest, like the northern valley, with elevations around 462 m a.s.l. at the northern end and 354 m a.s.l. at its southern end. The drainage system in the southern valley is more developed and drains to the eastern side of the valley (Figure 2.8). The Ashley River, Whistler River and Broom Stream all flow out of the west ranges and drain towards the eastern ranges. Tectonic uplift of the eastern ranges has diverted the drainage systems to the southwest where they coalesce with the Ashley River and exit the valley through Ashley Gorge. This results in erosion and over-steepening of the eastern rangefront slopes in the southern valley and obscuring zone.

Large overlapping alluvial fans have formed extending from the western ranges in the southern valley, with low rangefront uplift rates causing deposition in the more distal extremities of the fans (Section 2.2.4). No fans have been preserved along the eastern

rangefront due to the Ashley River actively eroding the base of the range. This has resulted in a predominance of a large fluvial terrace in the centre of the southern valley which has been incised by the active, braided drainage channels of the Ashley and Whistler rivers. There are some scattered localized swamp areas on the basin floor and ephemeral streams continue to build off the western ranges onto the terrace, joining into Broom Stream which flows into the Ashley River.

Other geomorphic features observed in the southern valley are attributed to tectonic uplift, including the mountain–piedmont junction, block-tilting and an uplifted terrace. These are further discussed in following sections (2.4.3 and 2.4.6).

2.4.2 Fault Zone Structure

Analysis of structural features helps to provide understanding on the development of the eastern rangefront thrust fault zone and consequent influence on the evolution of the valley. The main Lees Valley Fault extends along the foothills of the eastern rangefront, along with associated structural features such as, block tilting and coincident steps in adjacent ranges. Analysis of surface deformation through field mapping, surface geomorphic measurements and GPS profiling has provided information on factors such as fault dip, sense of motion and the cause of deformation with respect to surface expression.

Previous work has indicated the orientation of the fault as a NE-SW trending reverse fault and its location within the northern Canterbury rangefront (Cowan, 1992; Garlick, 1992; Pettinga 2001; Barrell & Begg 2013). As discussed in Chapter 1, the prevailing stress field within the PPAFZ has resulted in a hybrid fault zone with a pre-dominance of thrust/reverse faults and associated strike-slip. Estimated dips for the Lees Valley Fault span a range of 15-50º (Cowan, 1992) and 30-80º (Pettinga, 2001). There has also been some speculation of an element of strike-slip motion at depth along the Lees Valley Fault (Garlick, 1992; Pettinga et al, 2001).

The total Lees Valley Fault length is approximately 25 km, the fault expression varies along the valley as does the associated deformation (Figure 2.7 & 2.8). The main cause of variation in the surface expression of the deformation is effects of fluvial erosion and deposition, as the orientation of the drainage systems is parallel to the fault. The depositional tilt of the southern valley floor has caused the migration of the Ashley River to its current location directly above the fault where it has eroded away and obscured the fault trace. The fault expression

varies between the northern and southern valleys hence will be discussed individually in the "southern valley" and "northern valley" sections.

The Lees Valley Fault varies in apparent strike with an average strike of 048º in the northern valley and an average of 035º in the southern valley, with smaller variation in strike occurring throughout these sections. Variation in strike affects the zone of deformation associated with the Lees Valley Fault, where it may result in formation of fault splays and a wider distribution of folding, causing an increase in the fault deformation width. Deformation observed at the surface correlates directly to the complexity of faulting beneath as it extends to the surface and can often result from subtle differences in subsurface bedrock characteristics (Burbank and Anderson, 2012). For instance bedrock heterogeneity in density, joint spacing or depth below the surface can cause changes in fault dip and fault splays, altering the zone of deformation.

At its southern end the Lees Valley Fault connects into the Townshend Fault Zone (refer to Figure 1.7), and at its northern end, near Okuku, the fault scarp fades out and could either terminate here, or may project/step-over and link to other splays. This fault discontinuity will be discussed in the following sections along with other structural features.

Northern Valley Section

The fault trace is definite through the entire northern valley section measuring about 7.6 km long (Figure 2.7). It has offset the numerous fan deposits along the eastern rangefront and along the majority of its length displays a prominent, 1.5 – 11.5 m, fault scarp. The definite expression of the fault is due to the direction of the drainage systems here at approximately right angles to the fault zone.

The section of fault trending through the northern valley has a strike range of 020º – 065º. Apparent strike changes can in part be attributed to topographic variations as the Lees Valley Fault traces across a series of alluvial fans. It is also further enhanced by the rivers and streams that cross cut and degrade sections of the fault scarp.

There are no bedrock outcrops that show a clear exposure of the fault zone, although river cuts in Willow Creek and some smaller channels alongside, show zones of highly fractured bedrock that are the inferred result of displacement and strain associated with the nearby fault zone.

Features of note in the northern valley are the northern fault termination, the anastomosing and splayed fault sections, and the complex fault transition point between the northern valley and the southern valley.

Southern Valley Section

There are two main fault traces, inferred and projected through the majority of the southern valley. The main fault extends approximately 17.2 km along the entire length of the southern valley eastern rangefront, while the most western footwall thrust of the fault zone extends from the fault transition zone between the northern and southern valley into the basin floor (Figure 2.8). The footwall thrust varies in trend from the valley transition zone into the southern valley, approximating the shape of the rangefront. It may terminate near the centre of the southern valley fluvial plain or trace through and connect with the range-bounding fault at its southern end (Figure 2.8). The fault zone defining the eastern rangefront is locally exposed as outcrop exposures (refer to Figure 2.25) in the Ashley River, where it has thrust the Rakaia Terrane above Tertiary marine sediments. However, generally faulting can only be inferred where the Ashley River has removed evidence of any fault traces and alluvium covers bedrock. River flood deposits along the centre section of the southern valley eastern rage front have obscured any fault expression, consequently faulting can only be projected through here (Figure 2.8).

The base of the eastern rangefront in the southern valley and its associated fault bends and forms an arc shape, resulting in the bounding fault strike varying between 000º – 055º. Error is associated with these measurements as there is ambiguity in the exact position and orientation of the fault within this section, due to in its inferred and projected nature.

The position of the shorter most westward trace is mostly projected due to its location in the river bed however, evidence for its presence is the tilted block located in the valley floor (Figure 2.10). The trace is then projected southward beneath the central fluvial plains of the southern valley where it appears to have uplifted a section of the terrace (Figure 2.8). Due to the orientation of this uplifted section of terrace it could be mistaken for another terrace riser formed by the Ashley River. However, there are no other terrace risers at this height on the fluvial plain and it is a small raised section more likely present due to the hard resistant bedrock just beneath the surface, raised by tectonic uplift associated with fault rupture. While conjecture only, it is also possible it continues beneath the alluvial plain joining to a splinter fault at the southern end of the valley (refer to Section 2.4.6).

Figure 2.10: *Photo view looking north, of the tilted block in the northern section of the southern valley where Duck Creek from the northern valley joins to the Ashley River. The outline of the tilted block is indicated (white) with the direction of tilt (arrow) and the position of the westward active fault trace (red). Grid Reference: 2446 5786*

Complicating the structure in the southern valley is a splay off the main rangefront fault which splays to the northeast up Ribbonwood Stream (Figure 2.8) (refer to Section 2.4.6). Other features of note in the southern valley include splinter splays and monoclines, separate features from the rangefront fault zone which splay into the footwall. They are observed along the valley floor and trend north and north-east respectively (Figure 2.8) (refer to Section 2.4.6).

2.4.3 Mountain Front Sinuosity

Analysis of sinuosity using the mountain-piedmont junction as described by Bull (2007) can provide an indication on relative uplift rate. Episodic displacement along a range-bounding fault will result in a steep, straight mountain-piedmont junction with less embayments and induced stream downcutting. Using the 5 m DEM alongside vertical aerial photographic imagery the sinuosity of both the eastern and western rangefronts of the northern and southern valleys was analysed. Segments were chosen for the mountain-piedmont junction analysis based on the extent of the northern and southern valleys individually and then

combined, resulting in 3 sinuosity values for both the eastern and western ranges (Figure 2.11). The results are summarised in Table 2.3.

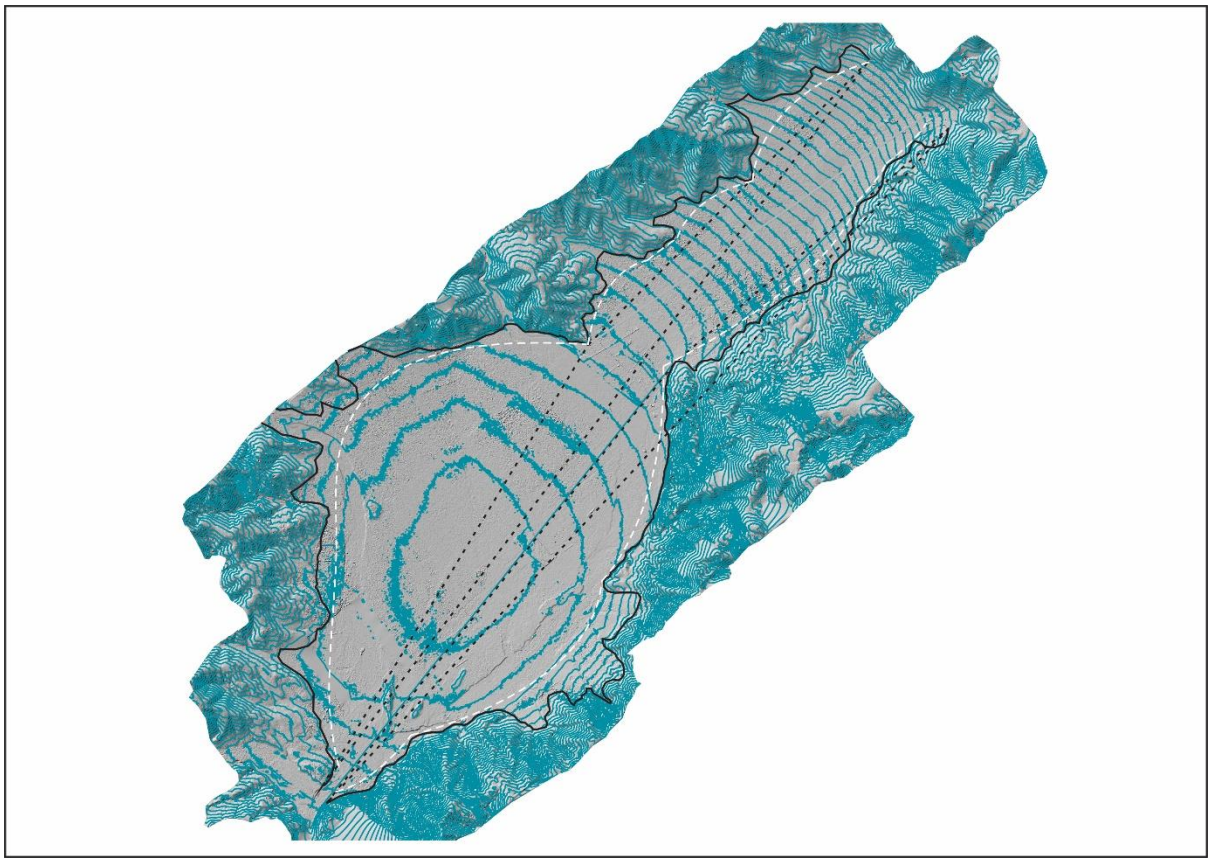

Figure 2.11: *A 5 m DEM of the Lees Valley with contour intervals at 20 m. Solid black lines represent planimetric length (Lj) and the dashed black lines represent straight line length of the mountain front segment (Ls). Dashed white lines represent where the range-bounding geologic structure is/would be for this reverse fault controlled basin.*

Results

Table 2.3: *Mountain front sinuosity for various sections in Lees Valley.*

Valley Section	Valley Side	Lj	Ls	J
Northern Valley	East	8,431.49	7,100.04	1.19
	West	13,155.48	7,879.52	1.67
Southern Valley	East	16,456.74	11,111.14	1.48
	West	21,069.95	10,175.10	2.07
Whole Valley	East	24,888.22	18,131.64	1.37
	West	34,225.43	17,967.53	1.90

The eastern range shows a sinuosity value closer to 1 and lower than that of the western range. This fits with the expectations and models as the range-bounding fault is located at the

base of the eastern range, actively uplifting and maintaining the straightened nature of the range-piedmont junction. This is evident in the values of 1.19 for the northern valley, 1.48 for the southern valley and a combined value of 1.37 along the eastern ranges. Placing the eastern rangefront in the highly active mountain front class of 1 – 1.5 (Bull, 2007).

Discussion

According to the model developed by Bull (2007), the lower the activity of a rangefront the more sinuous the piedmont junction due to the widening of the valley floor, and degradation which lowers the ridge crest and rangefront relief. The western rangefront shows higher sinuosity values than the eastern rangefront which is expected due to its lack of active rangefront faulting. In the western rangefront fluvial processes have dominated to the point where the Ashley and Whistler Rivers cut down to base level. These rivers and numerous streams along the rangefront have built large fan heads forming large embayments, altering the rangefront significantly over time. This has occurred on a larger scale in the southern valley than the northern valley. In contrast the eastern rangefront has numerous small streams due to episodic uplifts which alters stream paths, forms new ones and resets the rangefront for continual stream incision and modification. The sinuosity indices for the west range are 1.67 and 2.07 for the northern and southern valley respectively and 1.90 for the entire rangefront. This places it in the moderately active mountain front class (Bull, 2007).

The northern and southern valley display different sinuosity values of 1.19 and 1.48 respectively for the eastern range. It is possible the southern valley displays a higher sinuosity than the northern valley due to the range-bounding fault of the southern valley being inactive/less active and the active most westward trace of the southern valley more recently accommodating strain within the fault system (Figure 2.8). Over time the range-bounding fault may have become more sinuous due to its lack of uplift. However, erosion from the Ashley River has had significant effect on the rangefront junction expression, making it too difficult to attribute its expression purely to a shift in strain accommodation. It is possible a new thrust splay has formed in the footwall of the northern valley eastern rangefront and is starting to create a similar relationship of strain transfer here. However, no evidence was found for a more recent thrust in the footwall. This could be due to the nature of the interacting and overlapping fan deposits on the valley floor obscuring any evidence, the new thrust could be a blind thrust which has not yet reached the surface, or because no new thrust has yet formed.

Despite not being controlled by a range-bounding fault, the western range is classified as a 'moderately active' mountain-front, explanations for this mostly result from limitations of Bull's (2007) model. This model was developed based on features in the western USA, which leads to five main limitations when comparing to study areas such as the Lees Valley in New Zealand. These are: 1) The arid climate conditions of western USA versus the temperate climate of New Zealand, which results in higher rates of erosion (aggradation and degradation). 2) The difference in glacial-interglacial activity. In New Zealand glaciation cycles ranged from 100's-1000's years dominated by gravel cycles, aggrading and degrading. Higher erosion during the glacial period caused fans to build up relatively fast, developing back into drainage channels and significantly altering the mountain front junction. Therefore sinuosity reflects climate rather than fault uplift activity. 3) The dominance of normal faulting in the extensional setting in western USA while this study applies the model to a compressive setting resulting in thrust/reverse faulting. 4) Difference in bedrock materials of the two regions which could result in variation of fault and rangefront expression. 5) Difference in uplift rate, New Zealand has a relatively faster uplift rate of its mountain ranges due to its location within an active plate boundary collision zone, resulting in faster uplift and erosion cycles. This may account for the western range being classified as 'moderately active' although it is assumed to be in a mostly inactive state. It is also possible that tectonic features noted on the western front could be the cause for the more active classification than expected. A fault trace at the base of the Kingsdown Hills which continues east of the Whistler Fault Zone which may account for some uplift and lessening of the sinuosity in that section. It is likely that a combination of these factors has led to lower sinuosity values than expected.

These limitations highlight the importance of locality and tectonic regime when applying the mountain front sinuosity index. The index calculation involved including the straight-line length of the mountain front segment (Ls). However, the range-bounding fault structure in this basin in not straight but curves in an arc. Therefore, in order to represent the actual length of the range-bounding geologic structure 'Ls' should be calculated using a curved geometric line (indicated by the dashed white line in Figure 2.11 rather than a straight one. If this line was used for calculation instead, the sinuosity would be even lower than the current values. Using the index classification by Bull (2007) this would indicate a higher uplift rate even in sections of the valley where no range-bounding fault is present, such high activity classes would be incorrect. Therefore, it can be concluded that in this study area the sinuosity index is sensitive to fan development which has been significantly controlled by climate, rather than

fault uplift which Bull's model uses sinuosity to describe. Therefore sinuosity is not sufficiently sensitive to describe fault activity accurately in Lees Valley. This highlights the limited use of the sinuosity index for analysing reverse/thrust fault controlled basins in New Zealand, under this regime.

2.4.4 Faceted Spurs

Results

Faceted spurs are present along the entire eastern rangefront (Figures 2.8 and 2.9). Uplift has created steep, large facets that run along a semi-straight rangefront. There are numerous facets that display various stages of dissection and are nested, younger facets within older ones (Figure 2.12). Small piedmont fans build out from the base of these facets. Based on Bull's (2007) model for triangular facet dissection stages (Table 2.1) the rangefront section in Figure 2.12 shows Stages 1-3.

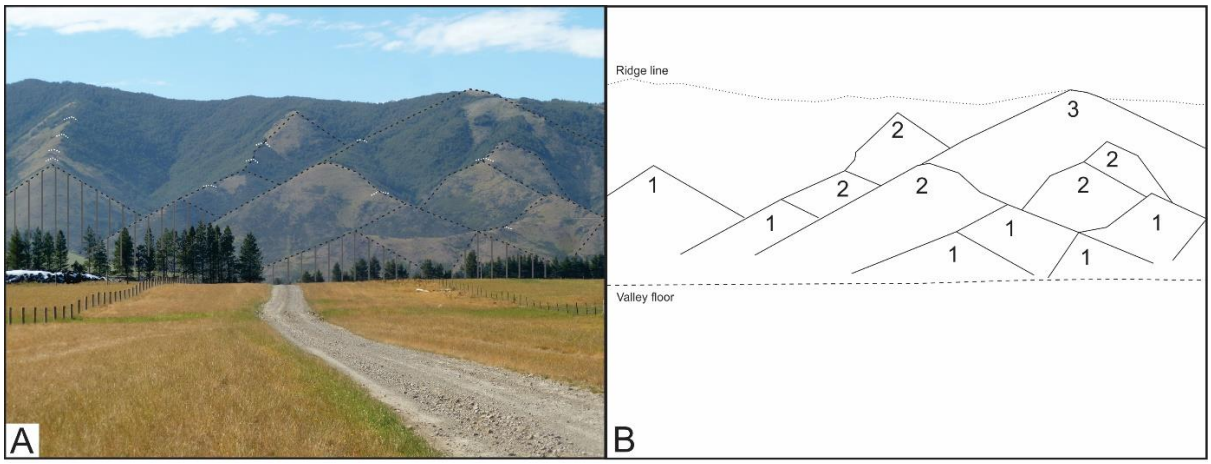

Figure 2.12*: Nested facets in eastern rangefront in the southern valley. A) Photo facing east displaying the faceted spurs and ridge steps of the thrust faulted eastern range. Grid reference: 2442 5783 B) Outline of faceted spurs with class of dissection indicated as described in Table 2.1. The younger facets nest within the older higher facets with more stream incision and erosion.*

Discussion

The dissection within each class of facets forms as a result of the relationship between uplift and erosion. Over time, facets become higher and more dissected, moving from Class 1 to Class 7. The low class rating of facets present along the eastern ranges indicates rapid uplift and moderate fluvial erosion, representing the tectonically active nature of the rangefront fault zone.

Faulting within the eastern ranges is complex, with numerous fault traces accommodating various rates of uplift. As new footwall splays break through forming the new rangefront, uplift of earlier fault traces and old rangefronts occur (refer to Section 4.1), these can become preserved within the ranges as uplifted faceted spurs and ridge steps. Old remnants of uplifted piedmont surfaces located adjacent to uplifted fault facets are recognized as low-relief benches ("UCB" in Figure 2.7). This complex nature of faulting is observed in the apparent separated facets higher in the ranges (Figure 2.12 A), the ridge steps noted above and between the facets (Figure 2.12 A and Figure 2.13) and the nested nature of the facets (Figure 2.12 B). The array of facet stages observed in the rangefront is an indication of renewed fault uplift. Recent uplift forms Stage 1 facets at the new rangefront fault trace, and ongoing uplift activity upslope heightens earlier facets and increases their dissection stage.

The western ranges have less steep slopes with smoother more degraded spurs than the eastern range (Figure 2.13). Facets are either small or not present at the range base. Fans building out from the range have a low gradient and are entrenched at the fan head. This is a result of less uplift, therefore no rapid base level change or formation of steep facets. The topography has lessened as erosion has lowered the ridge crests and built larger fans. The diverse nature between the ranges highlights the fault control on the eastern ranges.

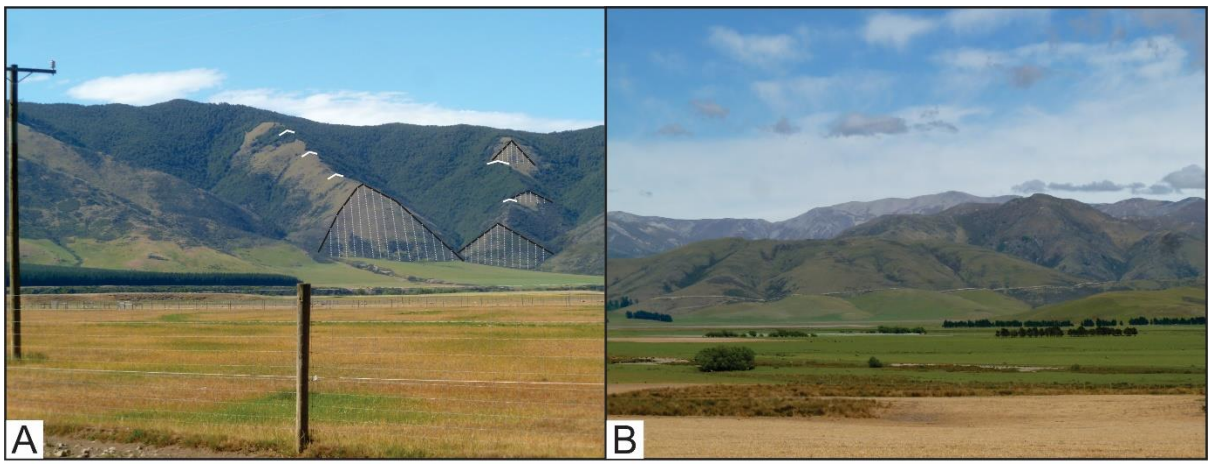

Figure 2.13: *Comparison of spur development. A) Photo view, looking south, of the eastern ranges in the southern valley. Grid reference: 2443 5784. Note numerous annotated faceted uplifted spurs within the range, and large, steep facets. B) Photo view, looking southwest, of the western range in northern valley. Grid reference: 2450 5791. Note the more subdued topography, more degraded spurs and low gradient fans.*

Using the classes of relative tectonic activity after Bull (2007) (Table 2.2), the Lees Valley falls within category Class 2 – rapid, defined by "$\Delta u/\Delta t < \Delta cd/\Delta t > \Delta pa/\Delta t$" where the alluvial fans have become slightly entrenched and the ranges display v-shaped valleys. Increasing

relief of the mountains, narrow river valley floors and triangular facets of Class 1 – 3 would suggest a Class 1 landscape, however, the entrenched fan deposits and slightly sinuous piedmont junction suggest Class 2. While sinuosity is heavily influenced by climate and not a reliable indicator of tectonic activity, what can be concluded is that the rangefront displays an active class of landscape either Class 1 or 2.

2.4.5 Fault Discontinuity

North of Okuku Hills homestead the Lees Valley Fault scarp height decreases and the fault trace terminates (Figure 2.7). Further north the fault position has been projected as approximate by Forsyth et al. (2008) and definite by Barrell and Begg (2013). The projected fault zone is shown as continuing for ~ 7 km with the same northeast strike, forming a range-bounding structure to the eastern side of a smaller basin. Analysis of vertical aerial photo imagery and topographic maps indicate there may be a trace above the main Lees Valley Fault that accommodates some of the deformation along this section (Figure 2.14). The ground surface undulates significantly making it difficult to pick out fault related geomorphic features, however, there is a change in slope that may be the result of overlapping deposits or an underlying structure (Figure 2.14).

Figure 2.14: *Photo view, facing southwest, of the hanging wall above the projected Lees Valley Fault Zone at its northern end. Bold dashed line is the now less active earlier range-bounding fault. Dotted black lines the potential trace accommodating offset/deformation at the transition into the basin north of Lees Valley. Grid reference: 2452 5793.*

2.4.6 Fault Splays

Thrust fault zones generally form imbricate splays as they propagate to the ground surface (McCalpin, 2009), while laterally they typically form an array of unconnected or anastomosing faults (McCalpin, 2009; Burbank & Anderson, 2012). When co-seismically ruptured, surface deformation is typically complex and not only impacted by the heterogeneity of the ruptured material but also through displacement transfer on the numerous splays which act to accommodate slip deformation. Furthermore their low angle of intersection at the ground surface can result in topographic effects on expression and highly sinuous traces. There are five locations where the Lees Valley Fault splays: i) Willow Creek (Figure 2.15), ii) Stock Pen splay (Figure 2.16), iii) Dalzell Splay (Figure 2.17), iv) Ribbonwood Stream splay; and v) the splinter faults of the southern valley (Figure 2.8). On a larger regional scale thrust/reverse faults often form long arcuate belts with a wedge shaped imbricate series of thrusts in the footwall block.

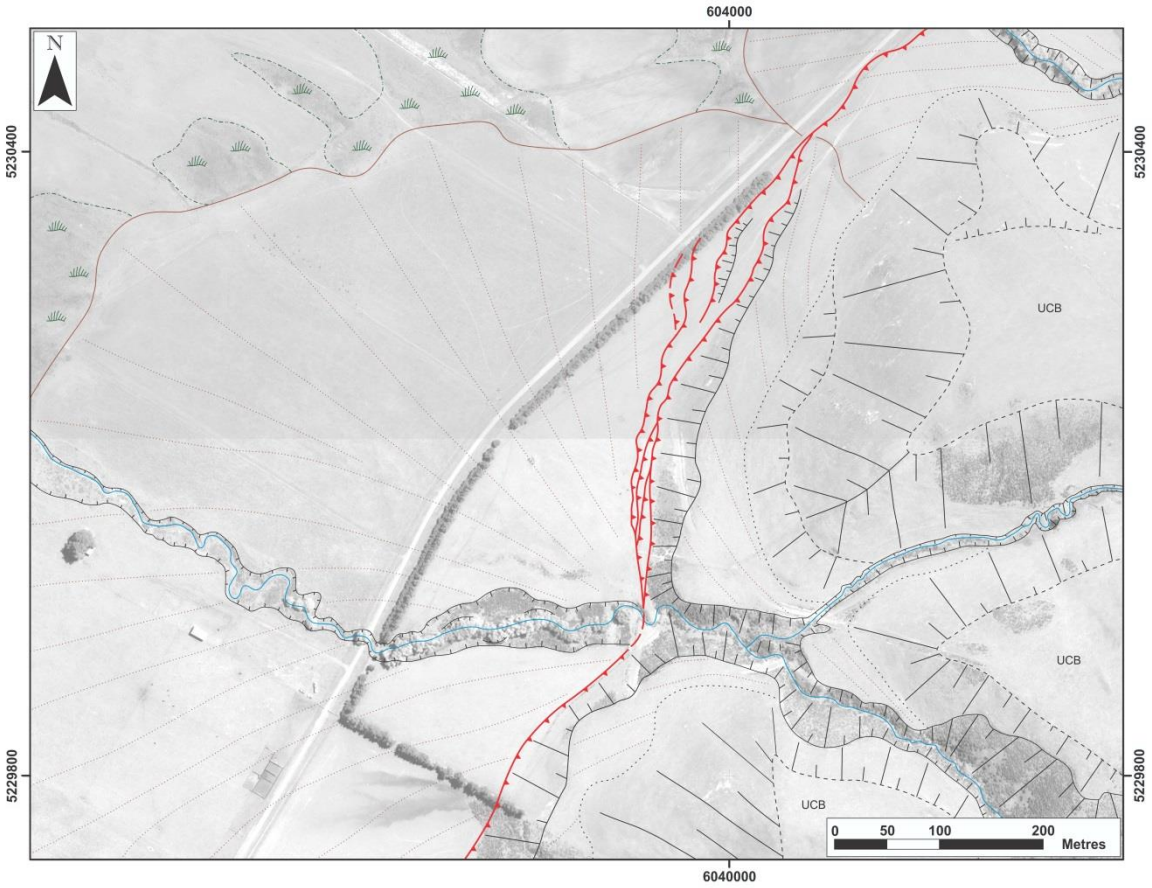

Figure 2.15 A: *Willow Creek structural and tectonic geomorphic map.*

Figure 2.15 B: *Photo View of the Willow Creek fault splays, looking north. Grid reference: 245107 579225.*

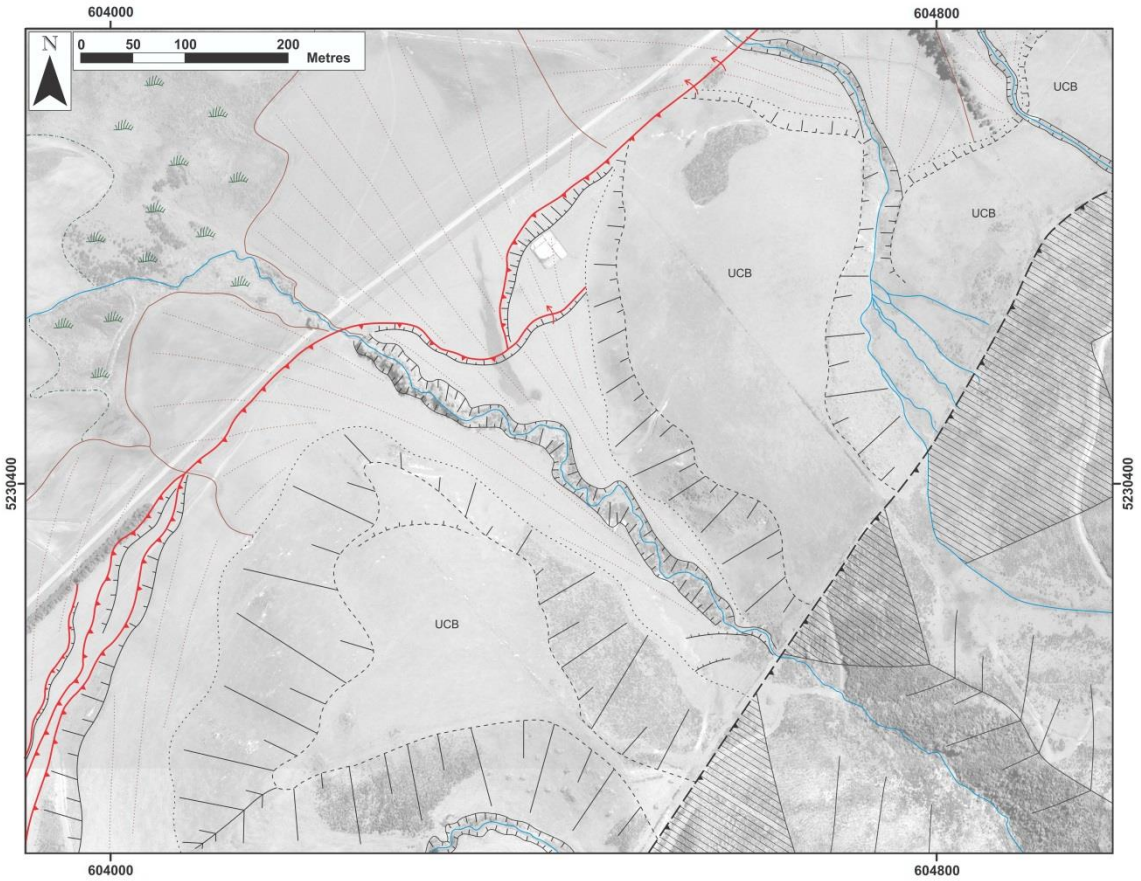

Figure 2.16 A: *Stock Pen splay structural and tectonic geomorphic map.*

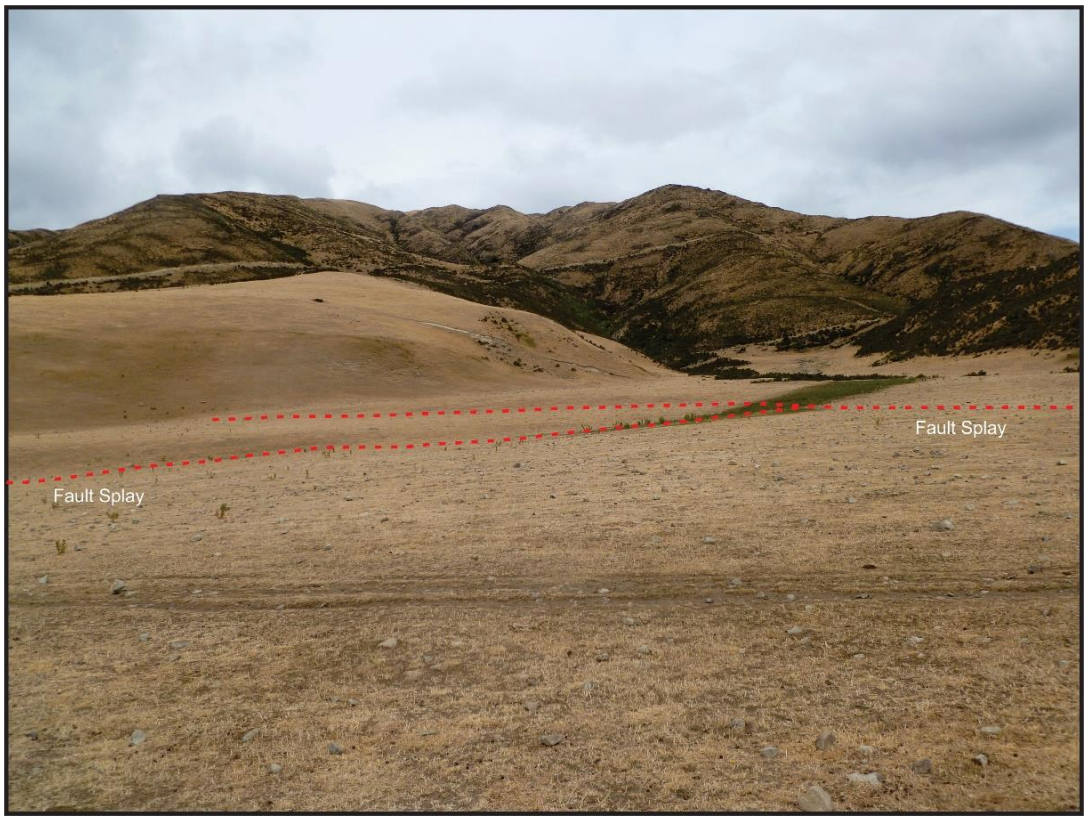

Figure 2.16 B: *Photo view of the Stock Pen splay, looking southeast. Grid reference: 245152 579272.*

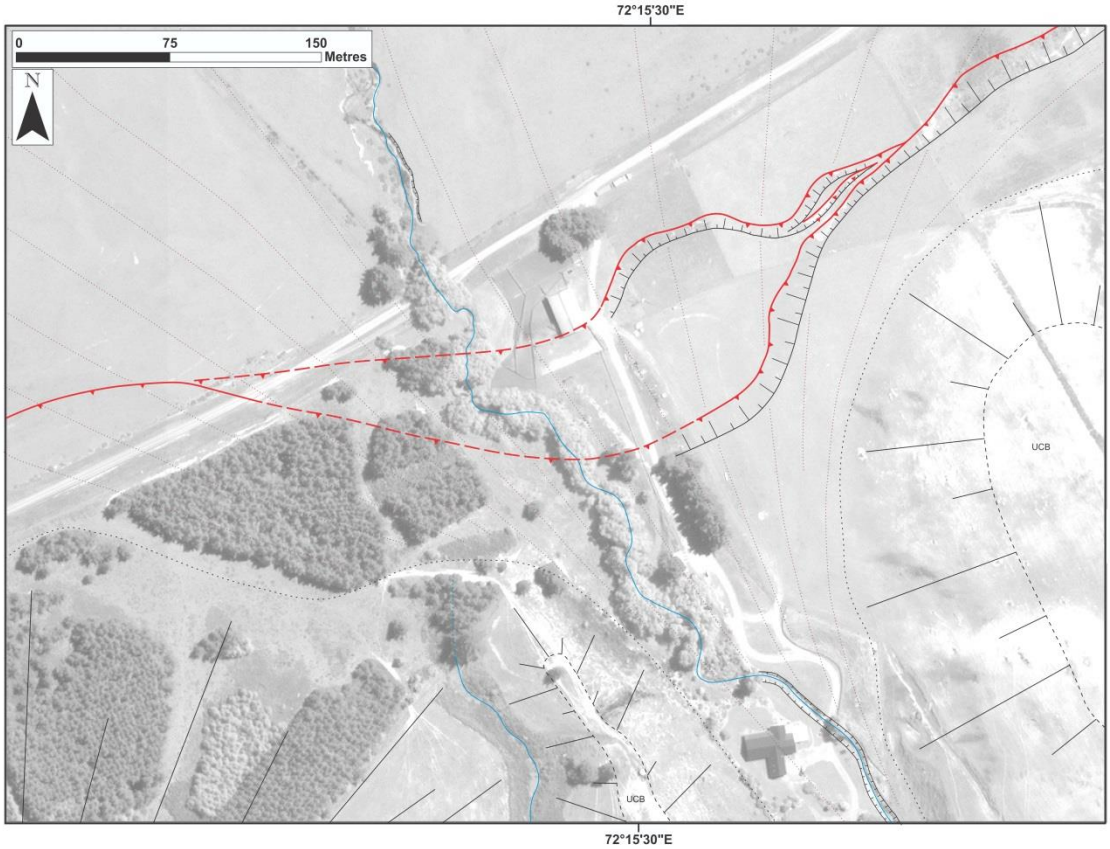

Figure 2.17 A: *Dalzell splay structural and tectonic geomorphic map.*

Figure 2.17 B: *Photo view of the Dalzell splay, looking southeast. Grid reference: 245000 579015.*

Willow Creek has numerous faults expressed at the surface in a complex anastomosing pattern (Figure 2.15). Each splay has accommodated a variable component of slip resulting in scarps of differing heights that decrease basinward of the main trace (refer to Figure 2.24 B and C). The main range-bounding fault at this location has produced the highest scarp (11.5 m) along the surface fault trace and the topographic slope directly upslope of the fault scarp traces is steep (~30˚). The variation in fault splay expression may be attributable to topographic loading of the hanging wall of each imbricate splay, propagating further footwall splays at the toe of the slope, as each splay accumulates slip and then exceeds its slip accommodation (as a function of shear stress vs normal stress). Heterogeneity in sediments may be the cause of differing number and expression of fault splays and why individual fault strand behaves independently. It is possible the bedrock is present at shallow depths and is complicating the response of the surficial deposits to the rupture or there is actually variation in displacement along the bedrock plane (McCalpin, 2009). The lower scarps have offset an alluvial fan consisting of alluvial gravels with high heterogeneity which can influence fault propagation (Lin and Stein, 2004). Variation in scarp expression either side of Willow Creek may be a result of the fault offsetting surfaces of different height and age. The alluvial fan surfaces either side of Willow Creek display different surface heights likely a result of the lower fan surface to the south of Willow Creek being younger and actively degrading at a later stage.

The Stock Pen splay (Figure 2.16) is located just 800 m northeast of Willow Creek and links directly to the Willow Creek splays (Figure 2.15). From the north the fault trace appears to terminate against the fault trace projected from the south at a very high angle. Fault offset and deformation has offset the lower slopes of a fan and the scarp formation here is significantly reduced. This is likely due to aggradation modification, where more erosion has reduced the scarp height. Shallow dipping thrust faults propagating through surficial fluvial/alluvial deposits may also result in the formation of low (< 1m) scarps. Heterogeneous deposits and/or subsurface bedrock relief may be the cause of significant changes in fault expression along this section, resulting in high scarps to the north and lower scarps within the fan deposit. Furthermore, variation in scarp height along the fault is also a result of variably aged surfaces. North of the small tributary the fan surface is higher than the fan surface south of the small tributary which is likely younger and has been more degraded. The Dalzell (Figure 2.17) and Stock Pen (Figure 2.16) splays offset the lower section of different fan surfaces,

although the Dalzell splay scarp height is larger (> 4m) than the Stock Pen Splay height (< 4m), it is likely these splays are influenced in different ways by these factors.

The fault splay at Ribonwood Stream is a large fault branch off the main fault trace in the southern valley (Figure 2.8). The splay continues on with the northeast trend of the main trace while the main range-bounding fault bends in an arc shape up to the southern to northern valley transition. The fault splay is approximately 2.5 km long and has a zone of associated shear fabric noted up the stream (Cowan, 1992). This splay indicates the start of the complex faulted shear zone at the southern to northern valley transition (Figure 2.8 and Figure 2.23), which has been mapped by Cowan (1992). It is possible cross-cutting inherited faults in the basement across the valley floor are affecting the expression of the main range-bounding fault here. This is further discussed in Section 5.2.1

Finally, significant splinter splays are inferred to break off the main fault close to the connection to the Townshend Fault at the south end of the southern valley, also recorded by Barrell and Begg (2013) (Figure 2.8). These faults extend ~ 3.5 km north-northeast into the southern basin beneath the expansive river plains. Fault zone displacements in the subsurface beneath the valley floor have formed a northeast oriented monocline ~ 2.5 km in length. Paleo relief spurs are observed in the southern section of the southern valley (Figure 2.18). There is a loose association of these paleo relief spurs with the surface splays. It is likely their presence is a complex relationship of faulting and folding of the bedrock at depth that has been covered by alluvial valley fill and the surface splays that have since deformed the alluvial fill.

Figure 2.18: *Photo view looking north at the paleo relief spurs in the southern basin. Grid reference: 244027 577950.*

2.4.7 Displacement and Fault Deformation Zone

Fault scarp expression in the northern valley has been extensively analysed by GPS profiling, allowing scarp heights to be analysed using the method from Xiaodong et al. (2015). Calculation of reverse-fault parameters such as scarp height, fault dip, dip slip of fault and vertical displacement depends on the type of fault scarp. Based on the relative dip of the ground topography and fault scarp, a reverse-fault scarp can be either a reverse-scarp or normal-scarp (Xiaodong et al., 2015) (Figure 2.19). A normal fault scarp for a reverse fault will display a relationship of less than or equal vertical displacement (VD) to the vertical separation (VS) of the hanging wall and footwall which will be equal or smaller than the value of fault scarp height (SH), ($VD \leq VS \leq SH$). An example of this analysis is given in Figure 2.22, a GPS profile directly adjacent and south of the Dalzell trench site. The Scarp height here is 10.5 m with a vertical separation of 10.25 m and a vertical displacement of 8.5 m.

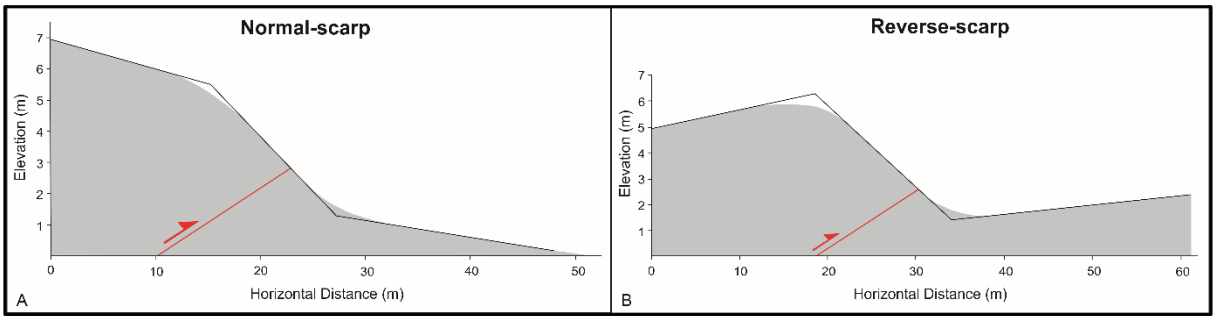

Figure 2.19: *Comparison of fault scarp types for a reverse fault. A) Normal-scarp B) Reverse-scarp. Modified from Xiaodong et al. (2015).*

Results

Fault displacement variation can be indicated by the variety of fault scarp heights in the northern valley which range from 1.5 - 10.9 m (Figure 2.23), as recorded from 72 selected fault scarp survey profiles (refer to Figure 2.7). Moving from the northern end to the southern end, discrete deformation is analysed. The smallest displacements (Figure 2.23) are recorded near the end of the fault trace (Figure 2.24 A) and along small splay segments (Figure 2.24 C). Larger displacements occur near the centre of the fault trace (Figure 2.23) at locations like Willow Creek (Figure 2.24 B) and the Dalzell trench site (Figure 2.22) (Figure 2.21). The shape of the fault displacement to length relationship can be described as 'Peak type' where there is a well-defined central maximum displacement, 'Plateau type' with a wide central section of relatively constant displacement or 'Bell-shaped' which is in-between (Fossen, 2010) (Figure 2.20). The Lees Valley Fault displacement varies considerably although generally shows a plateau type distribution with a section of maximum displacement between the Willow Creek splay and the Dalzell splay (Figure 2.23). Some locations with smaller displacement (Figure 2.23) are associated with fault splay sections where discrete offset is being accommodated on more than one trace such as the Stock Pen splay (Figure 2.24 D) and the Willow Creek splays (Figure 2.24 B and C). Other locations of reduced scarp height are associated with drainage systems (Figure 2.23).

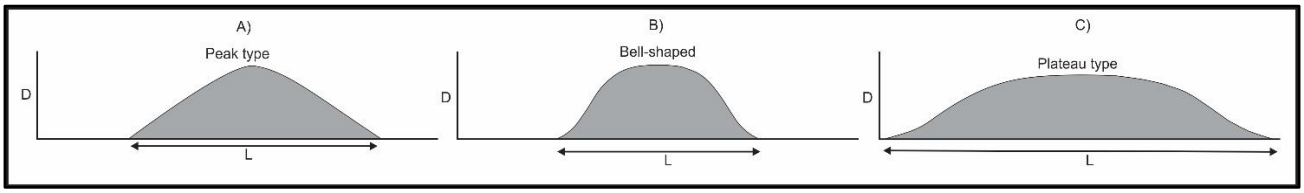

Figure 2.20: *Types of displacement (D) profiles along faults from Fossen (2010).*

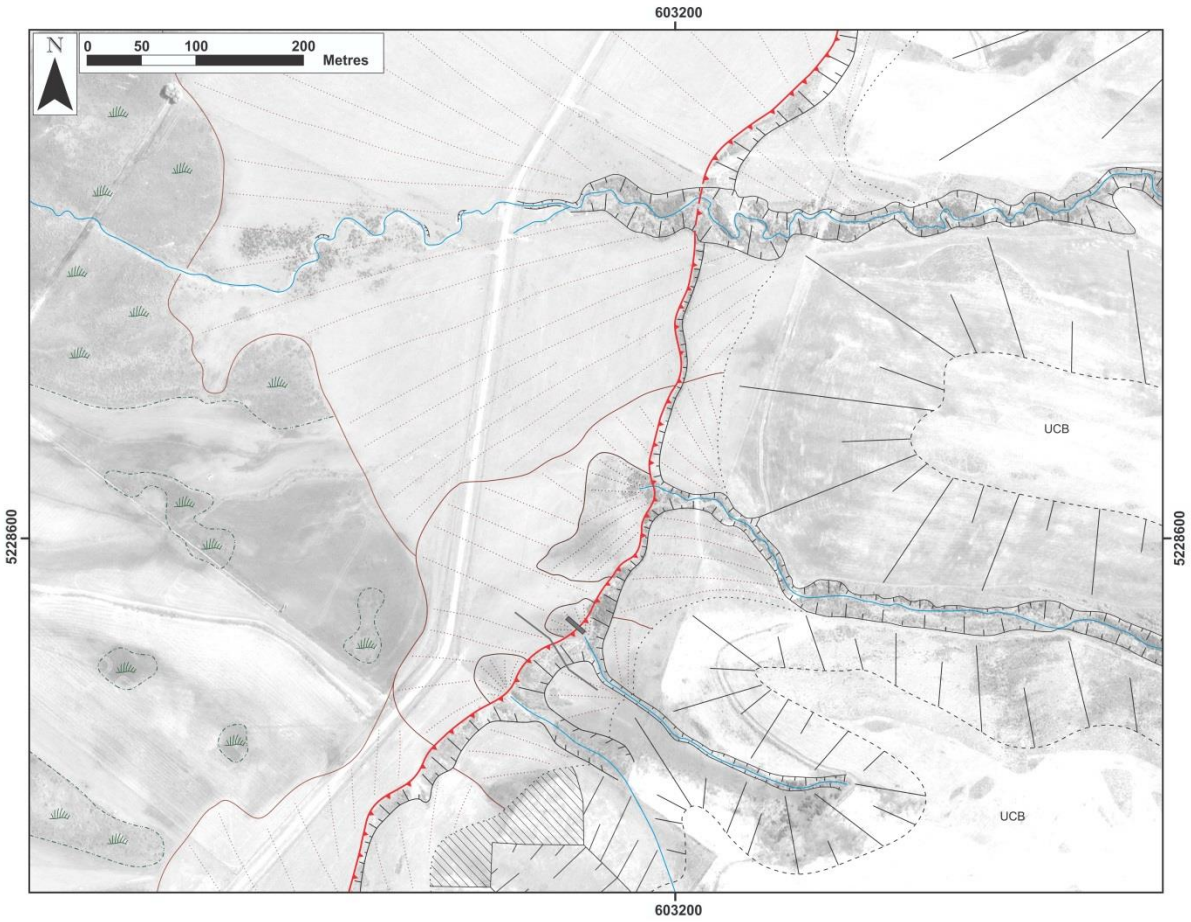

Figure 2.21: *Dalzell trench site structural and tectonic geomorphic map. Trench location indicated (grey box) and GPS profile (Figure 2.22) indicated (grey line)*

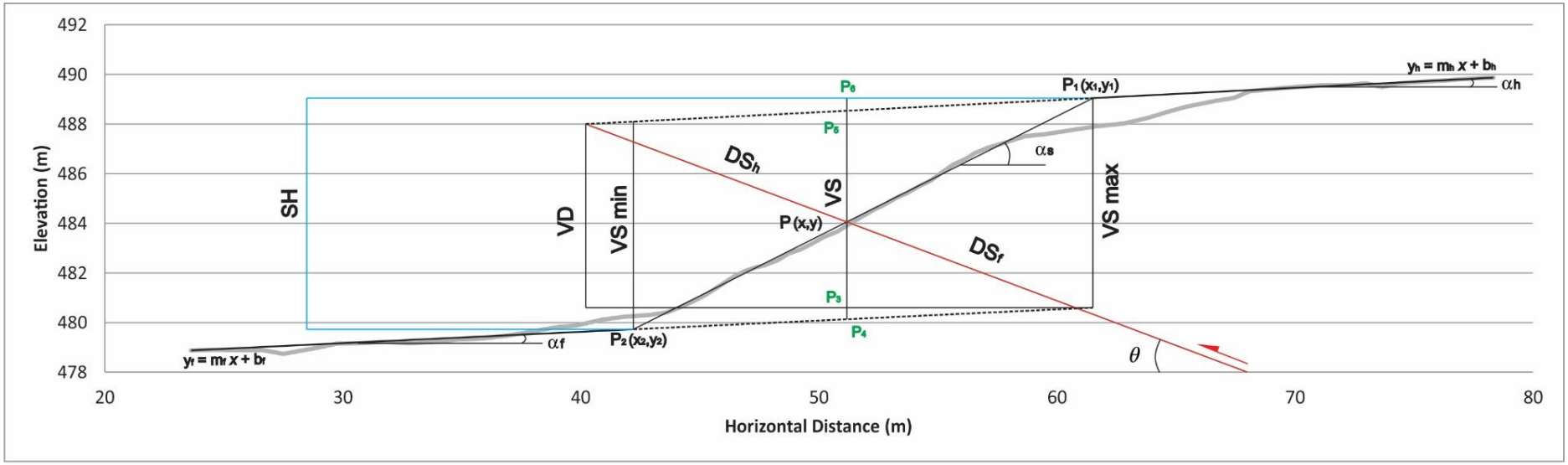

SH = Scarp height (10.5 m)

DS = Dip slip of fault

HD = Horizontal displacement

VD = Vertical displacement (8.5 m)

VS = Vertical separation of ground surface

VS min = minimum vertical separation of ground surface

VS max = maximum vertical separation of ground surface

θ = Fault dip (23˚)

αh = Angle of ground surface of the hanging wall (3˚)

αs = Slope angle of fault scarp (30˚)

αf = Angle of ground surface of the footwall (3.5˚)

P (X,Y) = Fault tip

$P_1 (X_1, Y_1)$ = Intersection point of hanging wall

$P_2 (X_2, Y_2)$ = Intersection point of footwall

Figure 2.22: *GPS Profile south of trench site (Figure 2.21) with fault parameter annotations (Using the method from Xiaodong et al., 2015).*

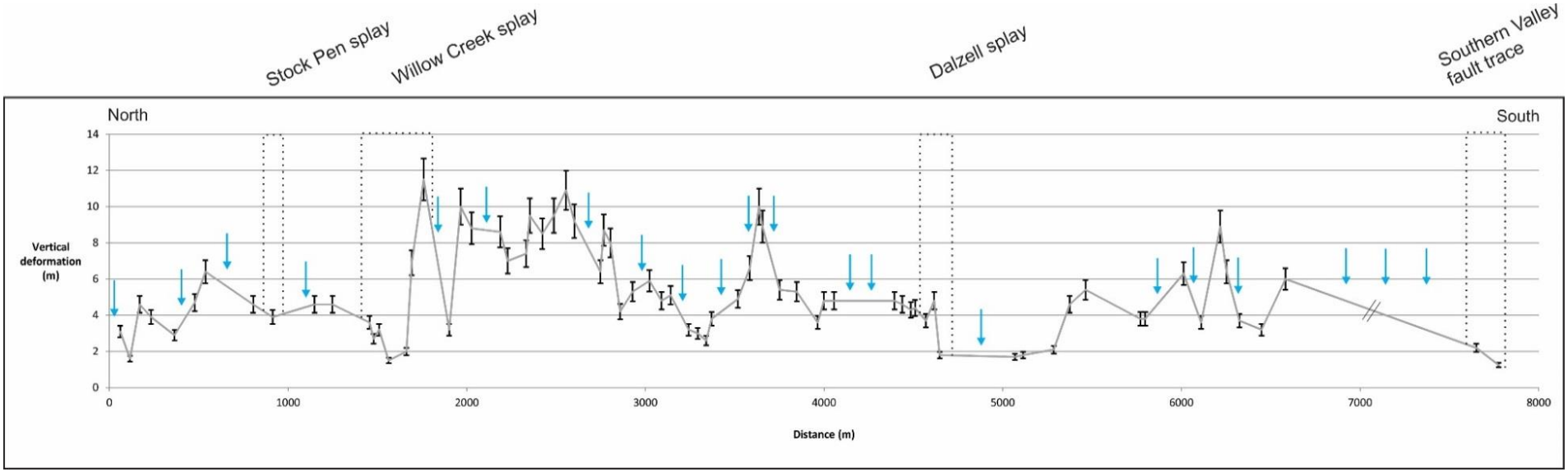

Figure 2.23: *Graph of deformation (vertical displacement) distribution along the length of the northern valley section of the Lees Valley Fault. Locations of fault splays and drainage channels (blue arrows) indicated.*

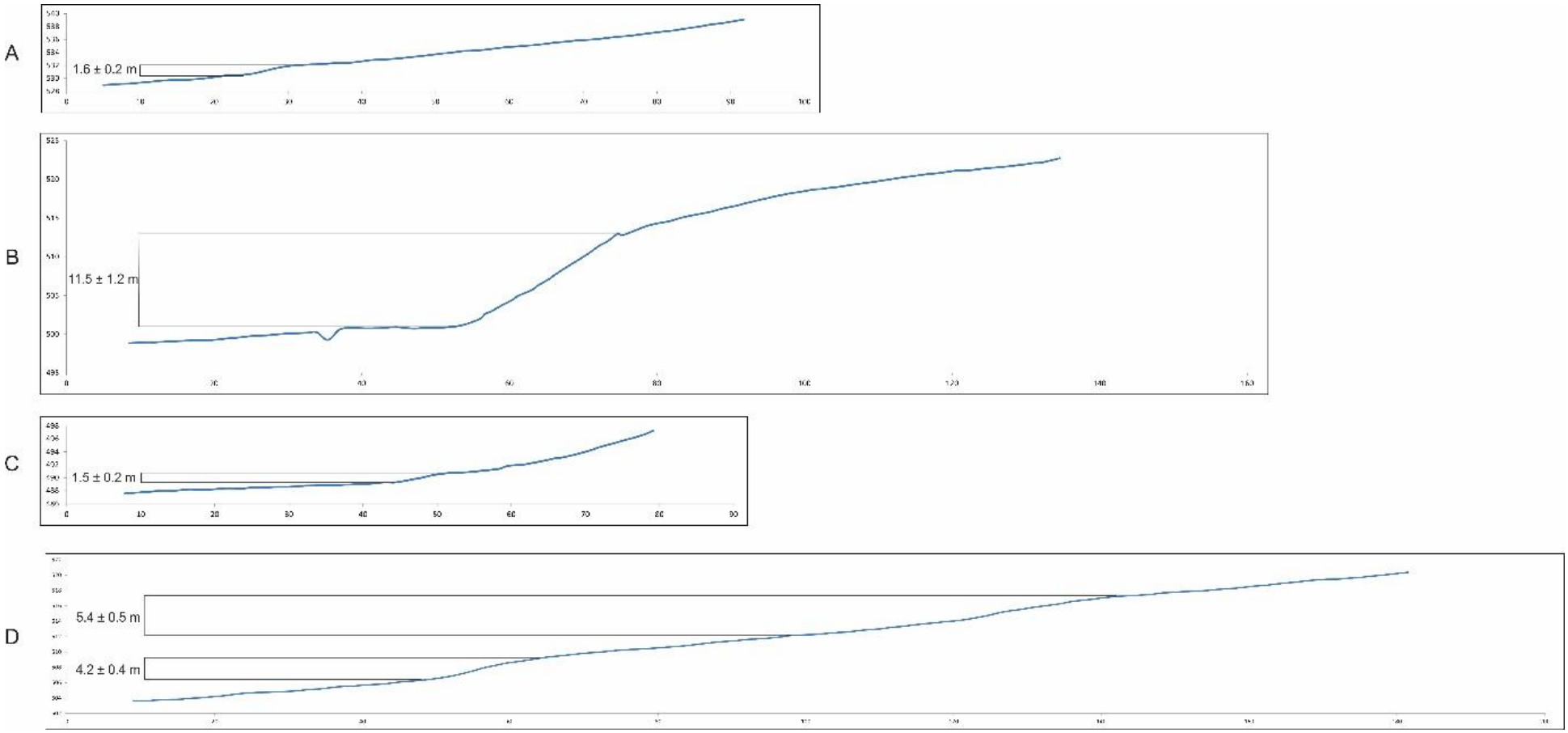

Figure 2.24: *GPS fault scarp profiles (profile numbers correlate to those found in digital appendices). A) Profile 2, indicating the reduced offset at the northern end of Lees Valley Fault. B) Willow Creek, profile 18, displaying the highest topographic offset nearing the centre of the fault section. C) Willow Creek, profile 15, a small splay within a system of four splays indicating some of the distribution of strain accommodation within an imbricate thrust system. Profile B demonstrates a scarp accommodating all of the deformation within this section. D) Stock Pen splay, profile 9, where two traces accommodate offset.*

Discussion

Deformation on reverse/thrust faults can be accommodated through discrete vertical offset and distributed folding within the hanging wall. Furthermore, not all deformation will occur co-seismically, as ongoing fluvial/alluvial processes can cause some modification to ground surface levels. While it is not possible to work out the relative timing of the distributed deformation, most of it is likely to have formed co-seismically. In some instances, the separation of components of deformation into folding and vertical offset can be calculated by analysis of scarp profiles. However, for the majority of these profiles it is too difficult to distinguish if folding is present in the hanging wall or not and if so distinguish this from the topography of the adjacent range upslope of the fault scarp.

Variation in surface deformation along a fault ground surface rupture trace may result from fault segmentation, fault growth, slip variation, altered geometry, changes in fault dip and displacement transfer between imbricate splays (Cartwright et al., 1995; Burbank and Anderson, 2012; Bubeck et al., 2015). Drainage patterns can further complicate surface deformation, as their pathways may alter over time, changing the location of erosion and deposition, and modifying/eroding the fault scarp, lessening the vertical offset recorded. Additionally, changes in bedrock characteristics such as density, joint spacing or depth below the surface can cause variation in fault surface expression (Burbank & Anderson, 2012). Fault orientation also varies within both the northern and southern valleys. Possibly due to the variation in bedrock depth due to the presence of the paleo relief in the southern valley where bedrock is uplifted beneath the Quaternary deposits (Barrell & Begg, 2013). Variation in the relationship between faulting and associated folding also affects the distribution of slip along a fault, which can vary the height of offset. Significant variation in vertical offset is also likely due to the difference in fault location within the alluvial fans, the different ages and sizes of the offset fans, coupled with the unconsolidated sediments the fault breaks through, likely causes shallowing of the feature as it nears the surface (Lin & Stein, 2004). It is likely that many of these factors contribute to the variation in surface deformation of the Lees Valley Fault (Figure 2.23).

The fault deformation zone width is also a complex relationship that can alter with increased hanging wall topography and topographic relief (Khajavi et al., 2014). Consequently the effect of changes in topography to fault geometry and stress states increases the fault zone complexity and width. As previously discussed, topography and several other factors result in

imbricate fault development, resulting in deformation being accommodated on more than one fault trace, widening the fault deformation zone. Furthermore, an increased thickness of alluvial deposits over bedrock also coincides with an increase in surface fault splay density and consequently fault zone width. Lastly, fault deformation zone width can also change with variation in fault dip and segmentation.

While the Lees Valley Fault is not necessarily (seismogenically) segmented it does have a structural discontinuity/step-over at the transition between the northern and southern valleys where there is also a significant change in fault orientation (Figure 2.25 & refer to Figure 1.4).The orientation of the fault changes, the individual sections of the fault trace do not directly join but rather overlap, and the deformation is distributed between the two main traces. This is apparent in the reduced height of a small splay off the fault trace from the southern valley (~2.2 ± 0.2 and 1.25 ± 0.1) (Figure 2.26). Segmentation is often defined by structural discontinuity evident in a step-over zone, when faults terminate against bedrock extending into a basin and en-echelon steps in range-bounding faults (Burbank and Anderson, 2012). The step-over gives the appearance of an en-echelon arrangement of fault splays, although no strike-slip motion is documented. The nature of faulting here is likely impacted by the change in orientation of the fault, while the overlapping splays cause an increase fault deformation zone width.

Reverse/thrust fault surface ruptures are often discontinuous, comprising several separate fault traces that transfer through step-overs with a combination of faulting and folding, and rupture continuously (Wesnousky, 2006; Wesnousky, 2008; McCalpin and Carver, 2009). During rupture the separate fault traces move together providing a rupture length much longer than what would be expected for the individual sections. Reverse faults are often underestimated in surface rupture length and earthquake magnitude when segmented and can be interpreted as segmented due to the tendency of the scarp expression to be discontinuous. (McCalpin & Carver, 2009). Although the Lees Valley Fault appears to be segmented between the two valleys, it is likely the fault ruptures continuously with strain passing through a complex transition zone. This is evident in the distributed deformation of fault splays in Figure 2.23 and the large deformation accommodated on the fault scarp in the upper valley, which would not be likely given a fault trace length of only 7 km (Quigley et al, 2012).

Range-front faults intersected by a cross fault or inherited feature trending at a high angle to the main fault could also result in the apparent fault segmentation (Burbank and Anderson, 2012). The continuation of the Whistler Fault Zone into the Lees Valley basin does cut through the valley at a high angle to the Lees Valley Fault (refer to Figure 2.8). It is possible the continuation of this feature or a remnant structure oriented east-northeast is complicating the surface expression of the Lees Valley Fault Zone within the eastern ranges (Figure 2.25).

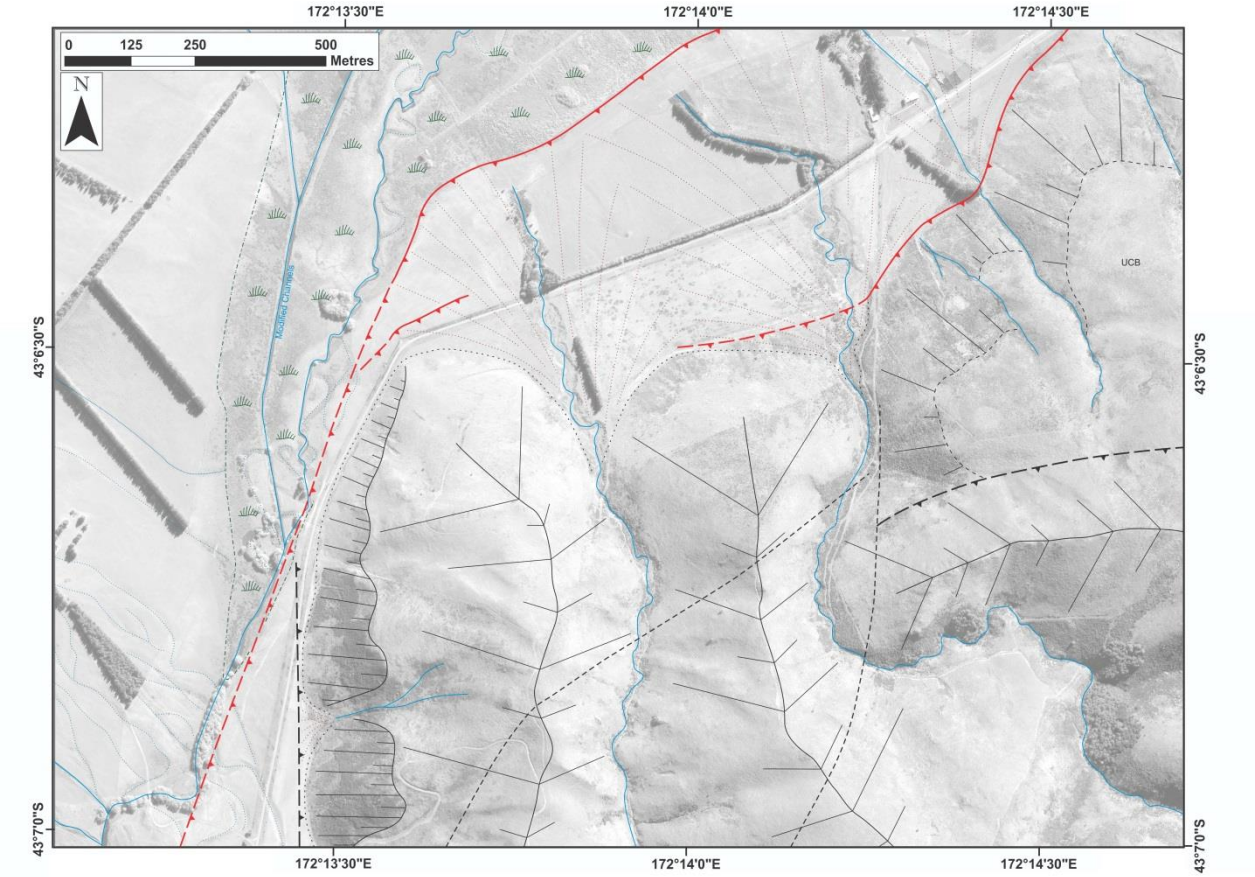

Figure 2.25: *Structural and tectonic geomorphic map of the transition zone between the northern and southern valleys.*

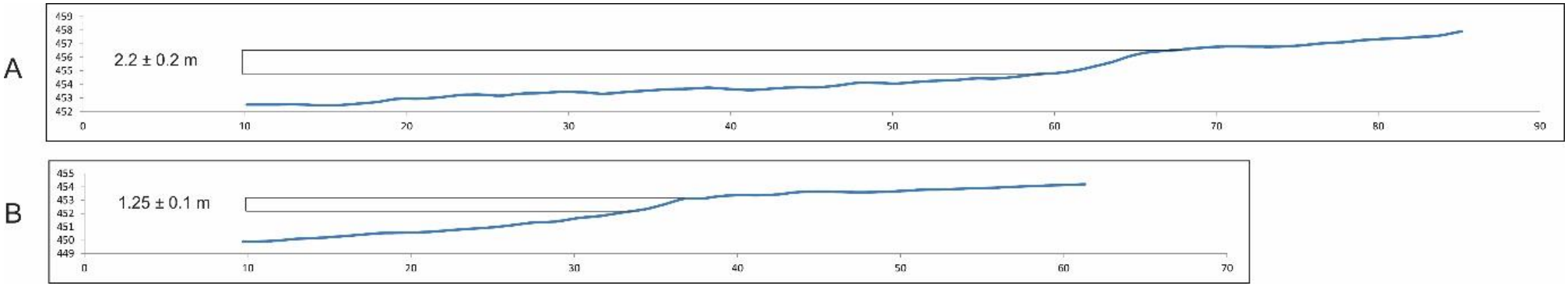

Figure 2.26: *GPS fault scarp profiles 72(A) and 73(B) of a splay off the most westward southern valley fault trace in the transition zone, indicating the reduced scarp height of this trace (profile numbers correlate to those found in digital appendices).*

2.4.8. Thrust Plane Exposure of the Lees Valley Fault

The principal thrust plane is exposed in outcrop within the Ashley River along the eastern rangefront about ~2.6 km southeast of where Duck Creek joins with Ashley River (refer to Figure 2.8). The outcrop has been extensively described by Garlick (1992) indicating Torlesse is thrust above Tertiary marine and non-marine sediments (Figure 2.27 & 2.28). Oriented north-south the thrust plane dips to the east variably ~ 20 - 40º (Figure 2.28). Highly polished surfaces and slickensides indicate that recent movement on the thrust plane has been accommodated by shears in the fault gouge adjacent and slightly oblique to the thrust plane (Garlick, 1992). Oriented to the east-west a series of steeply dipping faults offset the thrust plane and are likely to be the driving force behind failure in the river outcrop. Furthermore a major fault splay breaks off from the main fault here, tracing up Ribbonwood Stream (refer to Figure 2.8), which has resulted in intense crushing over a wide zone. Bedding of the Tertiary sediments below the thrust plane demonstrates a variety of orientations and their structural relationship to the surrounding deposits is indeterminate. Significant shearing and some tectonic mixing have affected the deposits. Greensand and coal are found close to the thrust plane and contain small reverse faults and minor folds. Lying above the outcrop is gravel and loess from former channels and possibly loess colluvium.

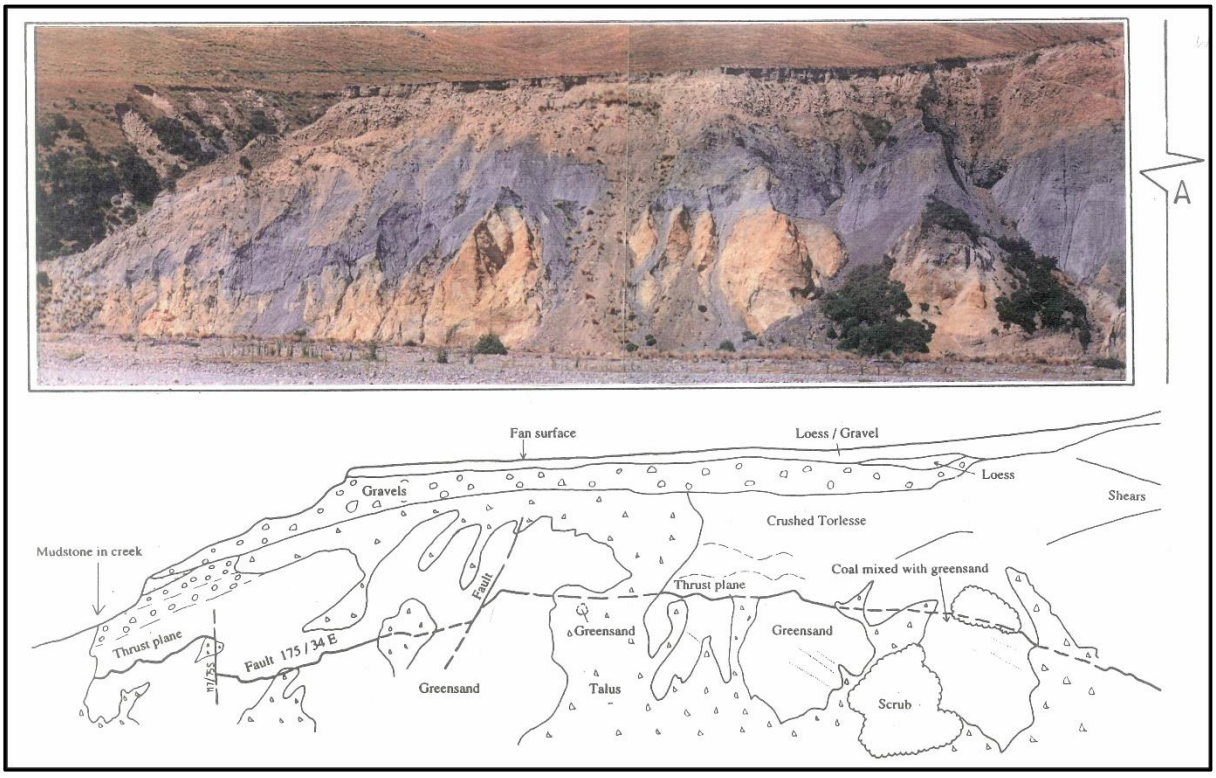

Figure 2.27: *Photo view of bedrock outcrop in Ashley River with structural interpretation and lithology indicated (from Garlick, 1992).*

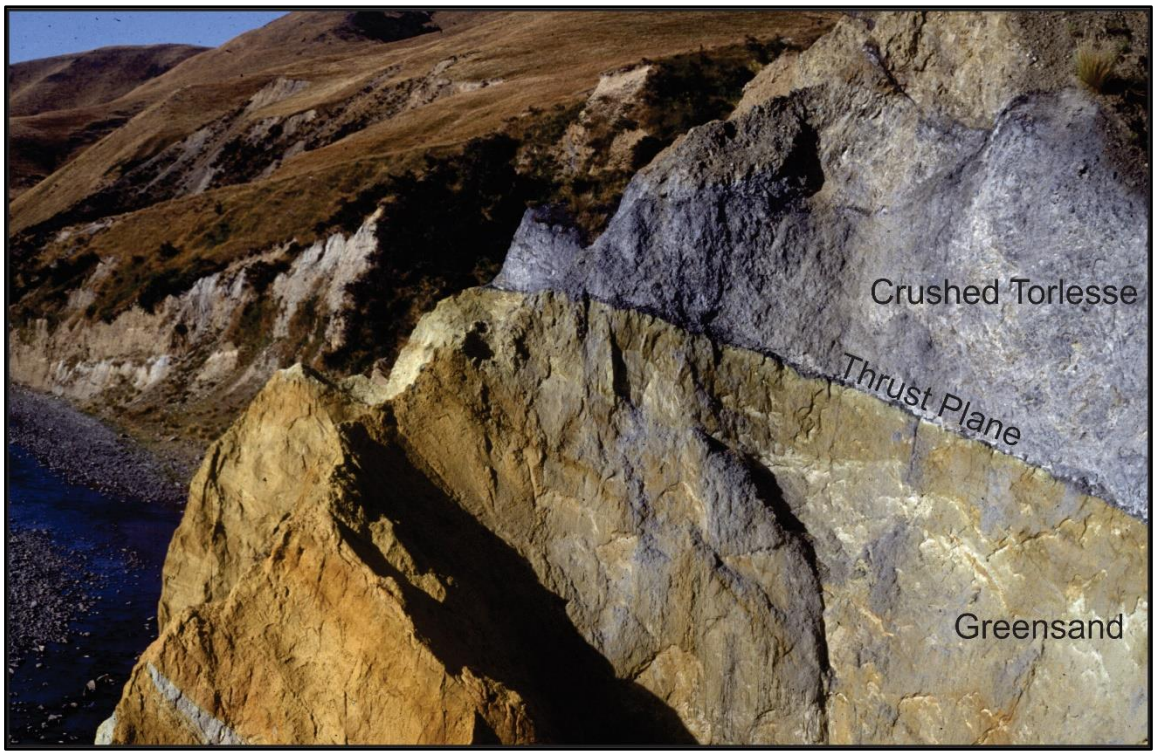

Figure 2.28: *Photo view of bedrock outcrop in Ashley River looking North along strike indicating thrust plane dip. Photo courtesy of Andy Nicol (Department of Geology, University of Canterbury).*

The fractured Torlesse yields fault and slickenside striations which can be measured in the hanging wall near Ribonwood Stream. Garlick (1992) measured and analysed this data to show the majority of striations plunge to the north and west quadrants. The majority of minor faults are steeply dipping and trend parallel to the Torlesse beds in a northwest-southeast direction. Motion sense from a selection of faults produced stress tensors indicating σ_1 plunges to the southwest at a low angle. The regional compression is oriented northwest-southeast (Nicol, 1991) and may be revealed in the smaller concentration of σ_1 to the northwest. Garlick (1992) inferred it is likely the deformation described in this data formed during late Cenozoic and the stress tensors demonstrate local stress variations in the regional stress field likely a result of the Ribbonwood Stream splay.

Orientation of principle stress directions was investigated by Garlick (1992), analysis of slickenside striations on the surface of shear planes using the M-planes method of Aleksandrowski (1985). Measurements from the fault exposure in the Ashley River have revealed two main sets of shear planes. One oriented parallel to the thrust plane and a second with variable orientation and some westward dip. There is a complex relationship of slickenside striations with one set mostly dip-slip resulting in eastwest trending M-planes and

a second showing mostly strike-slip resulting in northeast-southwest trending M-planes. The data is insufficient to identify the principle stresses, although it does suggest one does lie in a plane oriented northwest-southeast. This data mostly highlights the complexity of faulting within the valley although it does indicate a variation in stress field from what is normal in the region at this location which may reflect a more complex structural nature of the entire valley or just the complexity of this location due to the Riboonwood Stream fault splay.

One possible suggestion is that the Lees Valley Fault may be undergoing a change in the nature of faulting. The PPAFZ has a young strike-slip fault system that has developed to the south where is it overprinting and combining with pre-existing thrust faults (Cowan, 1992). Due to the transitional nature of the Lees Valley Fault into the PPAFZ it is possible some of this strike-slip motion is being accommodated on the valley fault. Late Quaternary development of the Porters Pass - Amberley Fault Zone was a result of a new transpressional fault zone relay forming through links between contractional step-over zones (Pettinga et al., 2014). Furthermore, it may be a reflection of near surface strain partitioning similar to that in the Marlborough Fault System which has resulted in complex patterns in the upper crust. The Marlborough Fault System has four principal oblique-slip structures that have accommodated strain through a gradual temporal south-eastward migration in the loci of strike-slip displacement (Eusden et al., 2005).

2.5 Chapter Summary

This chapter has highlighted the limitations of applying Bull's (2007) model to the development of reverse/thrust fault controlled basins in South Island New Zealand. Differences in the type of faulting, climate and bedrock materials has led to unexpected results from standard measures such as the lower than expected sinuosity values in Lees Valley. Although given these limitations comparison with the model was still useful in identifying geomorphic features that indicate active uplift and relative classes of activity such as faceted spurs.

Analysis of structural features including fault discontinuity, thrust plane bedrock exposure, variation in displacement and fault deformation zone has helped identify the complexity of faulting within the basin. Alongside analysis of the geomorphology the results from this data indicate an active tectonic zone and help to build a picture of the fault behaviour, influence of cross cutting/inherited structures and a model of development for the fault zone and associated ranges (discussed in Section 4.1).

3. Paleoseismicity

3.1 Introduction

Analysis of tectonic geomorphology helps to provide an understanding of the interactive relationship between tectonic deformation and surface processes along the Lees Valley Fault. However, evidence of pre-historic earthquakes is required to quantify the net slip rate and timing of ruptures of the Lees Valley Fault and provide constraints on the hazard to the region in a future fault rupture event.

This study includes Optically Stimulated Luminescence (OSL) dating of material collected from a paleoseismic trench across the range-bounding trace of the Lees Valley Fault in the northern valley. Dating is used to constrain the timing of the most recent surface rupture and to calculate/constrain average Late Quaternary slip rates and recurrence intervals. This can be combined with fault scaling relationships to determine likely paleoearthquake magnitudes. No paleoseismic trenches have previously been completed on the Lees Valley Fault; this study aims to fill this knowledge gap and provide more accurate information on past fault parameters and give more precise estimates on possible future fault characteristics.

3.1.1 Aims

Undertaking a paleoseismic investigation to provide more accurate quantitative data alongside the geomorphology work from this study and that presented in previous work. Data from the trench logs and dated sample material from the trench has allowed investigation into:

1. The potential age and number of Late Quaternary faulting events, in the northern valley.
2. The slip rate of the northern segment of the Lees Valley Fault most recent event trace.
3. The recurrence interval of past earthquakes along this segment.
4. The potential magnitude of large ground rupturing earthquakes along this segment.
5. Overview the seismic hazard the Lees Valley Fault poses in the region.

3.2 Methodology

3.2.1 Pre-trenching Site Investigations

Prior to trenching, extensive field mapping and DEM analysis was used to aid in trench-site selection. The Lees Valley Fault has a distinct change in expression in the southern valley versus the northern valley due to the orientation of the fault and the drainage systems in each section. The fault appears to be segmented between the two sections as discussed in Section 2.4.7 and its surface expression is obscured in the southern valley, due to erosion. In the northern valley, clear extensive scarp formation provided more trenching opportunities (Figure 3.1). The fault scarp trace in this section of the valley is 7.6 km long and varies considerably in height due its location at the foot of the rangefront, where it offsets fan deposits of various ages and differing heights. Furthermore numerous drainage channels have eroded the fault scarp resulting in reduced scarp height.

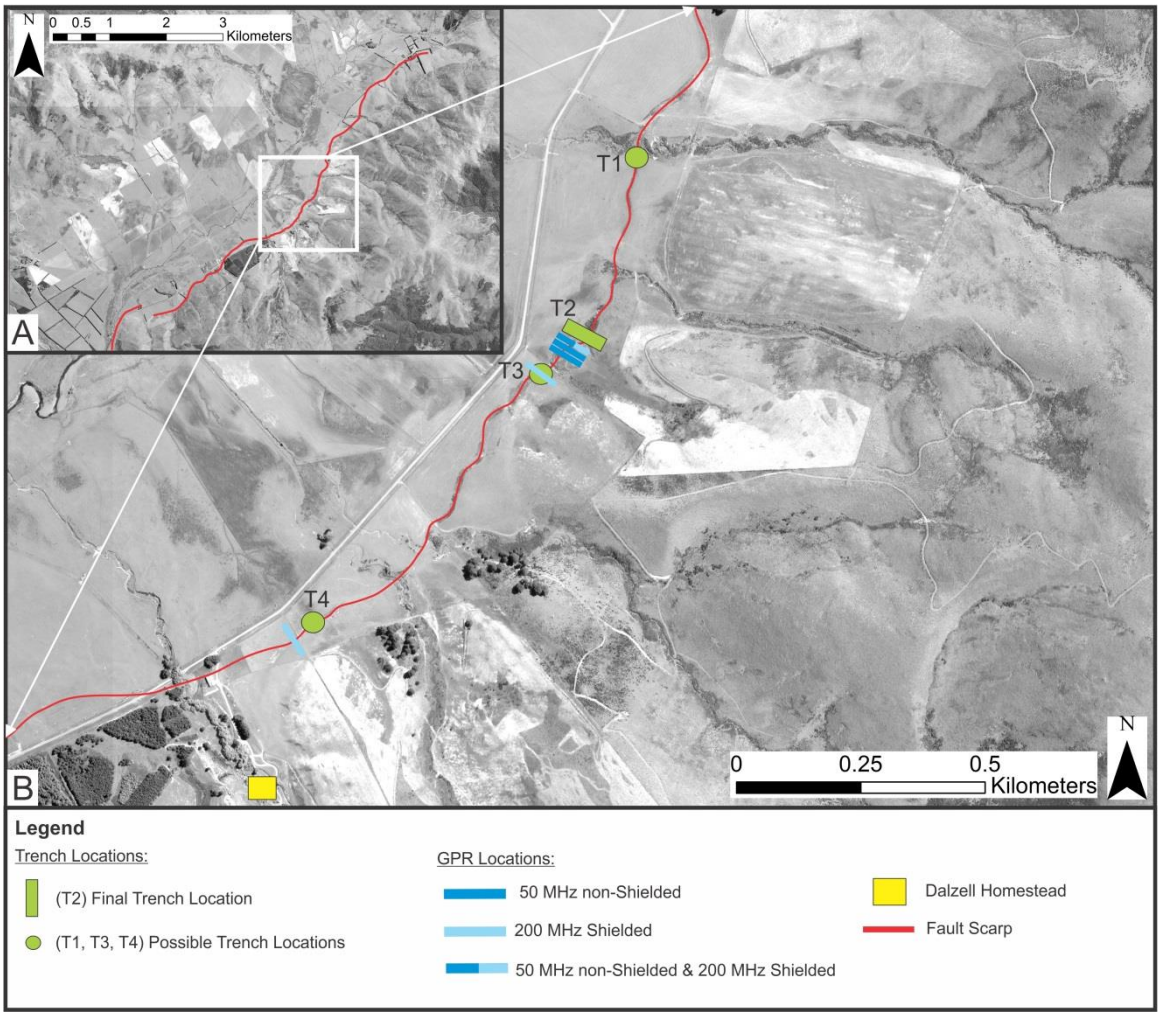

Figure 3.1: *A) Northern Valley fault expression. B) Dalzell property fault expression trench locations and GPR investigation locations indicated.*

Several locations along the northern valley were evaluated for a possible trench site. Important in site selection was a prominent and confined fault scarp indicating significant localized displacement in the near surface. Also important was less topography directly behind the scarp which simplifies analysis of deformation and folding related to the fault at the selected location. The most well defined scarp is located in the paddocks of the Dalzell's property immediately east of the Lees Valley Road (Figure 3.2). The Dalzell's property is situated in the middle of the northern valley and begins at the Dalzell homestead (Figure 3.1). Height of the scarp here varies but reaches up to 8.5 m. There has been extensive alluvial fan development at this location and the fault has offset several large, Late Pleistocene and Holocene fan deposits sourced from the eastern ranges. In some locations along the length of the fault scarp, continued drainage from the ranges has initiated younger, smaller fans to form at the foot of the scarp which are mostly all abandoned now.

Figure 3.2: *Photo of prominent fault scarp on Dalzell property looking east-northeast from Lees Valley Road. Grid reference: 245006 579029.*

A trench location was chosen from four possible sites (Figure 3.1). Location 1 and 3 had a clear scarp expression and would potentially provide a good comparison of deposits either side of the fault. A short "scoop style" trench would be most appropriate for these locations,

it was decided if the final trench location did not provide adequate information these sites could be investigated as a fall-back option. Location 4 has a prominent scarp and is partially located within a low-lying swamp area which indicates there has been ponding in this location over time. Consequently it was surmised there may be radiocarbon samples that would be useful for dating. However, significant vegetation is present and the site would require extensive clearing. Furthermore the height of the scarp at this location would make it difficult to trench safely to the inferred depth required to reach the fault.

Location 2 was chosen as the most promising site for trench investigation and will be referred to as the Dalzell Trench. This site was chosen because of the 10.5 m high scarp at this location (refer to Figure 2.22) and the young fan deposit at its base estimated to be Holocene in age based off its formation following offset of fan surfaces estimated to be Late Pleistocene. The smaller fan has been deposited on top of the older fan surface, sourced from an incised stream channel into the up-faulted larger fan above the fault scarp, indicating its formation post offset of the larger fan (Figure 3.3). The clear difference in age of fan deposits was considered likely to constrain the timing of faulting due to the older fan being offset followed by formation of fault scarp deposits, such as a colluvial wedge, which would be in turn overlain by the younger fan deposits. Older deposits would show offset and younger fan deposits would display an unconformity by draping over the faulted material. Absolute dating these various deposits could provide age bracketing for the faulting event. Their relative relationship and potential for correlatable units either side of the fault trace would identify fault behaviour. Field mapping and analysis of aerial photos indicated the small fan deposit to be relatively young as there was little vegetation on the fan surface, although estimates of the actual age are uncertain. The height of the scarp here suggested there could be accumulation of sediment on the downthrown side of the scarp following paleoearthquakes, while colluvial wedges could help identify individual faulting events from the trench log. Furthermore field observation and aerial photo analysis indicated active drainage processes in the past suggesting potential for radiocarbon dating of material may provide ages of the deposited material and if this was absent OSL samples would be taken.

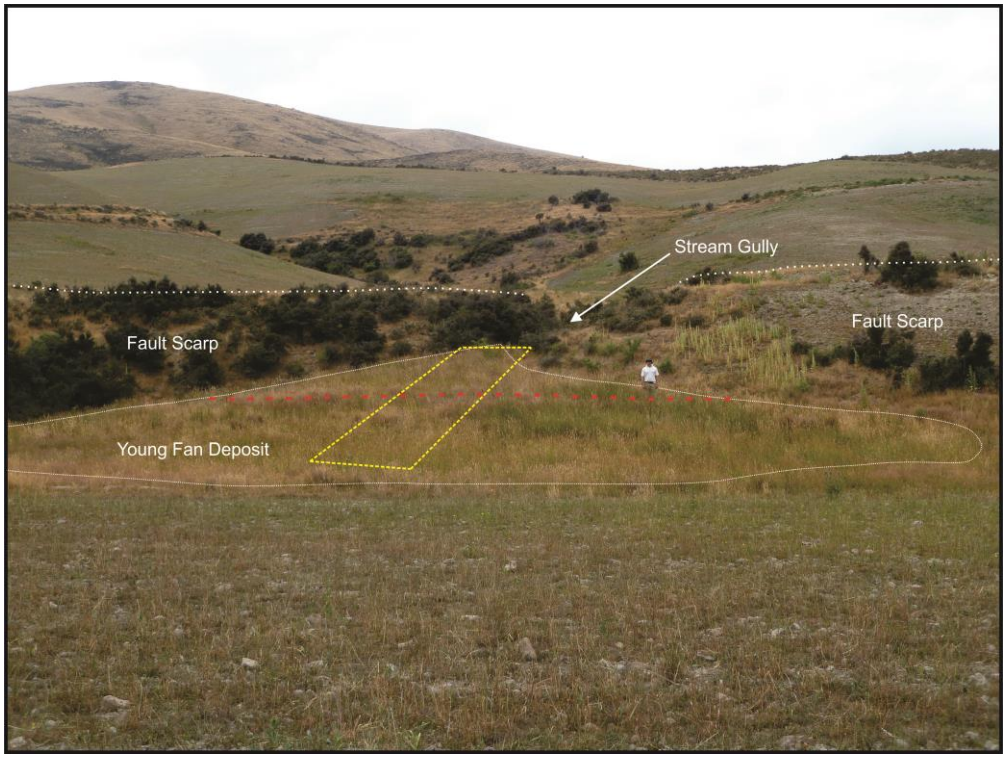

Figure 3.3: *Photo view of trench site, looking east-southeast, before trench excavation with geomorphic features labelled. Proposed trench location indicated in yellow. Expected trace of fault through trench indicated in red. Geologist for scale ~1.7m. Grid reference: 244998 579016.*

3.2.2 Paleoseismic Trenching

The paleoseismic trench was excavated to investigate the near-surface geometry and paleoearthquake history on this trace of the Lees Valley Fault. It was excavated in early March 2015 perpendicular to the fault scarp in an East-West orientation. The trench began near the top of the fault scarp above the apex of the younger fan deposit, extending to near the end of the fan deposit with a width, length and depth of 6 m, 25 m and 5 m respectively (Figure 3.4). Benches were cut halfway down the sides of the trench to stabilise the walls for exposure face logging. Before logging, the trench walls were thoroughly cleaned, measured and gridded, in 1 m^2 grids, following which unit contacts and structures were distinguished and traced using coloured nails. The trench walls were logged at a scale of 1:10 and photographed. The field paper logs were converted to digital logs from which the photo logs were scaled to match and facilitate comparisons.

Figure 3.4: *Photo view of trench excavation site, looking East-Southeast, note surrounding geomorphic elements are labelled and dimensions of trench indicated. Grid reference: 244998 579016.*

North, East and West walls of the trench were logged as each illustrated different aspects of the deposits. The north wall enabled description and sequence of the range of units found in the trench to be recorded, the south wall clearly showed the active structures and the east wall gave the correlation between both sides. Stratigraphic units and structures were described and recorded, and then samples from each unit were collected and described using the Munsell soil colour chart. There was no organic carbon material found in the trench for radiocarbon dating, the more cost effective, highly accurate and most widely used technique for dating Late Holocene and Pleistocene seismic activity. Therefore, the optically stimulated luminescence (OSL) method was used to date samples of fine grain size such as sands and silts taken within selected units.

3.2.3 Optically Stimulated Luminescence Dating

Eight Optically Stimulated Luminescence (OSL) samples were collected from within the trench of which five were sent to be dated, two samples from the east wall and three from the south wall (Figure 3.5). These samples were sent to the Luminescence Lab in the School of Geography, Environment and Earth Sciences, Victoria University of Wellington.

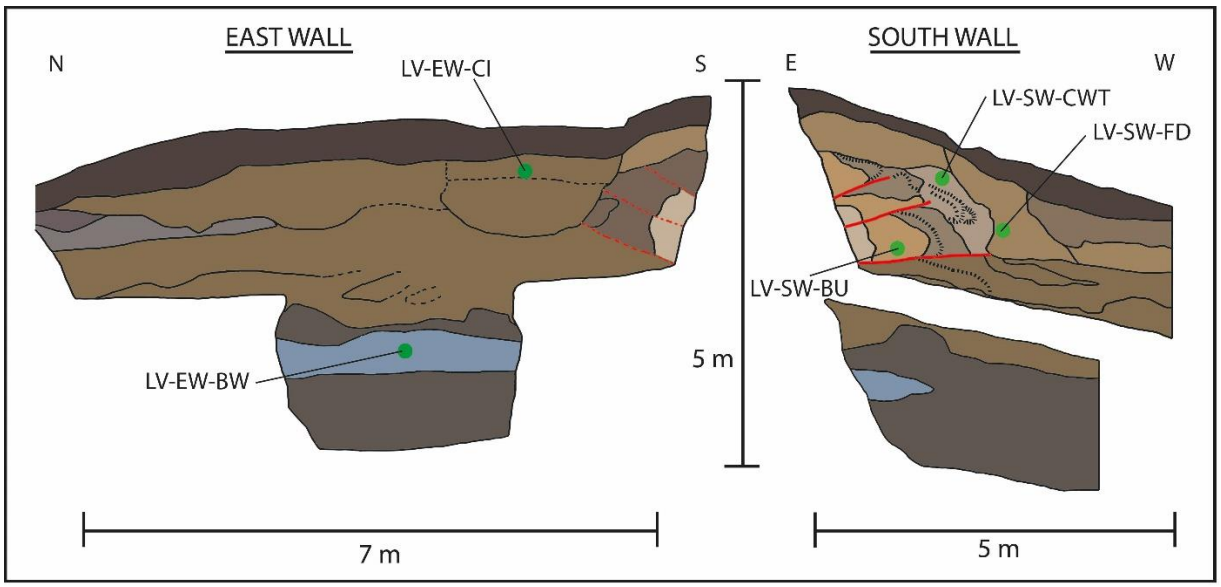

Figure 3.5: *Location of OSL samples within trench, labelled with field codes.*

The OSL samples for dating were chosen based on their suitability to be dated such as; their successful extraction from a section of fine grained material in the unit and if their location would help age constrain the movement events on the fault. Of those not sent to the lab, one tube was damaged during collection, and the remaining two samples were not considered suitable to constrain event horizons in the trench. Samples were collected in long stainless steel tubes from a representative section in the unit that had been cleaned. Care was taken not to disturb the sample excessively during collection and precautions were taken to eliminate any chance of light contamination. For further information on the field techniques used refer to the appendices (Appendix A).

Once collected and sent to the Luminescence Lab in Wellington the samples were prepared using the fine grain (4-11 µm) technique (Wang, 2015). The samples were then analysed for paleodose (equivalent dose) using the Multiple Aliquot Additive Dose method (MAAD) and dose rate determined by gamma spectrometry measurements. Water content was measured two different ways based on variation in location within the trench and unit type, which indicated differences in water content. All samples had water content measured in lab as weight of water divided by dry weight of the sample (including 25% uncertainty) and two of the samples were also treated as being saturated. Further discussion of these techniques can be found in the appendices (Appendix B and C).

3.2.4 Ground Penetrating Radar

Ground penetrating radar (GPR) was performed alongside the trench site (post-trenching) and at two locations south of the trench site along the fault scarp (Figure 3.1). Initial GPR analysis was done using 200 MHz shielded GPR which was followed with analysis using the pulseEKKO PRO system with CMP (Common Mid-Point) velocity sounding design. Surveys conducted at the trench site were done in attempt to determine the subsurface fault dip, and plunge beyond what was visible in the trench. Those performed at the two southern locations indicated in Figure 3.1, were to investigate any relationship between variation in scarp expression and fault behaviour at depth along its length.

The target depth was 3 - 6 m below the surface for the profiles next to the trench site. It was expected it might be difficult to distinguish the fault splays as the host material was similar either side of two of the splays in the trench, however, it was expected there would be sufficient contrast between the silt and gravel properties either side of the bottom fault splay which would show up in the GPR profile. The fault scarp along this section varied in vegetation cover therefore sites were selected with as flat a surface and as little vegetation as possible up the fault scarp, the remaining vegetation was cleared before the profiles were conducted. Before the surveys were conducted the area was also cleared of the majority of cobbles, small boulders and plants.

Two radar operating frequencies were tried in the field and selectively chosen to maximise penetration depth while still maintaining as clear a spatial resolution as possible. First a 100 MHz trail was run, due to the resultant high penetration depth and low resolution it was changed to 50 MHz in order to balance best resolution for the most penetration possible. A survey point spacing of 25 cm was selected as the best option for the frequency chosen, in order to remove the chance of spatially aliased ground response by not exceeding the Nyquist frequency. The Antenna separation was set at 1.5 m to balance the refraction focusing peak converging at depth with ease of sampling up a steep scarp. Their orientation was set at the commonly used PR-BD (Perpendicular Broadside) so the electric field was polarized parallel to the long axis and strike direction of the fault splays. Due to the rough surface conditions and obstructions the system was set up for a step mode survey technique, however, due to the height of the scarp and difficulty of shifting the antennas they were set up to be dragged via sledge mode to enable easier surveying, while still recording at step intervals. Radar velocity was set between 0.12 and 0.15 m/ns to match the mix of dry sand and dry rock in the sampled

material. Surveys were conducted perpendicular to the fault scarp (Figure 3.6). Those sampled next to the trench site were set out in three parallel surveys to enable a 3D image to be produced with the data. A tape measure was set up along the length of each survey location, and survey points marked on the ground with spray paint at 25 cm distances. The data was acquired through beeper activated trigger at each survey point. GPS points were taken at the start and end point of each survey line in order to spatially locate the data. To enable post processing GPS points were taken at the bottom and top of the scarp and any other point of significant height change.

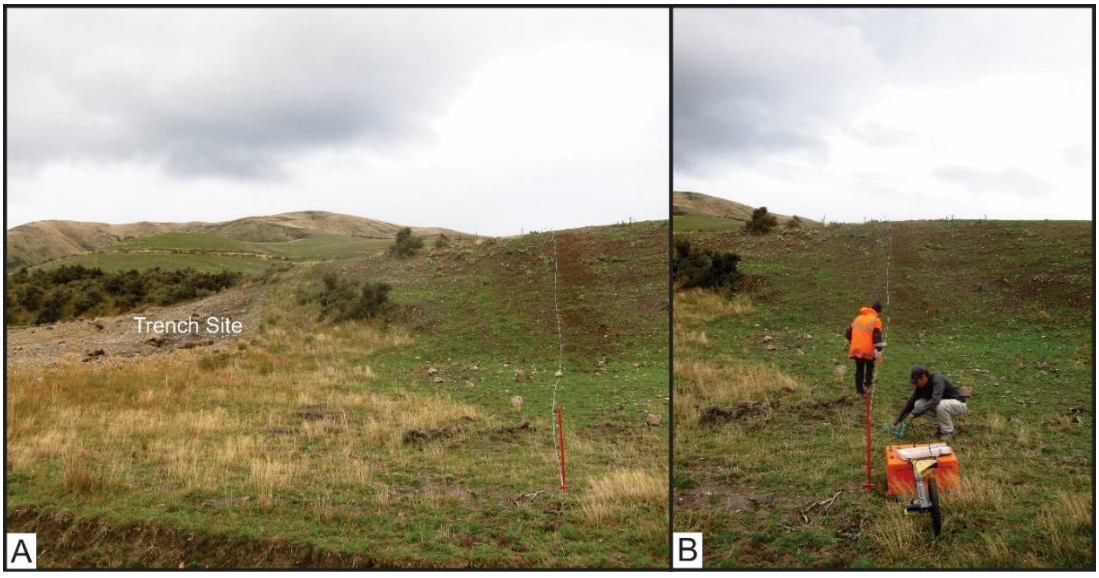

Figure 3.6: *A) Photo view of GPR trace parallel to trench site. B) Photo view of GPR survey in progress. Grid reference: 244996 579016.*

3.3 Results

3.3.1 Trench Stratigraphy

The paleoseismic trench was excavated into alluvial fan deposits. Full description and characterisation of all trench units is given in Table 3.1. The units display a series of channel deposits and a clear recent younger channel incised and infilled set into the older fan deposits. Some variation in grain size and sorting occurs within units both along and across the trench. The extent and definition of paleochannels was difficult to distinguish as they overlap and some are only partially visible due to erosion and re-deposition. In general, the deposits display fining of material from the bottom to top. Full trench logs of the north, east and south walls are presented in Figures 3.7, 3.8 and 3.9 respectively.

Table 3.1: *Summary of trench units and their characteristics.*

Unit Name	Deposit	Colour	Texture	Notes
1	Top soil	10 YR 2/1 10 YR 2/2	Soil	Some root matter, occasional small pebble, some large pebbles in lower section of unit.
2 (differentiated on South Wall only)	Wash deposit	10 YR 5/4	Silty gravel	Pebble to large cobble size clasts. Matrix supported. Poorly sorted.
3a (differentiated on South Wall only)	Fluvial deposit	10 YR 4/1	Silty gravel	Pebble to large cobble size clasts, clast supported, poorly sorted.
3b (differentiated on South Wall only)	Colluvial wedge Two	10 YR 4/1		Pebble to cobble size clasts, clast supported, some root material, displays evidence of faulting, sorting (large clasts at base of wedge)
3c (differentiated on South Wall only)	Wash deposits (Reworked fluvial deposit)	10 YR 4/2	Gravelly silt	Pebble to cobble size clasts, with significantly less cobble size clasts than "Unit 2a", less clasts in general, poorly sorted, some root material (modern), no evidence of faulting.
4 (differentiated on South Wall only)	Colluvial wedge One	10 YR 5/4	Gravelly silt	Some pebble and cobble size clasts, less iron oxidation then "unit 3), and evidence of folding in fabric.
5 (differentiated on South Wall only)	Fluvial channel deposits	10 YR 6/2 10 YR 6/3	Silty gravel	Some pebble size clasts, significant iron oxidation, and evidence of folding in fabric.
6	Stream Flood Deposit	2.5 Y 6/1	Sandy silt	Occasional pebble size clast, significant iron oxidation.
7	Fluvial channel deposits	10 YR 6/1	Gravelly silt	Large proportion of gravel sized clasts with occasional cobble size clast, small amount of iron oxidation present.
8a (differentiated on East Wall only)	Most recent Channel infill	10 YR 6/1 10 YR 5/2	Gravelly silts to silty gravel	Clasts range from pebble to cobble. Most recent channel infill. Gravel fining upwards to silt.
8	Channel deposits	10 YR 4/2 10 YR 5/2 10 YR 6/1 10 YR 6/2 10 YR 7/2 10 YR 7/1 10 YR 8/1	Gravelly silts to silty gravel	Clasts range from pebble to cobble. Channels reworking present.
8b (differentiated on North Wall only)	Fluvial deposits	10 YR 5/2 10 YR 4/2	Gravelly silt	Pebble size clasts. Occasional small cobble size clast.
8c (differentiated on North Wall only)	Fluvial deposits	10 YR 7/1 10 YR 7/2 10 YR 8/1	Silty gravel	Pebble size clasts. Occasional small cobble size clast. Some fining towards top of unit.
8d (differentiated on North Wall only)	Fluvial deposits	10 YR 6/2 10 YR 7/1 10 YR 7/2	Gravelly silt	Pebble size clasts. Occasional small cobble size clast. Poorly sorted
9	Stream flood deposits	10 YR 7/1	Medium to fine silt	Predominantly pebble size clasts, significant iron oxidation. Has large pockets of gravel with some cobble clasts
10	Stream flood deposits	Gley 2 5/5 BG Gley 2 6/5 BG Gley 2 6/10 BG	Silty clay	Occasional small pebble clasts
11 (differentiated on North Wall only)	Fluvial channel deposit	10 YR 5/3 10 YR 5/4 10 YR 5/2	Gravel	Poorly sorted, pebble size clasts to cobble size clasts. Pockets of brown silt near top of unit and lenses of blue-grey clay near base of visible unit.

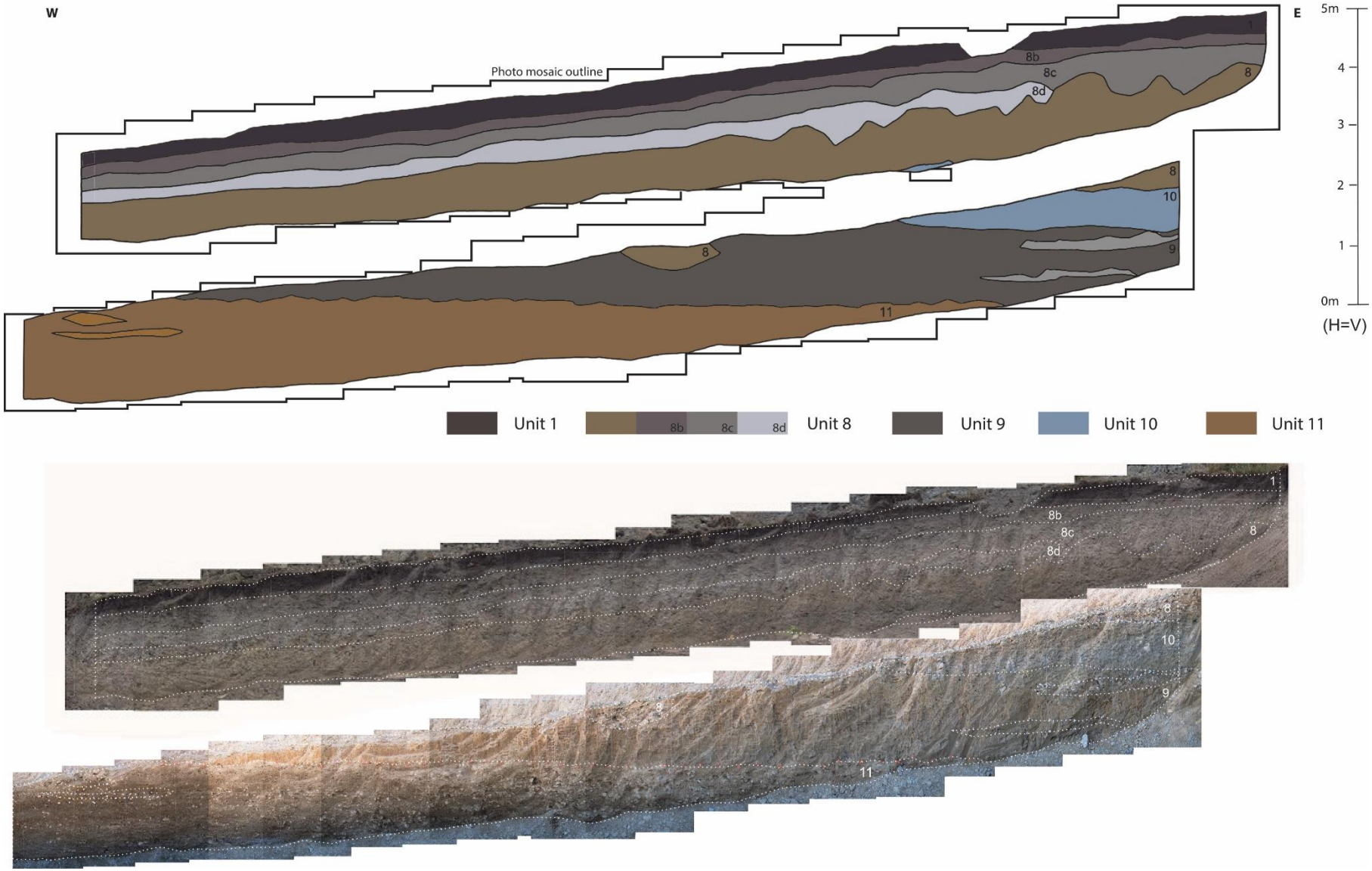

Figure 3.7: *Face log of North trench wall with accompanying photo mosaic.*

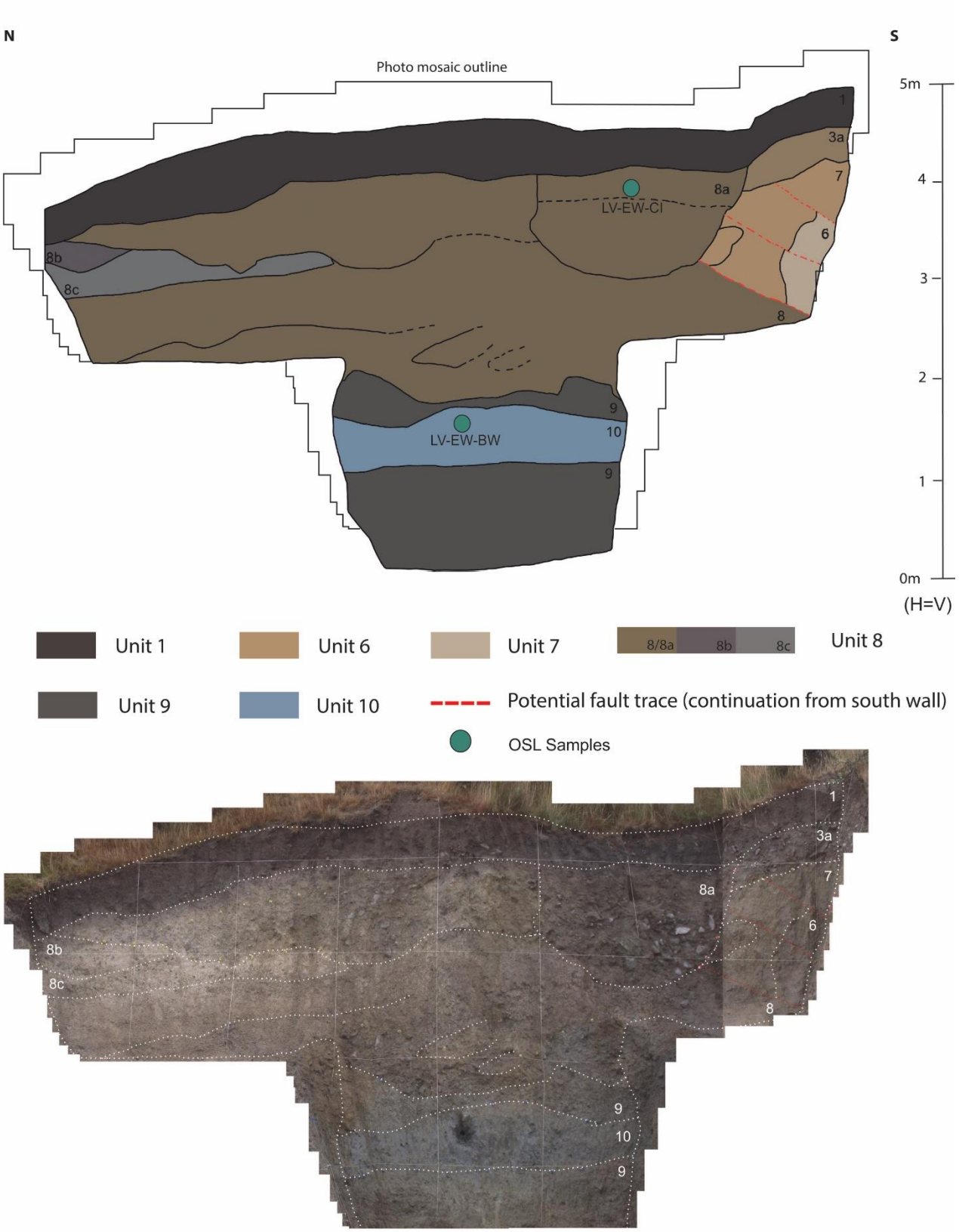

Figure 3.8: *Face log of East trench wall (end of trench) with accompanying photo mosaic.*

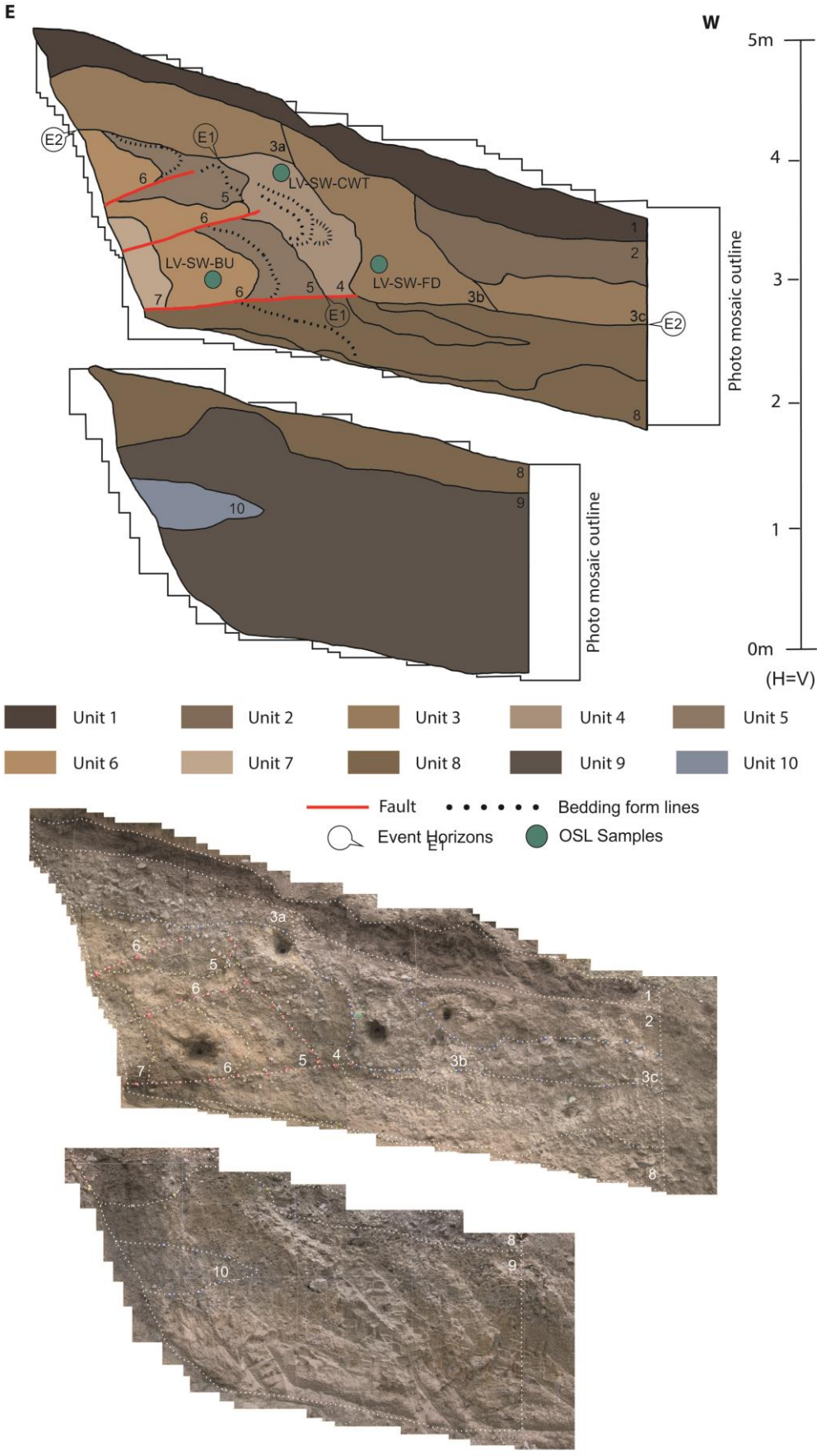

Figure 3.9: *Face log of South trench wall with accompanying photo mosaic.*

3.3.2 Optically Stimulated Luminescence Dating

The five OSL samples sent to the luminescence lab were selected in order to bracket the timing of the faulting events by indicating the age of materials deposited before, during and post faulting. Table 3.2 presents the results of the OSL ages received. Some recalculation accounting for variability in water content was performed although the adjusted results did not vary significantly therefore they have not been included in the final results. For these additional results see the attached appendices (Appendix C).

Table 3.2: *Summary of OSL samples and assigned ages (Figure 3.5).*

Laboratory code *	Field code	Depth (m)	Water %	Total dose rate (Gy/Ka)	Equivalent dose (Gy)	Optical age (ka) **
WLL1165	LV-EW-BW	3.33	17	3.79±0.19	21.24±0.65	5.6±0.3
WLL1166	LV-EW-CI	0.70	10	4.19±0.15	57.12±3.98	13.6±1.1
WLL1167	LV-SW-CWT	0.60	9.3	4.63±0.13	97.12±4.35	21.0±1.1
WLL1168	LV-SW-FD	1.09	9.9	4.37±0.15	96.62±7.14	22.1±1.8
WLL1169	LV-SW-BU	1.82	13.1	4.39±0.16	95.13±6.17	21.7±1.6

*All samples analysed at the Victoria University of Wellington OSL Laboratory with measurements taken of blue luminescence from fine-grained feldspar produced during infrared stimulation.
**All ages for the multiple aliquot additive dose method (Wang, 2015), reported with 1 σ uncertainties.

Sample LV-EW-CI was taken from a gravel infilled channel, representing the youngest material in the trench (Figure 3.8). The channel fill displays no evidence of being faulted within the trench (Unit 8a). The gravel infill fines upward with large cobbles in a sand matrix at the base grading to small cobbles and pebbles then sandy gravel at the top. The OSL sample was taken 23 cm below the top of the unit in the sandy gravel section. The sample yielded an optical age of 13.6 ± 1.1 ka suggesting a Late Pleistocene deposition.

Sample LV-SW-BU came from an alluvial sandy silt with occasional pebble clasts (Unit 6) (Figure 3.9). The unit has been offset by all three fault splays and correlates with unit 9, below the main, lowest fault, and is continuous across all three trench walls. The sample was taken 38 cm below the top of the unit and yielded an optical age of 21.7 ± 1.6 ka.

LV-SW-CWT was obtained from a gravelly silt colluvial wedge with large cobble clasts at the base fining upward to pebble size clasts (Unit 4) (Figure 3.9). This unit also displays evidence of faulting as the fabric displays fault related folding. 15 cm below the top of the unit in the finer grained silt this sample gave an OSL age of 21.0 ± 1.1 ka.

From the unit above, sample LV-SW-FD was obtained from a silty gravel, colluvial wedge (Unit 3b) (Figure 3.9). It has clast sizes from pebble up to cobble, with the large clasts

situated at the base of the unit where there is little to no matrix and it is clast supported. The unit fines upwards to silt. From within the fine grained silt 78 cm at the top of the unit the OSL sample yielded an age of 22.1 ± 1.8 ka.

The final sample LV-EW-BW was taken from a silty clay with rare small pebble clasts (Unit 10) (Figure 3.8). Unit 10 is most prominent in the East wall and quickly pinches out in both the North and South walls giving it a wedge shape. The OSL sample taken from the East wall, 26cm from the top of the unit gave an age of 5.6 ± 0.3 ka.

3.3.3 Faulting Events

There are three fault splays evident on the South wall above the bench that trace into the top south corner of the east wall (Figure 3.9). Each thrust fault splay has a shallow dip to the South-East and offsets both gravel and silt units. The visible section of the bottom splay has a length of 1.9 m. The trace is clearly defined by a sharp boundary between Unit 8 beneath and the series of cut off Units 7, 6, 5, and 4 above. It is not possible to correlate the offset units directly across the lower fault but there is at least a 1.9 m separation, based on the offset of Unit 6 across the trace, the exact net slip offset cannot be measured. The second splay extends over 1.3 m and cuts through units 7, 6, 5, and 4. Unit 6 is offset by separation of 50 cm across the fault here. The top splay extends 0.9 m and unit 6 has been separated here by 38 cm. An unconformity lies between the units 6, 5, 4 and 8 that have been eroded and overlain by unit 3. The units 8, 9, 10 and 11 all below the lowest visible fault trace, reveal no evidence of faulting within the extent of the trench excavation.

The dip and projection of the faults logged in the trench walls show they extend eastward. The full extent of the faults and their offset are not measurable, ideally the trench would have extended further east into the scarp. However, the trench was ideal for exposing the fault, its offset, revealing the nature of the fault dip and slip, and the fan deposit relationships. GPR was undertaken to investigate the nature of the fault and units at depth beyond the extent of the trench is discussed now.

3.3.4 Ground Penetrating Radar

The 200 MHz shielded GPR investigation provided insufficient data for post processing data interpretation, no irregularities or offset features were picked up within the reflectors hence further testing with different configuration was undertaken. 100 MHz non-shielded provided poor resolution and indicated there was a lack of penetration at this location. Hence 50 MHz

was used to increase resolution with the penetration possible. The limited penetration using 50 MHz meant very few reflectors could be resolved at depth, resulting in reflectors imaged to a depth of 2-3m. While there was an increase in resolution, clear relationships from reflector offsets were still not imaged in the profile data.

It is possible the deformational structures were at a depth not imaged clearly in the data due to the lack of penetration. It is also likely the fan gravel units have severely affected the ability of the radar to pick up the structural offset/dislocations needed to produce a clearly imaged reflection. The chaotic mix of the gravel beds and channelized units make it hard to pick up structural features as there is a lack of difference in material properties either side of the target features. Furthermore the presence of very fine silt and clays with high water content may be present at shallower depths alongside the trench than what was found within the trench which could explain the lack of penetration achieved.

Due to the lack of clear and accurate data it is not possible to make any interpretations, beyond highlighting the difficulties of using GPR to study faults in this type of terrain. Hence, this method of investigation and results will not be discussed further. For additional information see attached appendices for the GPR profiles.

3.4 Discussion

3.4.1. Limitations of Trench Findings

While the Lees Valley Fault surface expression is discontinuous through the valley as indicated by the step-over (refer to Figures 1.4 & 2.25) and varies in expression between the northern valley and the southern valley, it is likely linked at depth and ruptures simultaneously. This indicates its behaviour during a faulting event may vary as a result of different topographic loadings and material properties. As a consequence, findings from the paleoseismic trench can only be definitively linked to that particular section of fault trace investigated. However, it is likely that given the linked nature and structural continuity of the fault, these findings can be inferred to the entire fault trace.

3.4.2 Trench Stratigraphy

The range of grain sizes reflected in the trench deposits indicates both high and low energy environments, from large cobble down to clay respectively. This type of variation is to be expected in a fan deposit environment where channels wind over the fan surface, shift around

over time, become eroded and refilled. Characteristics of the deposits is controlled by the rate and duration of uplift of the nearby ranges and regional climate (Bull, 1974). The various deposits from such a setting can include; stream flow channel deposits, debris flow lobes and levee deposits, sieve deposits and stream-flood and old channel deposits (Figure 3.10).

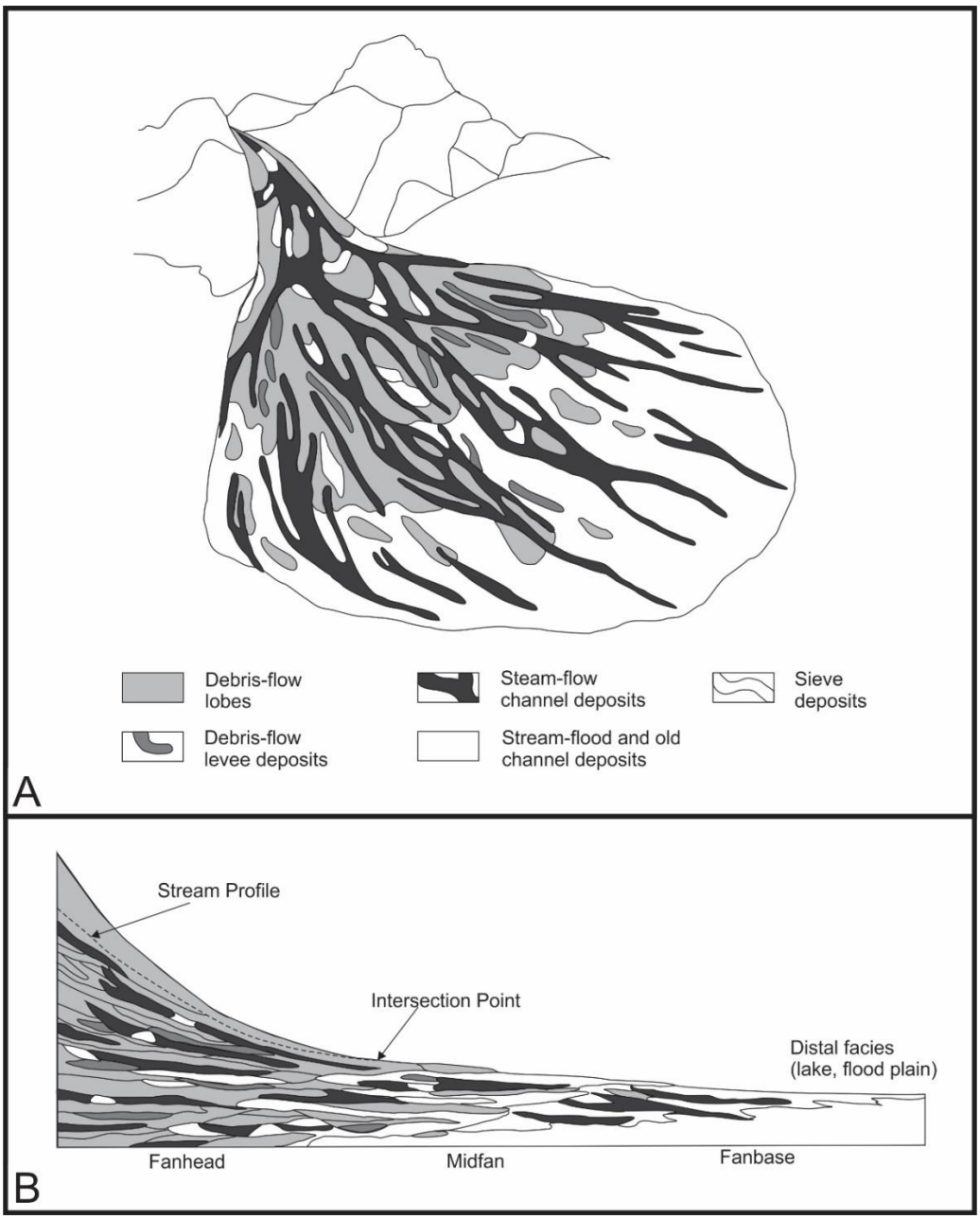

Figure 3.10: *A) Schematic diagram of a fan deposit environment. B) Expected nature of deposits. Modified from Spearing (1974).*

The trench cut directly into the middle of the small fan deposit which is why variation in grain size occurs both across and along the trench as the drainage system deposition changes during the evolution of the fan. Both cross section aspects of the channel deposits can be seen in the trench, lengthwise and crosswise. The cross-cutting braided nature of fan deposits

makes it difficult to trace individual channels within the trench. Some fining is noted within units due to nature of high energy system shifting to low energy as the flow levels change and the sinusoidal nature of channels resulting in different sections of the channel being exposed in the trench walls.

3.4.3 Optically Stimulated Luminescence Dating

The position of Unit 10 near the base of the trench and its stratigraphic relationship to the other sampled units would suggest the unit is the oldest of those sampled. The determined age was expected to help bracket the faulting events. However, the OSL sample (LV-EW-BW) gave an age of 5.6 ± 0.3 ka, displaying the youngest OSL age determined. The relationship of Unit 10 to the thrust fault is not recorded within the trench exposure. Although given the age inconsistency with the other samples obtained from units stratigraphically higher in the trench, it is possible it has been faulted causing it to display a younger age. The structural relationship behind this result cannot be determined from information provided by the trench.

Samples of channelised sands and gravels from the Canterbury Plains have returned OSL ages from feldspar between 20 – 33 ka (Hornblow et al., 2014). Other OSL ages from coarse-grained quartz have indicated the Canterbury plains formed during two sediment accumulation periods between 18 ± 1.3 ka and 36.7 ± 2.9 ka as a result of glacial outwash followed by river reworking (Rowan et al., 2012). The most recent deposition 18 – 24 ka had the most sediment accumulation and coincides with the LGM ice maxima. Although not directly correlatable to Lees Valley, these ages match most of the OSL dates found in the Dalzell Trench. Assuming the OSL ages are a true representation of the units depositional age this would indicate a corresponding deposition in Lees valley during the LGM. While no glaciers entered Lees Valley they reached a glacial extent to the Puketeraki Range, west of the Pancake Range (Rother, 2006) and climate at the time would have increased erosion and corresponded to gravel deposition. The three OSL ages that constrain the faulted sediments are very similar and overlap within error and the modern channel deposit is younger as is expected and stratigraphically correct suggesting these ages are reliable. However, this correlation is tenuous and further explanations need to be investigated.

There are many potential explanations for unexpected or inconsistent ages in OSL dating. They can be caused by insufficient bleaching before burial, which would result in an older than expected age or mixing of sediments which could cause older or younger ages (Aitken, M. J., 1998; Cunningham et al., 2015). Uncertainty factors such as moisture content and

heterogeneity of sediments also have significant effects on the accuracy of dose rate and therefore age estimations (Guerin et al., 2011). The depositional environment has an effect on age determination accuracy as water lain deposits can display significant grain to grain bleaching variability (Aitken, M. J., 1998; Cunningham et al., 2015). Reworking of sediments and intermittent exposure to sunlight also causes unexpected ages. Furthermore anomalous fading, leakage of electrons from thermally stable electron traps, can result from disequilibrium in the uranium decay chain and disparities in past sediment water contents. Systematic error also causes inconsistencies in results through calibration of laboratory radiation sources, possible light contamination during field sampling and accurate determination of the environmental dose rate.

During field work all of the samples were collected on the same day, seven days after opening of the trench, except one (LV-SW-CI) which was obtained on day three. Care was taken to obtain every sample from the centre of each unit and let no light enter the sample tube while taking the sample and removing it from the trench wall. The sample tubes were long enough that should there be some light contamination at the ends the majority of the sample in the centre of the tube would remain uncontaminated for testing in the lab. Each sample was carefully sealed and packed in order to prevent light contamination and any material agitation during transport. They were all stored in the same place under identical conditions, not exposed to direct sunlight or extreme heat. Therefore it is unlikely that any unexpected age relationships have occurred as a result of error during field attainment of these samples

Sample LV-EW-BW was taken from a silty clay which appears to have not been deformed by faulting from evidence within the trench. As it is a clay deposit and water content may vary significantly to the coarser grained gravel deposits, water content was recalculated for the samples to take into account full saturation for finer grained sediments. The adjusted results did not differ significantly indicating variation in water content is not responsible for the significant difference in ages between the samples.

Given the consistency of the other samples it is possible the age determined for LV-EW-BW is not a true reflection of the unit age. The most likely causes of the age inconsistency with sample LV-EW-BW, given this scenario, could be tunnel gully erosion and infill, bioturbational sediment mixing or complex subsurface morphologies. No tunnel gully erosion is observed at the surface elsewhere along the valley, so it is unlikely this process has

influenced the deposit. Likewise there is no evidence for sediment mixing in the trench deposits which indicates this is an unlikely cause. Hence the most probable explanation for an anomalously young age, that is a true reflection of the deposition age, is that there is a complex subsurface structural relationship beyond what is visible in the extent of the trench that is affecting the morphology of this unit.

The final scenario to consider is that the sample LV-EW-BW is the only true reflective depositional age out of all of the samples. This would suggest the other samples are showing older ages than their true unit depositional age as a result of insufficient bleaching before burial. Therefore, their ages are more reflective of their source material age. Given the overlap within error (excluding the young channel infill, sample LV-EW-CI), it is possible they have come from the same source material. It is not possible to give a definitive explanation for the anomalous relationship between the ages, however, the most likely explanation is that these samples have not been sufficiently bleached and their deposition age is likely to be younger than indicated.

3.4.4 Timing of Past Events

In order to assess the probability of a future surface rupturing earthquake on the Lees Valley Fault, the timing of paleoearthquakes must be constrained. The timing of the most recent surface rupturing event (MRE) has been constrained by ages obtained from the Dalzell trench. Structures in the trench indicate the number of events and fault behaviour. The three fault splays exposed increase in their dip upwards, indicating stacking of fault splays may have occurred due to accumulated slip (McCalpin & Carver., 2009) (Figure 3.11). However, due to the ambiguity of the age constraint and the uncertainty in the timing of these events there may be alternative explanations for these findings

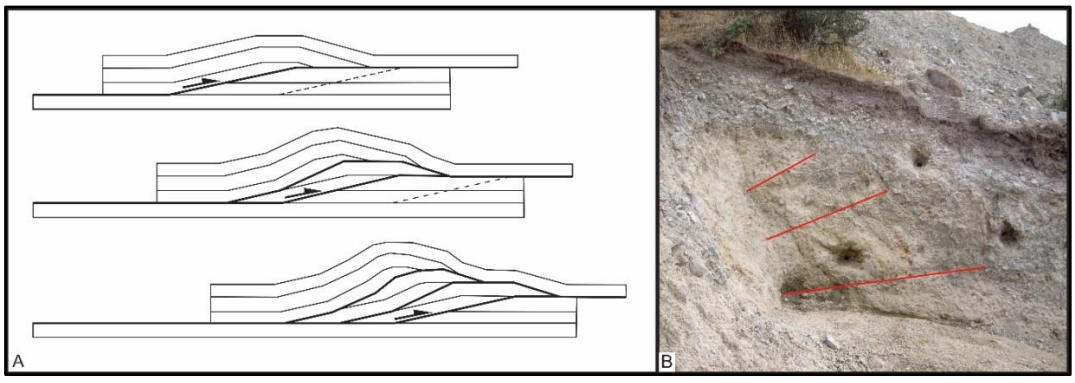

Figure 3.11: *A) Schematic diagram of a thrust fault duplex development through progressive failure. Diagram after* Souque *et al. (2003). Note comparison to B) fault splays exposed in trench.*

Sample LV-SW-CWT was obtained from a colluvial wedge that suggests deposition shortly after scarp formation, and provides an age of 21 ± 1.1 ka (Figure 3.9). The event horizon (E1) at the base of the unit is inferred to closely correspond to the timing of the rupture. Sample LV-SW-BU was obtained from sediment deposited prior to faulting which has been offset and deformed during the faulting event, which gives an age of 21.7 ± 1.6 ka (Figure 3.9). The two ages overlap within error; their correlation could indicate these units have close timing in deposition. Sample LV-SW-FD was obtained from the unit above sample LV-SW-CWT within what has been interpreted as another colluvial wedge. These two units are separated by an event horizon (E2) extending along the whole trench south wall and unconformably overlies Units 4, 5, 6 and 8. This sample also has an age within error of the previous samples, 22.1 ± 1.8 ka. The similarity of these ages could suggest that while there may be two discrete faulting events, they have occurred very close together in time.

Alternatively, the two colluvial wedges (samples LV-SW-FD and LV-SW-CWT) may be derived from reworked sediment (~ 21 ka) that has not been adequately exposed to light during re-deposition, and therefore not completely bleached. As discussed in the previous section (Section 3.4.3) they may be displaying significantly older OSL ages than their actual age of re-deposition. This is a plausible scenario and the most likely explanation for these close deposition ages. Therefore, the only conclusion that can be made from this data is that two events occurred after 21.6 ± 2.3 ka at undetermined times. Furthermore, any further interpretations of fault characteristics based on the trench data should be regarded as minimum estimations, as incomplete bleaching may have led to anomalously old OSL dates for faulting.

Separating the timing of the fault rupture events or the period of time elapsed between events is not possible due to the overlap in ages. The interpretation of faulting and unit relationships gives the impression the timing is close together as the two events appear to have offset sediment of close ‘depositional’ age. Additionally there is no evidence for paleosoils occurring between the units indicating there has not been sufficient time for organic soil development. However, given the depositional environment of highly variable alluvial deposits of low water holding capacity and low organic matter, it is unlikely there would be rapid soil formation regardless, particularly during the LGM. Given the apparent close timing in deposition, the second colluvial wedge may have formed from an aftershock following the main event. Furthermore, given the minimum age calculations of deposition and possible gap

in deposition, a second separate faulting event may have formed the second colluvial wedge. A possible and preferred most likely sequence of events is outlined in Figure 3.13.

The maximum age of faulting is constrained as 21.6 ± 2.3 ka, the average age gathered from the faulted deposits. As these alluvial units must have been deposited prior to faulting. Likewise, the minimum age of faulting is constrained by the oldest undeformed deposit, as it is the first unit to form following fault rupture. The only unit visible within the trench that can confidently be identified as unfaulted is the most recent channel infill, dated by sample LV-EW-CI at 13.6 ± 1.1 ka. This is evident in the fault trace terminations against the channel edge in Figure 3.8, indicating the channel has cut through and eroded the faulted deposits, hence it must have formed post faulting. Furthermore at the surface the uplifted fan deposit and fault scarp have been cut into and degraded by this channel, supporting its post faulting age of formation. However, the age of this sample may be subject to the same limitations of insufficient bleaching as the others and the unit may be younger than the sample suggests, indicating faulting may also be younger than shown by this data.

Therefore, assuming these constraints are reliable, the faulting episode recorded in the trench can be roughly constrained to an 8,000 year period between 21,600 years ago and 13,600 years ago. However, given the ambiguity of the ages the faulting episodes may be younger. Due to multiple possible interpretations from the trench data, a logic tree was created to show each of these scenarios and select the most likely (Figure 3.14). Consequently, the most likely scenario infers the majority of faulting and deformation observed in the trench occurred during a single seismic event which formed all three fault splays and first colluvial wedge. Following this, there was erosion and a reactivation of the fault splays, causing further offset and creating another colluvial wedge.

A recent historic event in Taiwan, the Chi-chi earthquake of 1999 provides insight into thrust fault-ground surface (structural style) interaction similar to that found in the Dallzell Trench. The rupture on the Chelungpu fault formed a principal thrust scarp 2-3 m high (west-facing) with smaller back-thrust scarp (east-facing) (Lee et al., 2004). The basal thrust dips 12˚-35˚ and flattens towards the ground surface and the footwall strata displays only minor drag deformation (Lee et al., 2001). Borehole data revealed Holocene alluvium and fluvial Quaternary deposits, overlies the Pliocene bedrock (Lee et al., 2004). Exposed in the Wufeng trench is lower cobbly gravel fluvial deposit and upper overbank sand deposit capped by cultivated soil (Figure 3.12), similar to the lithology exposed in the Dalzell Trench. A multi-

stage process of faulting, folding and scarp development has been interpreted from the trench where the primary thrust ruptured then became more complex as it approached the surface as the wedge thrust structure formed and then the buckle, aniticlinal fold with two secondary thrusts forming coincident with the anticline growth (Figure 3.12) (Lee et al., 2001 and 2004). The anticline is interpreted as forming in the 1999 event due to the warping of sediments and the youngest deposits do not thin over the crest of the fold (Chen et al., 2007). Similar strata and thrust faulting in the Dalzell Trench has likely led to a similar multi-stage process, structures and characteristics such as the shallowing basal thrust, secondary thrusts, folding of strata and slump deposits.

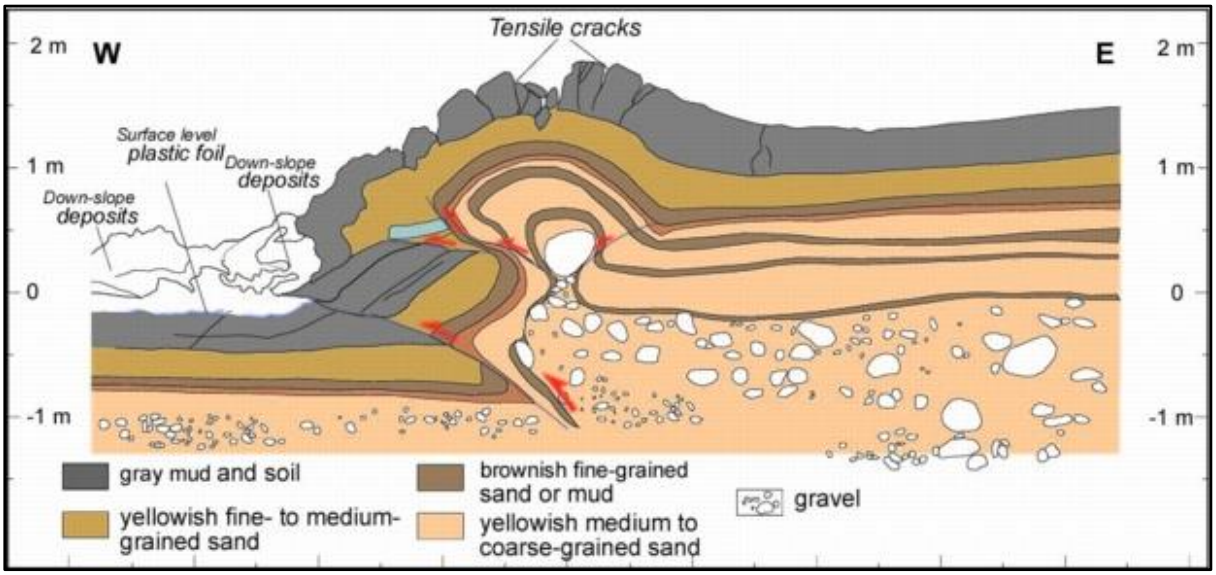

Figure 3.12: *Wufeng trench wall log showing geologic contacts, faults and associated structures from Lee et al. (2004).*

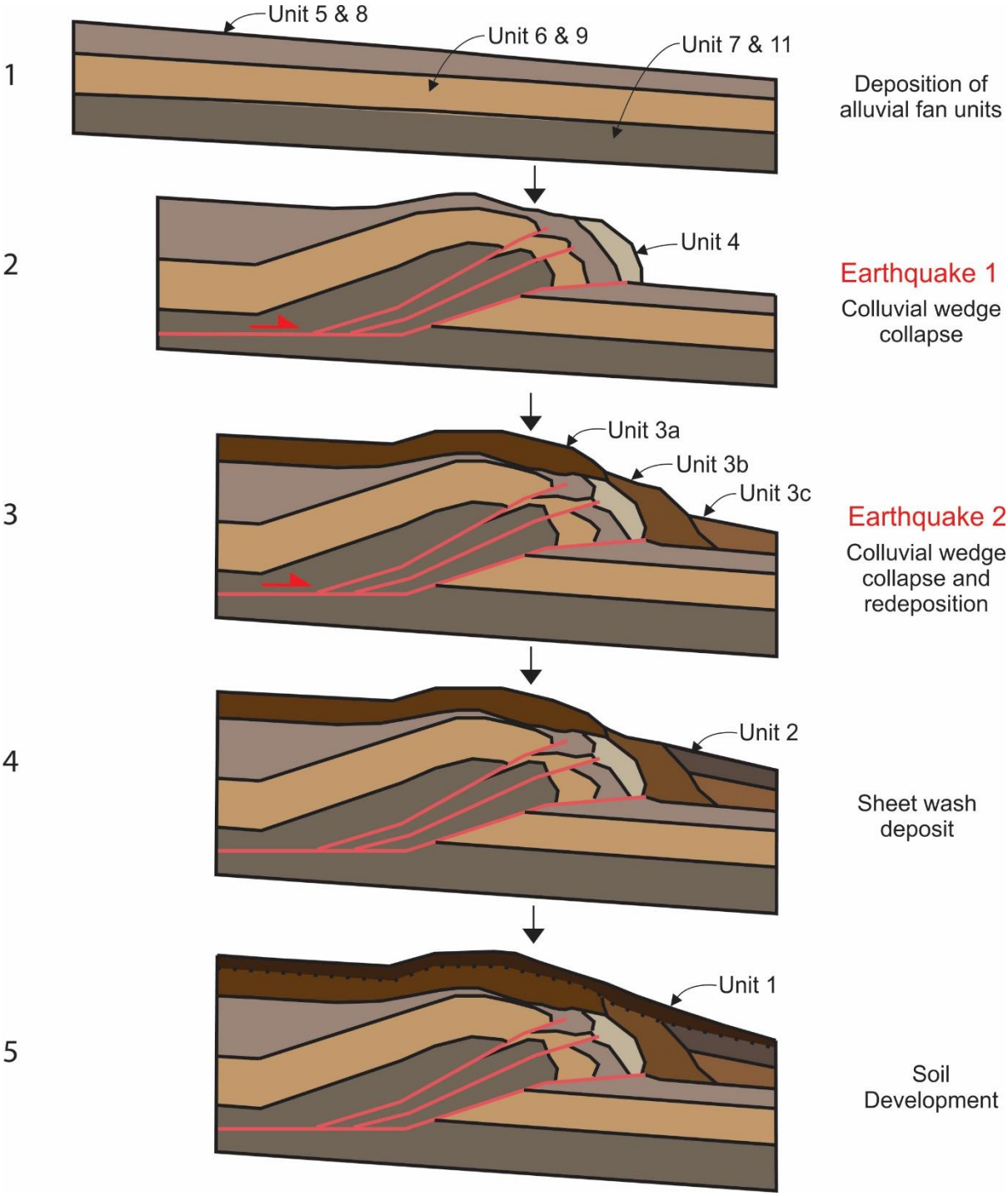

Figure 3.13: *Reconstruction diagram of series of events that led to present formation in trench. 1) Deposition of fan units channel gravel and stream flood deposits (Units: 5, 6, 7, 8, 9 & 11). 2) Earthquake 1 which caused colluvial wedge collapse (Unit 4). 3) Earthquake 2, reactivation on fault, another collapse and formation of a second colluvial wedge – redeposition within wedge (Unit 3b) and reworking and redeposition (Unit 3c). 4) Channel flood/Sheet wash deposit (Unit 2). 5) Soil formation (Unit 1).*

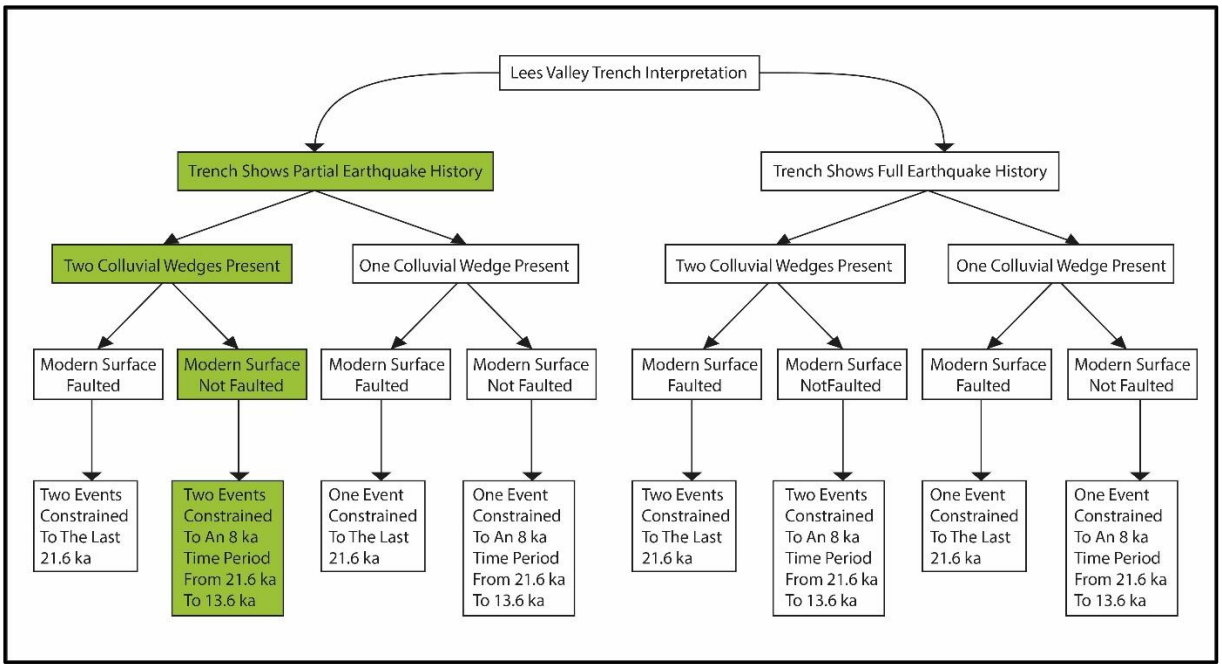

Figure 3.14: *Logic tree for possible scenarios interpreted from the trench with the most plausible scenario highlighted.*

3.4.5 Slip Rate for Lees Valley Fault

Based on data from the trench, the slip rate has been calculated using two different methods. The first is using measured offset (minimum offset) on each fault and the average age of all three OSL samples from offset material of 21.6 ± 2.3 ka. The upper fault and middle fault exposed in the trench have measured offsets of 38 ± 1 cm and 50 ± 1 cm, respectively. The full extent of offset in the lower fault splay is not visible in the trench and there is no direct correlation of units either side of the fault, however minimum offset is 86 ± 1 cm. These offsets give minimum slip rates of 0.02, 0.02 and 0.04 mm/yr respectively, and a combined slip rate of 0.08 mm/yr. However, because the full offset cannot be measured in the trench, this is a conservative minimum estimate only. Furthermore offset measurements are limited to one unit due to the lack of correlation for the other units either side the fault traces. Substantial ground movement is also accommodated by fault related folding (McCalpin, 2009), as these estimates are based only on fault slip they will significantly underestimate total movement and true slip rate. Folding is evident in the nature and fabric of the trench deposits (Figure 3.9) indicating that deformation has been accommodated in both discrete faulting and associated folding in this location. Therefore true slip rate calculation must also account for this deformation, as this estimate has not taken folding into account the true slip rate is expected to be significantly higher (~0.4/0.5 mm/yr).

The second method of calculating slip rate is to use the total vertical displacement calculated from GPS profiles of the fault scarp. This method includes all deformation along each fault splay and folding within the fault scarp into the slip rate estimations. Hence the parameters calculated from a profile scarp adjacent to the trench site are likely to be closer to the true cumulative offset in the scarp. The scarp height is 10.5 m at this location, using fault parameters measured in the trench (fault dip of 23º) the calculated dip slip cumulative from hanging wall and footwall is 24.5 m while the total vertical displacement is 8.5 m (refer to Figure 2.18). Combining this offset data with the maximum faulting age of 21.6 ± 2.3 ka, this produces a slip rate of 0.4 mm/yr, a more realistic estimation.

Each method gives very different slip rate results. The first method describes discrete fault slip rate only, it does not account for entire deformation in scarp, and is limited by the extent of fault traces visible in the trench. While the second method describes the vertical slip required to produce the entire deformation in the scarp. However, this method is limited by GPS data accuracy and ambiguity in OSL ages and therefore also contains some uncertainty. Therefore the more reliable method in this instance is estimating from GPS profiles, as it provides a better estimate of the slip rate required to produce the observed deformation. Hence the most likely slip rate for this section of the Lees Valley fault is ~0.4 mm/yr. Furthermore calculation of slip rate using the average slip per rupture and recurrence interval discussed in the following section (Section 3.4.6) also yields a slip rate of 0.4 mm/yr (1490 mm/ 3600 years = 0.41 mm/yr).

Previous estimates of slip rates for the Lees Valley Fault have indicated an average vertical slip rate of 0.4 mm/year (Barrell & Begg, 2013) and an uplift rate of 2.5 – 5.0 mm/yr (Garlick., 1992; Pettinga, 2001). Barrell and Begg (2013) used a cumulative vertical offset of ~10 m on the splinter faults/monoclines of the southern valley and an estimated age of 18,000 years for river plains they offset, to estimate a slip rate for the fault. Amount of offset was roughly estimated and the surface age is based on the termination of the last ice age and subsequent surface formations. Hence the slip rate estimate is not expected to be highly accurate and not applicable to the range-bounding fault given the estimate is based off structural and geomorphic features of different orientation distorting the basin floor. An uplift rate for the Lees Valley eastern ranges has been suggested between 2.5 – 5.0 mm/year since the fault became active (Garlick., 1992; Pettinga, 2001) although this estimate is not well constrained. Garlick (1992) based this estimation off data such as projected throw of the rangefront which incorporates folding and uplift from structures on opposing sides of the

range. Timing of events was based on broad time scale ranges such as fan aggradation during the Pleistocene, followed by quiescence, then uplift during the late Otirian – early Holocene. The minimum number of uplift events was suggested as four based on a series of uplifted fan surfaces. Given the significant amount of error and poor constraint on these estimations the given uplift rate suggested by Garlick cannot be associated to the expected slip rate along the Lees Valley Fault. The new calculated slip rate of 0.4 mm/yr does, however, match with the estimated value of Barrell and Begg (2013) despite its significant error margins and limited association with the range-bounding fault zone.

Limitations on the new slip rate calculated in this study include the uncertainty of the OSL dates, given the fan deposition environment and the complication of recycling of material and the possibility of the deposits not being completely bleached during transportation, and therefore displaying older ages than expected (Aitken, M. J., 1998; Cunningham et al., 2015). More accurate ages could be obtained if radiocarbon samples were located for dating offset deposits. Furthermore, these estimates of slip rate can only be applied to this section of the Lees Valley Fault as they have been based on measurements from fault scarp analysis of the one fault trace. There are multiple fault traces within the Lees Valley Fault system which may display variability in fault characteristics. Due to limited fault data in the southern valley and given the variability in fault slip orientation and expression it is not possible to infer the same slip rate as calculated for the northern valley fault trace. It is also possible there are other splays in the fault system which are active and accommodate a different slip rate given the nature of the basin-ward evolution of faulting.

3.4.6 Slip per Event and Recurrence Interval

The data gathered from the trench and scarp profile analysis indicates multiple events have produced the significant amount of deformation present along the rangefront fault trace, given the development of more than one colluvial wedge in the trench and a vertical displacement of 8.5 m. Historically in New Zealand it generally requires an earthquake with Magnitude Mw 7 or higher to generate ground surface rupture on faults, as demonstrated by the Mw 7.3 earthquake in Murchison in 1929, the Hawke's Bay Mw 7.4-7.6 earthquake in 1931 and the Darfield Mw 7.1 earthquake on 4 September 2010 (Townend et al., 2012; GeoNet, 2015a). A notable exception was the Mw 6.5 Edgecumbe Earthquake in 1987 (GeoNet, 2015a). Expected offset from a Mw 7 or above earthquake would be ~2 m given Wesnousky scaling relationships (Wesnousky, 2008). Therefore it is expected the scarp

height deformation recorded on the Lees Valley Fault is the result of multiple earthquake events.

To determine single event displacement, a simple estimation can be made when a characteristic earthquake model is assumed (McCalpin, 2009), while utilising the number of events and scarp height. The vertical displacement at the trench location is 8.5 ± 0.4 m. Using the most probable scenario from the logic tree, at least two events constrained to an 8.0 ± 3.4 ka time period from 21.6 ±2.3 ka to 13.6 ± 1.1 ka, a single event vertical displacement estimation would yield 4.25 ± 0.2 m.

Other methods include using scaling relationships. Wesnousky (2008) determines the average slip per event by assessing the relationship between fault type (strike-slip, normal and reverse) and surface rupture length. The equation Wesnousky provides for average single event displacement is; $Slip\ (m) = C\ x\ Length\ (km)$, where 'Slip' is the co-seismic surface slip. The constant '*C*' is 0.06 for calculating average geological slip, and 0.21 for maximum geological slip in relation to reverse faults.

The surface rupture length for the Lees Valley Fault can be divided into three possible rupture sections as measured in this study. The northern valley and the southern valley sections could rupture individually, or they could rupture together as a full fault trace event. The possible rupture section scenarios are listed with their single event displacements in Table 3.3 with fault length measurements from this study.

Table 3.3: *Variation in single event displacement using Wesnousky (2008) scaling relationship for reverse faults applied to the Lees Valley Fault.*

Section of Fault	Length (km)[1]	Average Single Event Displacement (m)	Maximum Slip (m)
Northern Valley	7.6 ± 0.38	0.46 ± 0.02*	1.60 ± 0.07*
Southern Valley	17.2 ± 0.86	1.03 ± 0.05	3.61 ± 0.18
Entire valley	24.8 ± 1.24	1.48 ± 0.08	5.21 ± 0.26

*Not reliable given the scaling relationship is most accurate for surface rupture lengths greater than 15 km (Wesnousky, 2008).

[1]Length error calculated using 5% to account for measuring inaccuracy.

Given these fault length measurements, the average single event displacement could be anywhere between 0.46 ± 0.02 – 1.48 ± 0.08 m, depending on whether the event has ruptured the entire trace or smaller segments. It is important to note the model is focused on faults larger than 15 km in length therefore estimations based on faults shorter than 15 km are not likely to be modelled accurately. Furthermore in order to generate surface rupture in the Canterbury region an earthquake should typically be ≥ Mw 7 which is unlikely to be

produced by faults of shorter length. During the Canterbury earthquakes of 2010 – 2011, reverse faults of lengths 8 – 12 km did not cause surface rupture. Hence it is unlikely the surface rupture observed in Lees Valley has been produced by rupture along an individual segment, rather faulting has occurred along the entire fault trace during a seismic event. Therefore, the minimum average single event surface displacement is most likely to be 1.48 ± 0.08 m. Similarly, the maximum slip possible on the fault at depth also has a range of 1.60 ± 0.07 – 5.21 ± 0.26 m, with a likely slip of 5.21 ± 0.26 m given full trace rupture. The ground surface rupture is more closely correlated with the average surface displacement, therefore the 1.48 ± 0.08 m average displacement per event will be used to calculate the recurrence interval.

This estimate is conservative as the actual length of rupture during a seismic event could extend beyond what is estimated to be the extent of the fault. The Lees Valley Fault has been noted to potentially extend beyond the Lees Valley into a smaller basin North of Okuku Hills (Barrell and Begg, 2013), which has not been investigated in this study. Furthermore the connection of Lees Valley to Townshend Fault is not well understood. Increasing the length of the surface rupture length would alter the displacement and slip calculations.

Given the interpretation from the trench, analysis of the fault scarp profile, OSL ages and the approximate single event displacement an estimate on recurrence interval can be made. The recurrence interval is dependent on the number of earthquakes interpreted to have formed the deformation observed along the fault scarp. With a total vertical displacement of 8.5 ± 0.4 m on the fault scarp adjacent to the trench and an estimated average single event displacement of 1.48 ± 0.08 m it would require six rupture events to produce this deformation. Given this information and the average age of the oldest offset material (21.6 ± 2.3 ka) a recurrence interval of 3.6 ± 0.3 ka is suggested for the Lees Valley Fault. This places the fault in Recurrence Interval Classification III of Kerr et al (2003) (Table 3.4). However, as the average single event displacement is dependent on the fault surface rupture length which is not well constrained, this recurrence interval is also not well constrained. Given the minimum estimation of the surface rupture length the calculated recurrence interval should also be treated as a minimum estimation. An expected longer fault rupture length would increase expected average single event displacement resulting in less events necessary to produce the observed offset. In turn this would produce an expected longer recurrence interval.

Table 3.4: *Fault recurrence interval classes from Kerr et al (2003).*

Recurrence Interval Class	Average fault recurrence interval of surface rupture
I	≤2000 years
II	>2000 years to ≤3500 years
III	>3500 years to ≤5000 years
IV	>5000 years to ≤10,000 years
V	>10,000 years to ≤20,000 years
VI	>20,000 years to ≤125,000 years

Barrell & Begg (2013) suggested a recurrence interval of 4,500 years based off a younger rupture age of 18,000 years and assuming a larger vertical deformation of 2 m per event. Garlick (1992) and Pettinga et al. (2001) gave a recurrence interval range of 3000 – 5000 years and 2000 – 5000 years respectively. This study found the offset deposits to be older than previously expected and the average single event vertical displacement to be less. This accounts for the difference in findings, although the new recurrence interval is within range and same recurrence interval class as previous estimates in previous studies.

3.4.7 Magnitude

Fault scaling relationships can also be used for calculating possible earthquake magnitudes. The scaling relationships of Wells and Coppersmith (1994) are widely used although some discrepancies exist between estimations using these relationships and historical records for South Island earthquake magnitudes (Stirling et al., 2002; Howard, 2005; Quigley et al., 2010). The Canterbury region displays high ratios of magnitude to surface rupture length in conjunction with high ratio of average and maximum displacement to surface rupture length (Stirling et al., 2002; Quigley et al., 2010). Therefore methods used to estimate magnitude have been chosen due to their applicability for the region and tectonic environment, as a low rate, <10mm/year reverse fault in a crustal plate boundary setting.

The Wesnounsky (2008) scaling relationship for surface fault rupture length versus magnitude can be used in this setting for faults with known surface rupture lengths greater than 15 km (Wesnousky, 2008; Stirling & Goded, 2012). Using a logarithmic scale to indicate moment magnitude the equation given is; $M\omega = A + B \times \log(Length(km))$. The constants A and B for a reverse fault are respectively; 4.11 and 1.88. Using the different possible rupture lengths from the previous Section 3.4.7 the possible magnitude ranges from

5.8 ± 0.04 to 6.7 ± 0.04 Mw (Table 3.5). The most likely scenario of a full fault rupture with a 24.8 km length gives a magnitude of 6.7 ± 0.04 Mw.

Table 3.5: *Variation in earthquake magnitude using Wesnousky (2008) scaling relationship for surface rupture length for reverse faults applied to the Lees Valley Fault.*

Section of fault	Length (km)[1]	Earthquake Magnitude (Mw)
Northern Valley	7.6 ± 0.38	5.8 ± 0.04*
Southern Valley	17.2 ± 0.86	6.4 ± 0.04
Entire Valley	24.8 ± 1.24	6.7 ± 0.04

*Not reliable given the scaling relationship is most accurate for surface rupture lengths greater than 15 km (Wesnousky, 2008).

[1]Length error calculated using 5% to account for measuring inaccuracy.

Stirling et al. (2008) suggests the method established by Villamor et al. (2001) and Berryman et al. (2002); $M\omega = 4.18 + 2/3\log(Width) + 4/3\log(Length)$, for magnitude estimation of reverse and oblique slip earthquakes in New Zealand (Stirling & Goded, 2012). While we have a minimum full rupture length of 24.8 ± 1.24 km the width of the fault cannot be identified within the valley although regional estimates can be used. The seismogenic crust in north Canterbury is estimated to be ~12-15 km deep (Cowan, 1992; Cowan & Reyners, 1993) and the average fault dip of 65º - 70º. A regional survey in north Canterbury of microearthquakes identified a sub-horizontal zone of seismic activity restricted to the upper crust (≤12 km) suggesting a thickness of 12 km for the seismogenic zone (Cowan, 1992). Given this thickness (12 km) and the most likely rupture length scenario (24.8 ± 1.24 km) using Stirling's method the expected magnitude is Mw 6.8 ± 0.03.

Magnitude estimates using methods from Wesnounsky (2008) and Stirling et al (2008) produce similar results, however, they can only be considered minimum estimations. This is due to the significant uncertainty in estimating a rupture length and the conservative length of rupture used. The Lees Valley Fault may extend further north past Okuku Saddle, giving a possible total length ≥ 31.8 km. This would produce higher magnitude estimations, perhaps resulting in an estimate similar to the M_w 7.1 Darfield earthquake produced by a fault trace in the Canterbury region with a length of 29.5 ± 0.5 km (Quigley et al, 2012). Also of importance is the connected nature of the fault. The Lees Valley fault is not a discrete feature as it splays off the PPAFZ system, linking directly with the Townshend Fault to the south. It is not possible to constrain the rupture length of the fault within this complex connection, hence the estimation of an Mw 6.7/6.8 earthquake is considered a minimum estimation with a likely scenario of a higher magnitude event, ≥ Mw 7.

Compared to other reverse faults in the region the minimum estimated Lees Valley Fault magnitude of Mw 6.7 ± 0.04 is on the lower end of the scale showing low magnitude for fault length (Table 3.6), which is expected given its limitations. The West Culverden Fault Zone and the Cheeseman Fault Zone both have similar lengths to the minimum estimated rupture length of the Lees Valley Fault although they display much higher expected magnitudes. It is possible there is strain partitioning between Lees Valley Fault and surrounding fault systems which may account for their variability, this is discussed in Section 4.2.1.

Table 3.6: *Surface rupture length of reverse faults and their estimated magnitudes (Pettinga et al., 2001).*

Fault	Length (km)	Magnitude (Mw) (Estimated)
Mt Grey	15	6.9
Mt Thomas	16	6.5
Cheeseman Fault Zone	23	7.0
West Culverden Fault Zone	24	6.9
Greendale	29.5	7.1*
Torlesse Fault	31	6.7
Springbank Fault	68	7.1
Esk Fault	71	7.0 – 7.5
Ashley Fault/Cust Fault	72	7.2

*Not estimated. Measured magnitude during the Darfield earthquake, September 4 2010.

3.4.8 Seismic Hazard

Lees Valley Fault is 55 km northwest of Christchurch and 20 km north of Oxford. A future rupture on Lees Valley Fault could impact upwards of 460, 000 people residing in the Waimakariri District, Christchurch City and Selwyn District (CERA, 2012). Consequently assessing the likelihood of a future large earthquake and its peak ground accelerations is of importance. Although not a focus of this study, it is important to note that the effects would be widespread and hazards would likely include landsliding (of which is evident in Lees Valley itself from past events), rockfall, liquefaction and ground shaking.

The timing of future events can be investigated using recurrence interval. The minimum estimated recurrence interval from this study of 3,600 years for a surface rupturing event of minimum M_w 6.7 on the Lees Valley Fault is within the range of previous estimates, 1,000 – 5000 years (Garlick 1992; Pettinga et al., 2001). This places it within the Recurrence Class III

from Kerr et al (2003) and in agreement with the Van Dissen et al (2003) fault avoidance recurrence interval of Class IIa. Although given the limitation of the scaling relationships using fault rupture length it is expected the fault may be capable of producing Mw ≥ 7 over longer recurrence intervals than estimated.

No exact age can be estimated for the MRE as the data from the trench only identified two events within an 8,600 year period between 21.6 ± 2.3 ka and 13.6 ± 1.1 ka. A conservative analysis of the fault scarp profile and fault length scaling relationships indicate six rupture events would be required to produce the 8.5 m vertical displacement of the fault scarp, given a single event displacement of 1.5 m. Consequently, we are unable to identify at what stage the fault is in its interseismic period, hence the current class of fault recurrence risk cannot be determined. Although given the evidence we do have of a rupture cycle ~21,600 years ago, it is possible the fault could be late in its intersesimic period and may have an equivalent class of Ia, <2000 years. Significant error is associated with estimation of interseismic period

In the event of a future earthquake the most heavily affected would be the farm homesteads within the valley that are mostly situated on the eastern side of the valley near the fault trace and three that lie directly on the fault trace. Strong ground shaking would likely to be felt on the other side of the eastern ranges in Oxford. During a worst case scenario of a Magnitude 7 or greater earthquake, ground shaking and damage could be measured in the wider inland Canterbury region and potentially reach damaging levels of high peak ground accelerations in parts of Christchurch city.

4. Discussion

The main aim of this study was to contribute to understanding the structural geomorphology and paleoseismic history of the Lees Valley Fault, with new data obtained in this study presented in the previous chapters. Additional aims included identification of factors controlling the development of the basin and adjacent ranges. This chapter combines the previous chapter's findings to discuss their implication on the behaviour of the fault network and provide a proposed model of development for the Lees Valley Fault Zone and associated basin and ranges. The structural link of the Lees Valley Fault within the regional fault system will also be discussed for the effects such a connection could have on the Lees Valley Fault findings.

4.1 Lees Valley Development

North Canterbury experienced a regional crustal extension phase during the Pre-Neogene which resulted in an inherited normal faulting fabric oriented east-west (Pettinga et al., 2014). These inherited structures have been overprinted by thrust faults and folds, oriented north-northeast, that formed due to transpression during the Neogene. Shortening in the northwest-southeast direction formed landward verging asymmetric folds in Late Cretaceous-Cenozoic cover sequences during the Pleistocene (Nicol et al., 1995). Sedimentary basins in North Canterbury such as Lees Valley and the Culverden basin to the northeast formed during this regional episode of contractional deformation, with asymmetric folding cored by greywacke basement warping and rangefront faulting.

The Lees Valley basin has formed in the footwall of the Lees Valley Fault above an asymmetric syncline (Figure 4.1) where subsidence from folding has resulted in warping of the ground surface below the base level of erosion. Folding related to faulting has significant effect on the location, dimension and geometry of the Lees Valley basin. The elongate basin has developed parallel to the strike of the fault and fold structures. The Lees Valley Fault intersects the steeper fold limb on the eastern side of the valley where beds are steeply upturned. The western side of the valley reflects the gentler dipping beds often found on the opposing limb of the syncline.

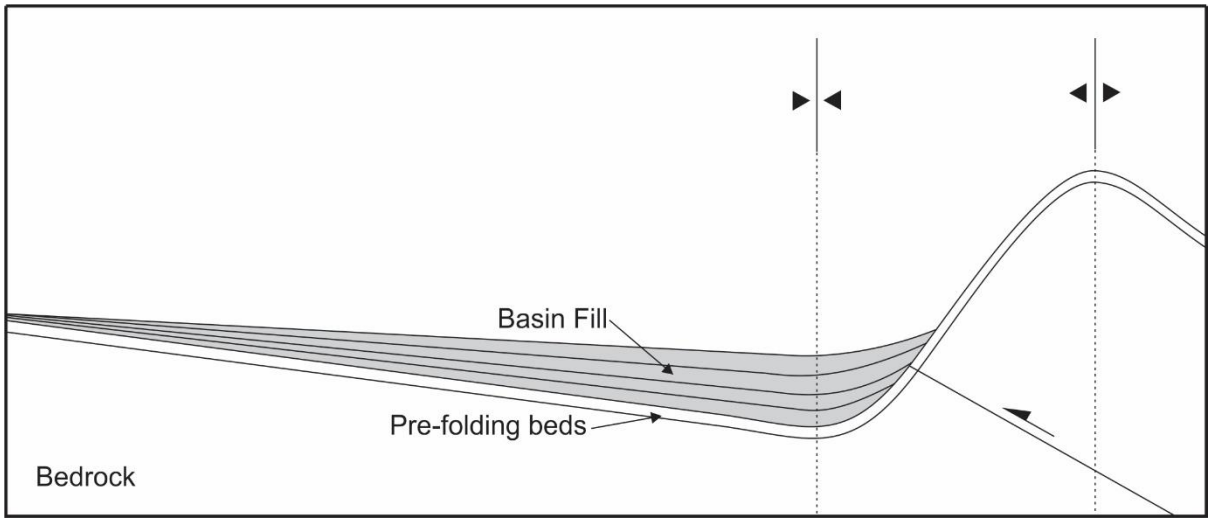

Figure 4.1: *Schematic cross-section of inferred geometry of reverse faulted and associated folded sedimentary basin. Modified from Nicol et al (1995).*

As indicated in Figure 1.6, the basin-fill succession is dominated by the Quaternary alluvial gravels which have been depositing into the basin since its formation. Drill holes from around North Canterbury indicate that basin sediments are relatively thin, varying in thickness up to 200 m (Nicol et al., 1995). There is no current subsurface evidence in Lees Valley to indicate the total basin-fill thickness. However, the basin setting, extensive fan development and the presence of the Lower Tertiary sediments exposed in the lower rangefront slope above the Ashley River suggests it may have relatively thin basin-fill similar to other North Canterbury basins.

The main fault present within Lees Valley, the Lees Valley Fault, has the same orientation (NNE-NE) as the majority of active thrust faults mapped extensively throughout North Canterbury. The three other faults which enter the Lees Valley; the Townshend Fault which transitions into the Lees Valley Fault at its southern end, the Whistler Fault which enters the valley in its centre along the western range and the possible Pancake Fault at the northern end of the valley all display a more general east-west trend (refer to Figure 1.8). It is likely these three faults have involved reactivation and progressive structural overprinting along the Pre-Neogene (normal) fault zones during the Neogene transpression and continuing today. These older structures are also involved and incorporated into the Quaternary thrust fault zones, leading to fault zone structural segmentation and complexity in surface trace expression in the valley. The Pancake Fault to the north may be influencing the nature of the Lees Valley Fault end or possible transition through Okuku Saddle.

In the centre of Lees Valley where the fault zone transitions between the southern and northern valley through a step-over, there is a significant change in fault surface expression (refer to Figure 1.4). The Lees Valley Fault increases in fault deformation zone width and fault complexity with several fault traces accommodating deformation and part of an imbricate array of splays. The ridges of each opposing rangefront extend out into the valley at this location defining the position/transition between the two sub-basins. The ridge extending from the western rangefront is bounded along its south margin by the east-west Whistler Fault Zone. The surface expression of the fault extends into the Quaternary basin fill deposits of the valley floor, although the structure may continue beneath these deposits, to or beyond the Lees Valley Fault. It is likely this structure or the inherited fabric of the Pre-Neogene crustal extension is adding complexity to the Lees Valley Fault surface expression at the northern and southern valley transition, resulting in the step-over structure. The Porters Pass Fault Zone is a result of this same style of interference and overprinted structural development. The hybrid dextral strike-slip fault zone has arisen from a complex and evolving Quaternary transpressional deformation (Pettinga et al., 2014). The array of fault segments comprising the fault zone display dextral strike-slip, oblique strike-slip, and thrust motion in a general east-northeast trend. These structures have overprinted an inherited east-west fabric of normal fault in the basement which have enabled the present structure to link and rupture through.

Basin development is an interaction of regional uplift, fault initiated uplift and erosional degradation and aggradation. The northern and southern valleys appear to demonstrate different stages of basin development with the northern basin being younger and more active than the southern basin. The smaller basin dimensions, lower sinuosity of the piedmont junction and the basinward projection of the active fault trace indicate the northern valley is more active. Faulting along the rangefront margin in the southern valley appears to be less active and drainage has a more significant influence resulting in increased rates of degradation and sediment transportation consequently widening the basin through deposition. The northern basin is inferred to be an earlier evolution stage of the southern basin as the focus of deformation has migrated north. A small basin north of Okuku saddle may be forming on a possible projection of the Lees Valley Fault (refer to Figure 1.7), and may be an even younger phase of basin development, controlled by the range-bounding transpressional faults. This evidence shows a temporal and spatial migration of basin development from south to north.

Differences between the eastern and western ranges are evident in the variation of surface geomorphic elements such as piedmont sinuosity. Geomorphic features such as faceted spurs, ridge steps, uplifted fan surfaces and nested fan deposits along the eastern ranges indicates a dominance of faulting along the eastern range compared to the western ranges. This indicates that while structures are present along the western range they are not active or as active and do not exert as much control on the current basin formation as the eastern Lees Valley Fault.

The Lees Valley Fault zone has a distribution of range-bounding and internal thrust and reverse faults splays (refer to Figure 1.4). The most westward trace in the fault zone is the most active and has vertically offset fan deposits in the northern valley and uplifted and warped the alluvial plain in the southern valley as a result of ongoing northwest horizontal contraction. The diffuse expression of the fault at its northern end (refer to Figure 2.14) is best attributed to a combination of the change in basement rheology from the Rakaia Terrane into the Esk Head Mélange (refer to Figure 1.8), and the complex interaction of the structural fabric with lithology. The fault zone may be transferring strain through small thrust segments affected/interuupted by the inherited east-west fabric onto a continuation of the Lees Valley Fault into the smaller valley over the Okuku saddle. Evidence for fault zone continuation is, however, tenuous and further detailed mapping in needed to confirm this continuation.

Fault expression along the valley is also complex at the surface with multiple splays identified through mapping of surface structures and located zones of shear fabric development which are suggestive of further faulting activity. Garlick (1992) identified shear rock mass fabric with decreased sizes of intact lozenges close to the internal rangefront fault zone in the northern valley, indicating recent uplift, although how recent was not defined. It is most likely major activity on these structures occurred over many co-seismic rupture cycles, while noting that there may have been a component of reactivation and further development during the latest faulting event (Figure 4.2). Pure dip-slip motion is observed at the surface along the Lees Valley Fault. The different observed fault traces display various stages of fault activity indicating a complex development of the fault zone (Figure 4.2), further complicated by the potential for spatial and temporal variation in slip rate along the active sections of the fault. Footwall imbricate thrust wedge development and fault zone propagation with a westward or basinward direction of migration of faulting is supported by the faulting pattern evident in the ranges and along the active rangefront (Figure 4.2). The oldest structures which would have formed earliest are inferred by the presence of ridge steps high in the range. An inactive/less active structure marking an uplifted former rangefront is marked by faceted

spurs and elevated fan surfaces ("UCB", Figure 2.7), and the current rangefront is marked by the youngest fault structure ("Current Rangefront Fault", Figure 4.2), the active trace in the northern valley (refer to Figure 2.7).

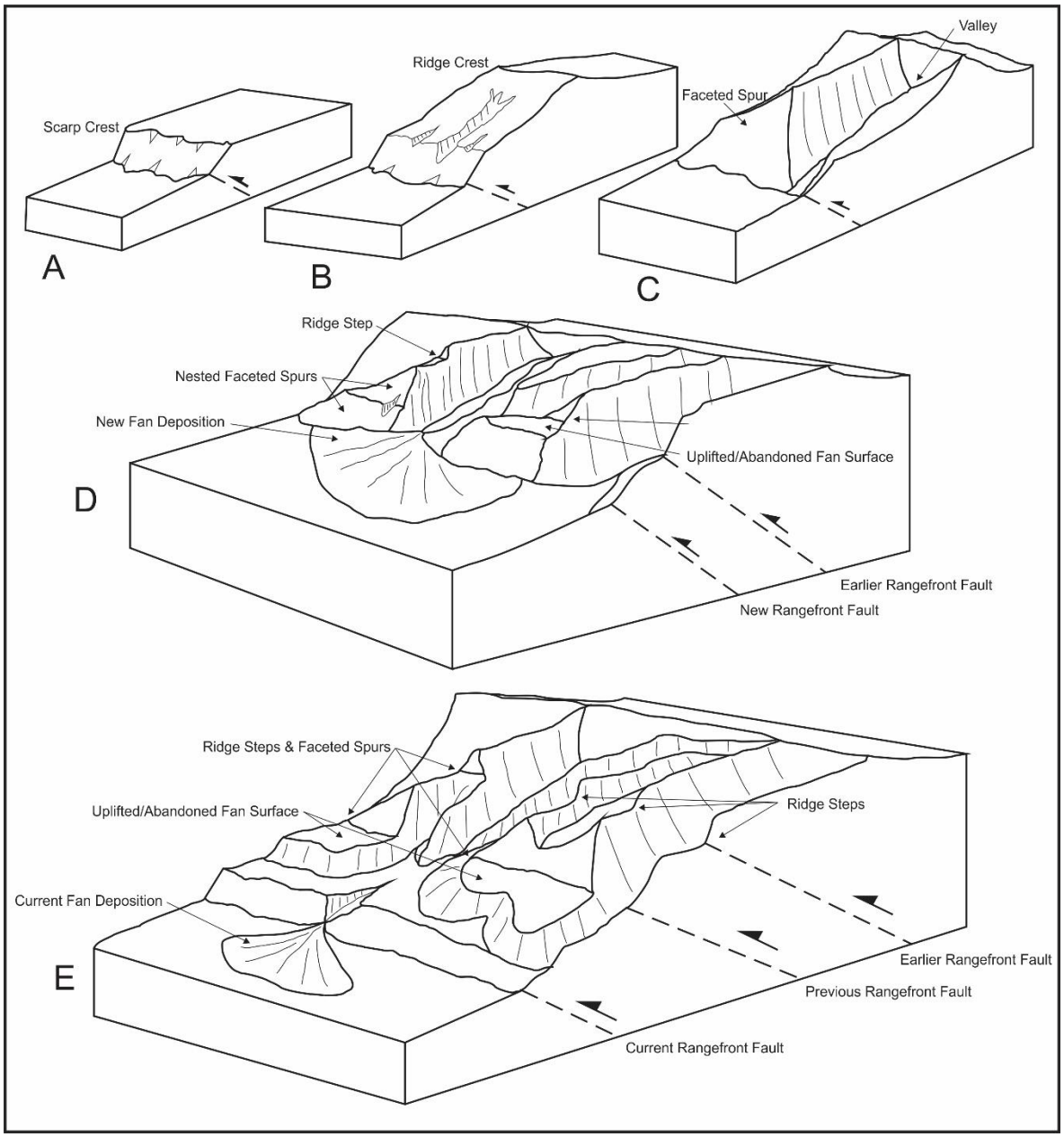

Figure 4.2: *Schematic model of rangefront and imbricate thrust wedge development along the fault generated escarpment of Lees Valley eastern range. A – C are based on Figure 2.1 from Wallace (1977) modified by Bull (2007). A) Linear scarp of initial faulting. B) Migration of scarp crest from rising range boundary to form range crest. C) Formation of valleys and faceted spurs in rising block. D) Footwall imbricate thrust wedge development through the basinward migration of faulting. Note original rangefront incorporated into the hanging wall of the ranges and identified by the ridge steps, and faceted spurs. Nesting of the faceted spurs indicates episodic displacement along the new range-bounding fault. E) Further migration of faulting and new footwall thrust, uplift and preservation of earlier rangefront. Degradation and downcutting of fluvial channels into uplifted fan deposits.*

4.1.1 Episodic Behaviour of the Lees Valley Fault

Episodic faulting behaviour has been observed on numerous fault systems worldwide (Crone et al., 1997; Gardner et al., 2009) including in New Zealand (Norris and Nicolls, 2004; Quigley et al. 2006, 2010; Stahl, 2014). Episodic behaviour on a fault is indicated by several earthquakes occurring during a relatively short period of time, followed by a significant period of quiescence, then further fault activity resulting in a pattern of earthquake clustering in a fault's history. Fault interactions can cause a change in stress field resulting in instability and relative clustering of earthquakes which in some instances may reactivate previously inactive faults as observed in Australia (Crone et al., 1997; Quigley et al., 2006; Gardner et al., 2009). The relationship of changing stress field due to fault rupture and increasing risk of rupture on surrounding faults has also been investigated in the central South Island (Steacy et al., 2013, 2014). The alternative fault behaviour is periodic faulting where earthquakes occur on a regular basis, and slip and time interval, or both are predictable (McCalpin, 2009).

Through observations and field data gathered on the Pre-Quaternary and Quaternary deformation the Lees Valley Fault appears to display cyclic or episodic fault behaviour. The ridge steps observed along the eastern ranges are a result of uplift of fan surfaces, behind the current active fault strand. The extensive alluvial fans formed during periods of tectonic quiescence and inferred cooler climate when mass movement (solifluction and slope failure) led to significant sediment flux from the ranges and fan formation. Uplift following fan formation lowers relative local base level causing downcutting onto the fan surfaces and is accompanied by the incorporation of the abandoned alluvial fans into the rangefront. Below the internal rangefront, recorded in the northern valley, uplifted fan piedmont surfaces are identified as UCB (Undulating Composite Benches) (refer to Figures 2.7, 2.14, 2.15, 2.16, 2.18 and 2.22). Uplifted fan piedmont surfaces indicates there was a significant period of time following fault uplift of the internal rangefront, during which fans formed at the base of the fault scarp extending out into the basin, followed by multiple faulting events which progressively uplifted these fan surfaces incorporating them into the lower hanging wall of the adjacent range.

The footwall imbricate fan development and migration of the range-bounding fault as discussed in the previous section describes the formation of these ridge steps (faceted spurs and benches). As faulting migrates westward into the basin margin it leaves abandoned faults represented by ridge steps, each new position of the active fault creates a new ridge step

(facet) that will consequently be uplifted, progressively degraded and incorporated into the range. Therefore the presence of ridge steps indicates periods of faulting interspersed with periods of tectonic quiescence evidence of cyclic tectonic activity. Furthermore, differential vertical offset recorded between sections of different surface ages, may be a result of the older surfaces accumulating deformation from more events. This would also indicate cyclic faulting over a relatively short period of time during formation of these surfaces. However, the relationship between these surfaces of various height and age is ambiguous and may just be the result of extensive fluvial modification. It is possible the variable offset is influenced by one or both of these tectonic or fluvial factors.

Evidence from the northern valley fault scarp also supports clustering of earthquakes. Analysis of the fault scarp indicates it is a composite scarp formed from multiple events supported by the evidence found in the trench of deformation of the units from more than one event. Age control from OSL samples within the trench constrain timing of these recent multiple ruptures to post 21.6 ± 2.3 ka. During this time, the fault scarp formed, offsetting fan surfaces followed by the current period of quiescence during which both features have been degraded and new fan surfaces have developed at the base of the fault scarp.

Active faults in stable continental regions often display episodic behaviour (Crone et al., 1997, 2003; Gardner et al., 2009) and it seems likely the Lees Valley Fault is no exception. There could be several explanations behind this behaviour on the Lees Valley Fault. One such explanation could be a change in regional stress field. The numerous fault structures in the basin have recorded a potential change in Pre-Neogene orientation of faults to the present Quaternary fault orientation which is a result of the northwest-southeast compression interacting with an inherited fault fabric accompanied by progressive structural overprint.

4.2 Surrounding Fault Systems Comparison and Structural Link

The Lees Valley Fault is part of the wider Porters Pass Alpine Fault Zone. The direct connection at the surface is with the Townshend Fault to the south, however, it is also likely that the east dipping Lees Valley Fault converges at depth with westward dipping faults, such as the Glentui Fault (refer to Figure 1.7). The structural convergence creates a fault bounded wedge forming the eastern ranges (Figure 4.3).

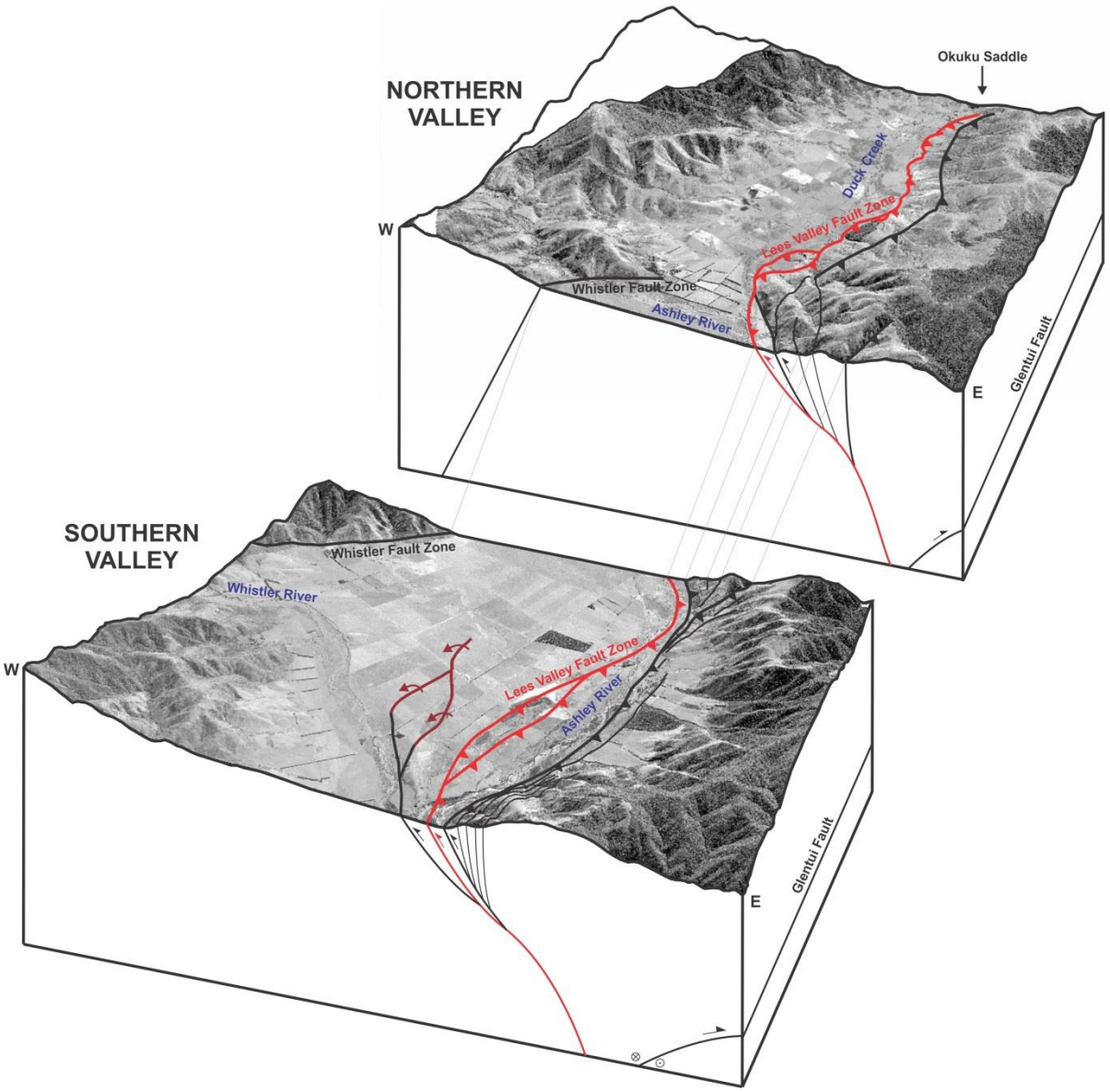

Figure 4.3: *A 3D block model of Lees Valley and surrounding range development showing links to regional structural features.*

4.2.1 Comparison of Slip Rates

Compared to other reverse faults in the region the calculated Lees Valley Fault slip rate of 0.4 mm/yr is relatively low. The Porters Pass Amberley Fault Zone (PPAFZ) has an estimated slip rate range of 3-4mm/year (Cowan et al., 1996), while the Porters Pass Fault has a slip rate of 0.3-0.9 to the west and 3.2-4.1 to the east and Mt Grey, 0.5-1.8 mm/yr (Cowan et al., 1996, Pettinga et al., 2001, Howard et al., 2003; Howard et al., 2005). However the Esk Fault to the north-west has a similar vertical slip rate of 0.31 mm/yr (Noble, 2011). Given the connectivity of the LVF to the PPAFZ it is possible there is interaction between them in regards to stress cycling. Within a network of faults the co-seismic rupture termination on

one fault can lead to changes in coulomb stress on adjacent and nearby faults, leading to increased activity on another, indicating associated strain transfer and loading between faults alters the slip rates measured for each fault (Roberts et al., 2002). It is likely faults with higher slip rates are oriented optimally to the regional stress field within the compressional tectonic setting and are hence able to accommodate more of the regional strain. The maximum contractional strain P-axes at shallow depths are relatively uniform across the region in a WNW-NW trend (Cowan, 1992). The Lees Valley Fault has a similar orientation as the Porters Pass Fault, the most significant structural feature in the PPAFZ accommodating much of the regions strain, therefore the Lees Valley Fault oriented NNE-SSW also has an optimal orientation for accommodating the regional strain orientated NW-SE.

The most likely scenario is that the calculated slip rate only applies to the active fault trace in the northern valley. Given the complex fault zone and multiple fault traces within the rangefront it is possible these are splays also accommodating a component of strain additional to the 0.4 mm/yr calculated in the northern valley. Furthermore, the splinter faults and monocline structures of the southern valley that splay off the main range-bounding fault zone at a different orientation also accommodate a component of strain which is not directly accounted for in the 0.4 mm/yr calculation. Therefore as strain is accommodated by Lees Valley Fault Zone it is distributed among a number of structural elements in the basin and a slip rate calculation from one such element cannot be representative of the slip rate for the entire Lees Valley Fault. Hence the Lees Valley Fault Zone slip rate is expected to be higher than 0.4 mm/yr and this estimation should be treated as a minimum. Further complication arises from the structural convergence either side of the eastern ranges indicating that uplift is a result of transpressional deformation being driven by active fault zones bounding the ranges to the west and east.

Slip within the PPAFZ is cumulatively estimated as 3-4 mm/year and the Porters Pass Fault is estimated to accommodate over half of this. The Lees Valley Fault accommodates a minimum of 0.4 mm/yr with an actual rate estimated to be significantly higher. Given these estimations, the Lees Valley Fault is an important structure in the region accommodating a portion of the deformational strain of the PPAFZ region.

4.2.2 Fault Segmentation and the Lees Valley Fault Structural Link to the Regional Faults

The Lees Valley Fault connects with the PPAFZ directly at its juncture with the Mt Oxford Duplex south of the Lees Valley. Here the Townshend Fault and the Coopers Creek Fault also relay into the Glentui Fault to the east of the Lees Valley Fault (refer to Figure 1.7). The Lees Valley Fault Zone bounding the eastern range of Lees Valley is interpreted to connect at depth with the west dipping dextral Glentui Fault on the opposing side of the eastern ranges creating a fault bounded transpressional wedge driving up the eastern ranges. This gives rise to the suggestion it may be possible for these structures to rupture simultaneously as energy is transferred through the fault relay.

Fault segments can be defined as earthquake, behavioural, structural, geologic or geometric segments each with varying degrees of likeliness of being a boundary to earthquake rupture (Knuepfer, 1989; dePolo, 1991; McCalpin, 2009), their descriptions are outlined in Table 4.1. Structural indicators include sharp changes in fault orientation, branch fault intersections and changes in dip or net slip (McCalpin, 2009). Geomorphic indicators include spatial variation in scarp height along fault strike, variation in height of uplifted hanging wall topography, sharp changes in strike and parameters of surface folding.

Table 4.1: *Types of fault segments and their defining characteristics from McCalpin (2009).*

Type of segment.[1]	**Characteristics used to define the segment.**[1]	**Likelihood of being an earthquake segment.**[2]
1.Earthquake	Historic rupture limits	By definition, 100%[3]
2.Behavioural	1. Prehistoric rupture limits defined by multiple, well-dated Paleoearthquakes. 2. Segment bounded by changes in slip rates, recurrence intervals, elapsed times, sense of displacement, creeping versus locked behaviour, fault complexity.	High Moderate (26%)
3.Structural	Segment bounded by fault branches, or intersections with other faults, folds, or cross structures.	Moderate-high (31%)
4.Geologic	1. Bounded by Quaternary basins or volcanic fields. 2. Restricted to a single basement or rheologic terrain 3. Bounded by geophysical anomalies 4. Geomorphic indicators such as range-front morphology, crest elevation	Variable [4](39%)
5.Geometric	Segments defined by changes in fault orientation, stepovers, separations, or gaps in faulting	Low-moderate (18%)

[1]Classification follows the segment boundary types of dePolo et al. (1989, 1991) and Knuepfer (1989).

[1]Percentages = percent of cases where historic ruptures have ended at this type of boundary, as opposed to rupturing through it (Knuepfer, 1989).

[3]However, restriction of a single historic rupture to the segment does not mean that all future ruptures will be similarly restricted.

[4]Small number of observations, accuracy questionable (Knuepfer, 1989).

While little is known of the Townshend Fault, the section observed in Lees Valley is a bifurcation from the lower Townshend Valley striking east across the Ashley River gorge opening and estimated to have a dip between 15 – 50º S (Cowan, 1992). It demonstrates very different characteristics to the Lees Valley Fault section which it is projected to join based on surface trace strike to the northeast, and an inferred 30 - 40º dip to the East. The abrupt change in orientation and dip suggests the fault interaction here could act as a rupture barrier. Mapped fault terminations, fault branches, and cross structures are often related to rupture barriers or 'endpoints' (McCalpin, 2009). It seems likely the faults behave individually given

the differing orientation of the structures. Mt Oxford Duplex is bounded by faults that change orientation from NE to EW or E-SE. Given the stress orientation required to trigger fault rupture along this structure it is unlikely the rupture would be continuous, although it is possible the stress loading at the end of the fault could transfer onto the Lees Valley Fault leading to an increased probability of fault rupture along this trace. Furthermore, given the lack of data on the Townshend Fault and its connection with the Lees Valley Fault the possibility of a joint rupture through stress transfer cannot be ruled out. In order to confirm linkage between the Lees Valley Fault and Townshend fault segments defining parameters such as slip rates and recurrence intervals need to be compared. Due to the lack of data on the Townshend fault and the limited paleo-data for the Lees Valley Fault, this is not yet possible.

The possibility of co-seismic rupture between the Lees Valley Fault and the PPAFZ has been previously raised by Garlick (1992). The PPAFZ has recorded seismic events at 8500 ± 200, 5300 ± 700, 2500 ± 200, 1000 ± 100 and 500-600 years B.P. (Howard, 2001; Howard et al., 2003; Howard et al., 2005). Garlick (1992) suggests the last two periods of scarp development on the Lees Valley Fault occurred co-seismically with the 2500 ± 200 and 500 - 600 year events, although his dates produced from weathering rind data in Lees Valley are somewhat tenuous. Likewise, OSL dating from this study is not conclusive enough on the exact timing of the Lees Valley Fault last earthquake rupture in order to link the events from the two structures. Evidence from this study indicates two events at an indeterminate time post 21.6 ± 2.3 ka, with a possible scenario where they occurred before 13.6 ± 1.1 ka, significantly older than the movements recorded on the PPAFZ, limitations on the age calculations from the Lees Valley Fault suggests movement could have been more recent than indicated and therefore a co-seismic event cannot be excluded. However, there is no evidence that supports regular co-seismic triggering of fault rupture on the Lees Valley Fault when compared to the PPAFZ, given the much more regular activity reported for the latter.

It is also possible strike-slip motion is occurring on the fault structure at depth, likely below the fault bounded wedge of the eastern ranges, supported by focal mechanisms that indicate strike-slip motion on a steeply dipping discontinuity at a depth of ~ 9 – 11 km (Cowan, 1992; Garlick, 1992). This further supports a structural and possible seismic link between the PPAFZ and the Lees Valley Fault. Evidence of faulting from the trench and observations within the northern valley suggests only pure dip slip motion at the surface. The Ashley River outcrop shows a more complex nature of faulting, where structures have been overprinted and multiple faults are complicating the structural expression. It is possible that some of this

complexity is a result of an accommodation of oblique strike-slip motion on the Lees Valley Fault. The strike-slip Mt. Oxford Duplex to the south is overprinting and incorporating older normal faults (Cowan 1992, Garlick 1992). The Lees Valley Fault splays off the duplex and may be accommodating an increasing component of strike-slip. There is little evidence to suggest this is the case on the Lees Valley Fault surface trace, other than local stress reorientations measured by Garlick (1992) in the Ashley River outcrop, although their exact origin is not certain. It is likely strike-slip motion is accommodated at depth given the focal mechanisms measured at depth and the expected structural connectivity of the fault zone. Although, there remains a high level of uncertainty what can be assumed is that there is a complex interaction between the two fault zones that is worth understanding in more depth.

5. Conclusions

5.1. Introduction

The purpose of this thesis was to investigate the tectonic geomorphology, structure, paleoseismology of the Lees Valley Fault and the model for development of the fault zone and associated ranges. Analysis on the Lees Valley Fault and associated geomorphic expression provided further understanding on the fault zones rupture characteristics, nature of deformation and paleoseismology. The field work and analysis completed in this study aims to build on previous studies, by providing updated and more quantitative work. The key findings of this thesis are summarised below alongside recommendations for future work on the Lees Valley Fault and its connection to the Porters Pass - Amberley Fault Zone.

5.2. Key Findings

5.2.1. Development of a Structural and geomorphic Model for the Lees Valley Fault Zone and Eastern Rangefront.

Developing a structural and geomorphic model involved investigating the deformation distribution along the strike of the fault, the various structures accommodating the deformation and factors which may be affecting their surface expression. Analysis of geomorphic features facilitated classification of the tectonic activity class for the fault and associated ranges and incorporation of all observations and analyses has enabled formation of a model for their development.

Deformation Variation along Strike of the Fault.

Numerous fault splays are noted along the length of the Lees Valley Fault at various scales and are likely a result of several contributing factors including; shallowing of fault splays near the surface, topographic effects (such as variable sediment loading) and heterogeneity of sediments. The splays distribute strain across multiple structures, resulting in less displacement on each individual structure but a cumulative total similar to that of the single fault.

The general displacement relationship shows smallest displacements at the ends of the fault trace with a wide central part that displays a section of larger displacements in the northern half of the fault trace. Vertical displacement along the fault scarp varies considerably and

ranges from 1.5 to 11.5 m with an average height of 5 m. This variation in vertical offset is observed in many cases to be modified significantly by fluvial drainage paths from the ranges, which erode and decrease the scarp height. Other contributing factors are the locations of fault splays, which distribute deformation among multiple structures and offset of variably aged surfaces, at different elevation. It is also possible some variation may be the result of fault dip changes, variation in bedrock depth below surface, or variation in slip due to differential accommodation of deformation in folding versus faulting.

Fault discontinuities are present at three main locations; the northern end of the fault trace in the northern valley, the transition zone between the northern and southern valley and the termination of the fault trace at its southern end. At the end of the northern valley trace displacement becomes unmeasurable indicating a termination of the trace, however, geomorphic evidence higher within the ranges indicates the fault may continue through Okuku saddle. A break in fault between the northern and southern valley is marked by an overlap of fault traces from each sub-basin, where deformation is distributed between the two sections of the fault through a complex pattern of numerous fault traces and folding. The southern end of the Lees Valley Fault is marked by its termination against the Townshend Fault. The location of each of these discontinuities is associated with cross cutting structural features.

Cross-cutting and Inherited Structures Affecting Basin Development.

East-west oriented structures such as the Townshend, Whistler and Pancake Faults have influenced development of the Lees Valley Fault. The interaction of the Townshend Fault and the Pancake Fault coincide with the southern and northern ends of the fault trace, respectively. The break in fault between the southern and northern valley coincides with the projected position where the Whistler Fault intersects the Lees Valley Fault if the trace continued across the valley. Variation in displacement and fault zone width is noted at these locations. It is suggested that the Lees Valley Fault has inherited these structures and fabric from the initial structural development in the Pre-Neogene faulting, altering its development and expression at the surface.

Tectonic Activity Class of the Ranges.

Sinuosity of the mountain-piedmont junction varied throughout the valley but consistently displayed low values indicative of ongoing active uplift of the ranges. The combined sinuosity value of the eastern range, 1.37, places it in the highly active mountain front class

of 1 – 1.5 from Bull (2007). Lower values for the eastern range in the northern valley compared to the southern valley suggest a higher level of fault activity. However, limitations of the models application to a thrust fault-bounded basin have resulted in a sinuosity index that is more sensitive to fan development (controlled by climate) than fault uplift. Therefore, range-front uplift activity cannot be accurately described from these sinuosity results alone.

Faceted spurs of Class 1 – 3 along the eastern ranges, predominantly in the northern valley indicate a 'Class 1' landscape of the relative tectonic activity provided by Bull (2007). This would also be supported by increasing relief of the mountains and narrow river valley floors. However, the alluvial fans of the eastern ranges have become slightly entrenched and the ranges display v-shaped valleys suggesting a move into the category of 'Class 2 – rapid'. This classification is also supported by the slightly sinuous piedmont junction >1, which would indicate some time, although relatively short, has passed since the last active uplift event.

Imbricate Wedge Development of Fault Zone and Rangefront.

Evidence of wedge development is present in older fault structures higher in the ranges bounded by the active trace at the current rangefront. Abandoned and uplifted fault splays lie alongside associated geomorphic features such as fan surfaces and faceted spurs. Interpreted from features observed mostly in the northern valley, it is assumed the entire fault zone and rangefront has developed through footwall imbricate splay propagation, leading to uplift and a "staircased" progressive temporal and spatial abandonment of earlier fault splays.

The Lees Valley Fault Zone is controlled by properties in the basement and cover sequence lithologies involved in thrust deformation and the inherited structures of the region. However, the primary control on the surface expression of faulting and present shape and nature of the basin, is the development of the structural and geomorphic thrust wedge of the Lees Valley Fault Zone at the rangefront.

5.2.2. Investigation of the Paleoseismic History of the Lees Valley Fault at a Selected Location.

Constraint on Timing and Number of Events on the Most Recent Trace in the Northern Valley.

Data from the paleoseismic trench indicates the most likely rupture scenario for the active northern valley fault scarp was at least two faulting events between 21.6 ka and 13 ka, although limitations of OSL dating in fluvial fan deposits has restricted conclusions from

these findings to two events after ~ 21 ka at undetermined times. Cowan (1992) and Garlick (1992) suggest faulting in the Holocene, which is likely given the offset of relatively young fan deposits. Analysis of the fault scarp profile indicates multiple events would be required to produce the deformation observed, 6 events given a single event displacement of 1.5 m. This is the more likely scenario, given the fault scarp profile analysis incorporates folding deformation into its calculations.

Estimated Slip Rate on the active trace – Northern Valley and Regional Comparison.

The calculated slip rate of 0.4 mm/yr obtained using scarp profile analysis matches the previous estimate of Barrell and Begg (2013), although their estimate was calculated from different structures within the basin, it does suggest a consistency of behaviour along the valley. Both are limited in their scope, the only firm conclusion possible is that the 0.4 mm/yr slip rate represents a minimum estimation for the fault zone. The true slip rate for the Lees Valley Fault Zone is expected to be higher potentially closer to lower estimations for the Porters Pass Fault slip rate range (2.7-4.0 mm/yr) as they both accommodate significant components of the PPAFZ regional slip rate of 3-4mm/year (Cowan et al., 1996).

Estimated Recurrence Interval and Magnitude of Past Earthquakes along the Lees Valley Fault.

Based on analysis of the active fault trace of the Lees Valley Fault in the northern valley, the estimated recurrence interval is 3,600 years, given a single event displacement of 1.5 m. Although limitations of OSL dating and modelling for the single event displacement introduces significant error to this estimate. An estimated magnitude is based on the surface rupture length of the fault and is ~Mw 6.7. However, the exact length of the surface rupture trace is conservatively estimated due to its possible extension to the north. Therefore it is expected, given surface rupture, the magnitude may be Mw $\geq$ 7, which in turn would produce greater single event offset and a longer expected recurrence interval.

5.3. Future Work

5.3.1. The Northern Continuation of the Lees Valley Fault

The study area of this thesis was restricted to the Lees Valley, consequently the Lees Valley Fault trace has been recorded up to the valleys northern end at Okuku saddle. It is suggested the Lees Valley Fault may project through to the small basin north of Lees Valley. Research

on this potential structure is important as it would represent a significant extension of the Lees Valley Fault Zone, which would affect the current understanding of the faults behaviour including the potential earthquake magnitude it could produce as well as structural connections to other structures in the region.

The potential section of fault extension is likely to show variation in its behaviour and surface expression from the rest of the Lees Valley Fault given the change in basement lithology from Rakaia Terrane into the Esk Head Mélange at the northern end of Lees Valley. It is also possible that the location of this fault trace further north brings it to the boundary of the PPAFZ and edge of the hybrid strike slip – thrust fault domain (refer to Figure 1.6).

Important future research should include identifying the presence and extent of the northern extension of the Lees Valley Fault, characterising its geomorphic expression and paleoseismic activity including type of motion, slip rate and timing of most recent fault ground rupture events. Such research would allow comparison to findings in this study and further our understanding of the Lees Valley Fault.

5.3.2. Inherited and Adjacent Structures and their Influence on the Current Range-Bounding Fault Zone

Not much is known about the other faults found in Lees Valley such as the Townshend, Whistler and Pancake Faults. The Pancake Fault in particular is a structural feature identified by Forsyth et al. (2008) and Barrell and Begg (2013), although it is not certain whether the linear feature is due to a rupture scarp, erosion, slope instability or merely a result of vegetation variation (Barrell and Begg, 2013) (Figure 5.1). Ridge renting within the pancake ranges has been described as a swarm of small discontinuous scarps, which have been upthrown on their southern side (Garlick, 1992; Cowan, 1992; Forsyth et al, 2008). The apparent fault trace trends east-southeast, following the ridge line, and is also upthrown on its southern side. The presence of this trace may be complicating the expression of the Lees Valley Fault at Okuku Saddle, where the Lees Valley Fault trace appears to terminate. Further investigation into the extent and true nature of this linear feature would aid in understandings the Lees Valley Fault expression at this location and its controlling effect on shaping the basin.

Figure 5.1: *Photo view of the Pancake ranges looking northwest. Ridge renting (dotted white lines) and possible fault trace (dashed white line) indicated. Grid reference: 245252 579312.*

Cowan (1992) has undertaken most of the study on the Whistler Fault Zone. Cowan identified the fault structure due to the intense crushed shear zone of basement rock exposed in Whistler Valley (Cowan, 1992). The crushed zone strikes east from the Whistler Valley and bounds the western ranges of the southern Lees Valley section (Figure 2.8). It consists of a network of vertical faults up to 1 km wide in the Whistler Valley where slickenside-striations record predominantly horizontal movement. The fault zone alters to dip ~ 50-70º N at its eastern end in the Lees Valley where it potentially accommodates vertical motion also. To the west the Whistler Fault Zone extent and expression is more complex, south of the Whistler River it is expressed in accordant topographic steps and further west it projects beneath the Puketeraki Range basement. Further research should focus on defining the exact extent of the Whistler Fault Zone and determining fault parameters such as, type of motion, slip rate, timing of last rupture, and recurrence interval to enable comparison with the Lees Valley Fault and other regional faults.

The Townshend Fault is part of the Mt. Oxford Duplex and a component of the Porters Pass - Amberley Fault Zone and is discussed in the following section.

5.3.3 The Structural Connection of Lees Valley Fault to the PPAFZ.

Little is known of the Townshend Fault which the Lees Valley Fault terminates against, other than its eastward strike and estimated near surface dip of 15˚ – 50º S (Cowan, 1992). Analysis and interpretation of such fault parameters as slip rate and recurrence interval would allow better comparison to the Lees Valley Fault. This would further our understanding of the interaction between these faults and importantly how the Lees Valley Fault connects to the PPAFZ. Important questions remain such as; how do the faults interact and transfer stress, do they rupture co-seismically and what is the rule of subsidiary structures in these processes? Further constraints on the timing of the Lees Valley Fault and its comparison and connection with PPAFZ could help understand the discussion behind the wider fault zones behaviour.

5.4 Research Summary

The research completed in this study on the tectonic geomorphology and paleoseismology of the Lees Valley Fault has furthered current understanding of the fault zone development and its control on the geomorphic evolution in the region. Paleoseismic analysis further emphasised the difficulty of undertaking GPR investigations in fluvial deposits and applying scaling relationships such as Wesnousky (2008) to reverse faults. However, the paleoseismic investigation proved successful in locating the fault beneath the surface and provided further constraint on fault characteristic estimations such as earthquake timing, potential single event displacements and earthquake magnitudes.

The following conclusions have been made on the Lees Valley Fault, based on the research completed in this study:

1. Faulting is complex within the valley and consists of numerous fault traces at the surface some more active than others. Their relationship indicates footwall propagating imbricate thrust wedge development of the fault zone and associated uplift of ranges.
2. Variability in surface vertical deformation ranges from 1.5 – 11.5 m with an average scarp height of 5 m. Variation is the result of offsetting surfaces of various ages and the degradation of the fault scarp by drainages from the ranges.
3. Through OSL dating, paleoseismic investigation and surveying the Lees Valley Fault is estimated to have a vertical slip rate greater than 0.4 mm/yr, a recurrence interval

greater than 3,600 years and the potential to generate earthquakes Mw ≥ 7. It was last active post ~21.6 ka and likely during the Holocene.

4. Fault scarp profile analysis of most recent trace in the northern valley indicates multiple events have produced the present deformation. Ridge steps and abandoned and uplifted fan surfaces within the eastern rangefront alongside the fault scarp analysis provide evidence for episodic behaviour of the Lees Valley Fault.
5. The Lees Valley Fault development has been complicated by inherited and cross-cutting features and its link with the wider regional fault zone.

References

Aitken, M. J. (1998). *An introduction to optical dating: the dating of Quaternary sediments by the use of photon-stimulated luminescence*. Oxford University Press.

Aleksandrowski, P. (1985). *Graphical determination of principal stress directions for slickenslide lineation population: an attempt to modify Arthaud's method*. Journal of Structural Geology, 7(1): 73 – 82.

Amos, C., Lapwood, J., Nobes, D., Burbank, D., Rieser, U., & Wade, A. (2011). *Palaeoseismic constraints on Holocene surface ruptures along the Ostler Fault, southern New Zealand.* New Zealand Journal of Geology and Geophysics, 54(4): 367–378.

Armstrong, M. J. (2000). *Geomorphological and Geophysical Investigation of the Effects of Active Tectonic Deformation on the Hydrogeology of North Culverden Basin, North Canterbury.* PhD thesis, Department of Geological Sciences, University of Canterbury, Christchurch.

Bannister, S., & Gledhill, K. (2012). *Evolution of the 2010–2012 Canterbury earthquake sequence*. New Zealand Journal of Geology and Geophysics, 55(3): 295–304.

Barrell, D. J. A, & Begg, J. G. (2013). *General distribution and characteristics of active faults and folds in the Waimakariri District, North Canterbury.* GNS Science Consultancy Report, 325: 52.

Bartram, K. L. (1958). *Lees Valley Intermont: Its Development and Present Geographic Character*. MSc thesis, Department of Geography, University of Canterbury, Christchurch.

Bebbington, M., Harte, D., & Williams, C. (2015). *Cumulative Coulomb Stress Triggering as an Explanation for the Canterbury (New Zealand) Aftershock Sequence: Initial Conditions Are Everything?* Pure and Applied Geophysics, 1-16.

Botsford, J. W. (1983). *The Esk Head Melange in the Esk Head/Okuku area, North Canterbury*. Unpublished MSc thesis. Department of Geological Sciences, University of Canterbury, Christchurch.

Bradshaw, J. D. (1973). *Allochthonous Mesozoic fossil localities in melange within the Torlesse rocks of North Canterbury*. Journal of the Royal Society of New Zealand, 3(2): 161–167.

Bubeck, a., Wilkinson, M., Roberts, G. P., Cowie, P. a., McCaffrey, K. J. W., Phillips, R., & Sammonds, P. (2015). *The tectonic geomorphology of bedrock scarps on active normal faults in the Italian Apennines mapped using combined ground penetrating radar and terrestrial laser scanning.* Geomorphology, 237: 38–51.

Bull, W. B. (2007). *Tectonic geomorphology of mountains: a new approach to paleoseismology*. John Wiley & Sons.

Burbank, D. W., & Anderson, R. S. (2012). *Tectonic Geomorpholog.* (2nd ed.). John Wiley & Sons.

Campbell, J., Pettinga, J., & Jongens, R. (2012). *The tectonic and structural setting of the 4 September 2010 Darfield (Canterbury) earthquake sequence, New Zealand.* New Zealand Journal of Geology and Geophysics, 55(3): 155–168.

Cartwright, J. A., Trudgill, B.D. and Mansfield, C. S. (1995). *Fault growth by segment linkage: an explanation for scatter in maximum displacement and trace length data from the Canyonlands Grabens of SE Utah*. Journal of Structural Geology, 19(9): 1319 – 1326.

CERA. (2012). *Recovery Strategy for Greater Christchurch Mahere Haumanutanga o Waitaha*. Christchurch: Canterbury Earthquake Recovery Authority. Retrieved August 18, 2015, http://cera.govt.nz/sites/default/files/common/recovery-strategy-for-greater-christchurch.pdf

Chen, W. S., Lee, K. J., Lee, L. S., Streig, A. R., Rubin, C. M., Chen, Y. G., Yan, H., Chang, H & Lin, C. W. (2007). *Paleoseismic evidence for coseismic growth-fold in the 1999 Chichi earthquake and earlier earthquakes, central Taiwan*. Journal of Asian Earth Sciences, 31(3): 204-213.

CLiFlo. (2015). *The National Climate Database*. Retrieved September 16, 2015, NIWA. http://cliflo.niwa.co.nz

Cowan, H. (1992). *Structure, seismicity and tectonics of the Porter's Pass-Amberley fault zone, North Canterbury, New Zealand*. PhD Thesis, Department of Geology, University of Canterbury, Christchurch.

Cowan, H. (1992a). *Porter's Pass-Amberley fault zone maps*. Unpublished. Held by University of Canterbury, Christchurch

Cowan, H., Nicol, A., & Tonkin, P. (1996). *A comparison of historical and paleoseismicity in a newly formed fault zone and a mature fault zone, North Canterbury, New Zealand*. Journal of Geophysical Research, 101(B3): 6021.

Cowan, H. A., Pettinga, J. R. and Smith, I. E. M. (1989). *Transtension and structural complexity along the Hope Fault: Glynn Wye to Hanmer Basin, North Canterbury*. Geological Society of New Zealand Miscellaneous Publication, 43, 31.

Cox, S. C.; Barrell, D.J.A . (compilers). (2007). *Geology of the Aoraki area*. Institute of Geological & Nuclear Sciences 1:250 000 geological map 15. 1 sheet + 71p. Lower Hutt, New Zealand. GNS Science.

Crone, A. J., Machette, M. N., & Bowman, J. R. (1997). *Episodic nature of earthquake activity in stable continental regions revealed by palaeoseismicity studies of Australian and North American quaternary faults.* Australian Journal of Earth Sciences, 44(2): 203–214.

Crone, A. J., De Martini, P. M., Machette, M. N., Okumura, K., & Prescott, J. R. (2003). *Paleoseismicity of Two Historically Quiescent Faults in Australia: Implications for Fault Behavior in Stable Continental Regions*. Bulletin of the Seismological Society of America, 93(5): 1913–1934.

Cunningham, A. C., Wallinga, J., Hobo, N., Versendaal, A. J., Makaske, B., & Middelkoop, H. (2015). *Re-evaluating luminescence burial doses and bleaching of fluvial deposits using Bayesian computational statistics*. Earth Surface Dynamics, 3(1): 55-65.

DeMets, C., Gordon, R. G., Argus, D. F., & Stein, S. (1994). *Effect of recent revisions to the geomagnetic reversal time scale on estimates of current plate motions*. Geophysical Research Letters, 21(20): 2191.

DeMets, C., Gordon, R. G., & Argus, D. F. (2010). *Geologically current plate motions.* Geophysical Journal International, 181(1): 1–80.

DePolo, C. M., Clark, D. G., Slemmons, D. B., & Ramelli, A. R. (1991). *Historical surface faulting in the Basin and Range province, western North America: implications for fault segmentatio*n. Journal of Structural Geology, 13(2): 123–136.

Eusden, J. D., Pettinga, J. R., & Campbell, J. K. (2000). *Structural evolution and landscape development of a collapsed transpressive duplex on the Hope Fault, North Canterbury, New Zealand.* New Zealand Journal of Geology and Geophysics, 43(3): 391–404.

Eusden, J. R., Dykstra, J., Pettinga, J. R. and Campbell, J. K. (2005). *Structural collapse of a transpressive hanging-wall fault wedge, Charwell region of the Hope Fault, South Island, New Zealand*. New Zealand Journal of Geology and Geophysics, 48(2): 295 – 309.

Field, B. D., Browne, G. H. and Davy, B. W. (1989). *Cretaceous and Cenozoic sedimentary basins and geological evolution of the Canterbury region, South Island, New Zealand*. New Zealand Geological Survey Basin Studies, 2.

Forsyth. PJ.; Barrell, D.J.A.; Jongens, r. (compilers). (2008). *Geology of the Christchurch area*. Institute of Geological & Nuclear Sciences 1:250 000 geological map 16. 1 sheet + 67p. Lower Hutt, New Zealand. GNS Science.

Fossen, H. (2010). *Structural geology*. Cambridge University Press.

Gardner, T., Webb, J., Pezzia, C., Amborn, T., Tunnell, R., Flanagan, S., Merrittsa, D., Marshalla, J., Fabel, D. & Cupper, M. L. (2009). *Episodic intraplate deformation of stable continental margins: evidence from Late Neogene and Quaternary marine terraces, Cape Liptrap, Southeastern Australia*. Quaternary Science Reviews, 28(1-2): 39–53.

Garlick, R. D. (1992). *Lees Valley Fault, North Canterbury*. Honours thesis, Department of Geology, University of Canterbury, Christchurch.

GeoNet. (2015). *Earthquake Catalogue*. Earthquake Commission and GNS Science. Retrieved August 3, 2015, http://quakesearch.geonet.org.nz

GeoNet (2015a). *Historical earthquakes*. Earthquake Commission and GNS Science Retrieved August 19, 2015. http://info.geonet.org.nz/display/quake/Historical+Earthquakes

Google earth, V 6.2.26613 (2013). *Canterbury, New Zealand*. 43˚23’14.25”S, 172˚20’40.72”E, Eye alt 174.89 km. SIO, NOAA, U.S. Navy, NGA, GEBCO. Landsat. Retrieved October 29, 2015, http://www.earth.google.com.

Google earth, V 6.2.26613 (2015). *Lees Valley, New Zealand*. 43˚07’52.81”S, 172˚12’52.19”E, Eye alt 32.33 km. DigitalGlobe 2015, CNESI Astrium 2015. Retrieved Retrieved October 09, 2015, http://www.earth.google.com.

Gregg, D. R. (1964). *Hurunui Geological Map of New Zealand 1:250,000*. Sheet 18. Wellington. New Zealand Department of Scientific and Industrial Research.

Guerin, G., Mercier, N & Adamiec, G. (2011). *Dose-rate conversion factors: update*. Ancient TL, 29(1): 5 – 8.

Hornblow, S., Quigley, M., Nicol, A., Van Dissen, R. & Wang, N. (2014). *Paleoseismology of the 2010 Mw 7.1 Darfield (Canterbury) earthquake source, Greendale Fault, New Zealand*. Tectonophysics, 637: 178 – 190.

Howard, M., Nicol, a., Campbell, J., & Pettinga, J. (2003). *Recent Paleoearthquakes of the Porters Pass Fault and Hazard Posed to Christchurch, New Zealand* . Proceedings of the Pacific Conference on Earthquake Engineering, (69): 1–8.

Howard, M., Nicol, A., Campbell, J., & Pettinga, J. R. (2005). *Holocene paleoearthquakes on the strike-slip Porters Pass Fault, Canterbury, New Zealand*. New Zealand Journal of Geology and Geophysics, 48(1): 59–74.

Howard, M, E. (2001). *Holocene surface-rupturing earthquakes on the porters pass fault*. MSc Thesis, Department of Geology, University of Canterbury, Christchurch.

Jongens, R., Tulloch, A. J., Spell, T. L., Rattenbury, M. S., Begg, J. G., & Lyttle, B. S. (2009*). Pember Diorite—an Early Jurassic intrusion in the Rakaia Terrane, Puketeraki Range, Canterbury, New Zealand*. New Zealand Journal of Geology and Geophysics, 52(1): 37–42.

Keller, E. A. (1986). *Investigation of Active Tectonics: Use of Surficial Earth Processes*. 8. National Academy of Sciences, Washington.

Kerr, J., Nathan, S., Van Dissen, R., Webb, P., Brunsden, D., & King, A. (2003). *Planning for Development of Land on or Close to Active Faults: A guideline to assist resource management planners in New Zealand*. Wellington, Ministry for the Environment.

Khajavi, N., Quigley, M., & Langridge, R. M. (2014). *Influence of topography and basement depth on surface rupture morphology revealed from LiDAR and field mapping, Hope Fault, New Zealand.* Tectonophysics, 630, 265–284.

Knuepfer, P. (1989). *Implications of the Characteristics of Endpoints of Historical Surface Fault Ruptures for the Nature of Fault Segmentation*. U.S. Geol. Surv. Open File Rep., 193–228.

Langridge, R., Campbell, J., Hill, N., Pere, V., Pope, J., Pettinga, J., Estrada, B and Berryman, K. (2003). *Paleoseismology and slip rate of the Conway Segment of the Hope Fault at Greenburn Stream, South Island, New Zealand*. Annals of Geophysics, 46 (5): 1119-1139.

Lee, J. C., Chen, Y. G., Sieh, K., Mueller, K., Chen, W. S., Chu, H. T., Chan, Y. C., Rubin, C. & Yeats, R. (2001). *A vertical exposure of the 1999 surface rupture of the Chelungpu fault at Wufeng, western Taiwan: structural and paleoseismic implications for an active thrust fault*. Bulletin of the Seismological Society of America, 91(5): 914-929.

Lee, J. C., Rubin, C., Mueller, K., Chen, Y. G., Chan, Y. C., Sieh, K., Chu, H. T & Chen, W. S. (2004). *Quantitative analysis of movement along an earthquake thrust scarp: a case study of a vertical exposure of the 1999 surface rupture of the Chelungpu fault at Wufeng, Western Taiwan*. Journal of Asian Earth Sciences, 23(2): 263-273.

Lin, J. & Stein, R. S. (2004). *Stress triggering in thrust and subduction earthquakes and stress interaction between the southern San Andreas and nearby thrust and strike-slip faults*. Journal of Geophysical Research: Solid Earth, 109(B2): 1978 – 2012.

McCalpin, J. P. (2009). *Paleoseismicity* (2nd ed.). Burlington: Academic Press.

McCalpin, J.P. & Carver, G, A. (2009). *Paleoseismology of compressional tectonic environments*. International Geophysics, 95: 315 – 419.

Nathan, S.; Rattenbury, M.S.; Suggate, R.P. (compilers). (2002). *Geology of the Greymouth area*. Institute of Geological & Nuclear Sciences 1:250 000 geological map 12. 1 sheet + 58p. Lower Hutt, New Zealand. GNS Science.

Nicol, A, Van Dissen, R. J., Robinson, R. & Harvison, A. (2012). *Variability of single event slip and recurrence intervals for large magnitude paleoearthquakes on New Zealand's active faults.* GNS Science Report, 41: 57.

Nicol, A. (1991). *Structural styles and kinematics of deformation on the edge of New Zealand plate boundary zone, mid Waipara region, north Canterbury*. PhD Thesis, Department of Geology, University of Canterbury, Christchurch.

Nicol, A., Cowan, H., Campbell, J., & Pettinga, J. (1995). *Folding and the development of small sedimentary basins along the New Zealand plate boundary.* Tectonophysics, 241(1-2): 47–54.

Noble, D. P. (2011). *Tectonic Geomorphology and Paleoseismicity of the Northern Esk Fault, North Canterbury, New Zealand*. MSc Thesis, Department of Geology, University of Canterbury, Christchurch.

Norris, R. J., & Cooper, A. F. (2000). *Late Quaternary slip rates and slip partitioning on the Alpine Fault, New Zealand.* Journal of Structural Geology, 23(2-3): 507–520.

Norris, R. J. & Nicolls, R. (2004). *Strain accumulation and episodicity of fault movements in Otago*. Earthquake Commission, University of Otago, Otago.

Pettinga, J. R., Cowan, H. A., Nicol, A., Quigley, M. C., Jongens, R., Campbell, J. K. (2014). *Structural styles of transpressional deformation along the margin of the New Zealand plate boundary: the Porters Pass-Amberley Fault Zone and 2010-12 Canterbury Earthquake Sequence.* Geological Society of America Conference in Vancouver.

Pettinga, J.R. Yetton, M.D. Van Dissen, R.J. Downes, G. (2001). *Earthquake Source Identification and Characterisation for the Canterbury Region, South Island, New Zealand*. Bulletin of the New Zealand Society for Earthquake Engineering.

Quigley, M. C., Cupper, M. L., & Sandiford, M. (2006). *Quaternary faults of south-central Australia: Palaeoseismicity, slip rates and origin*. Australian Journal of Earth Sciences, 53(2): 285–301.

Quigley, M., Van Dissen, R., Litchfield, N., Villamor, P., Duffy, B., Barrell, D., Furlong, K., Stahl, T., Bilderback, E. & Noble, D. (2012*). Surface rupture during the 2010 Mw 7.1 Darfield (Canterbury) earthquake: Implications for fault rupture dynamics and seismic-hazard analysi*s. Geology, 40(1): 55–58.

Quigley, M., Van Dissen, R., Villamor, P., Litchfield, N., Barrell, D., Furlong, K., Stahl, T., Duffy, B., Bilderback, E., Noble, D., Townsend, D., Begg, J., Jongens, R., Ries, W., Claridge, J., Klahn, A., Mackenzie, H., Smith, A., Hornblow, S., Nicol, R., K. (2010). *Surface Rupture of the Greendale Fault During the Mw 7.1 Darfield (Canterbury) Earthquake, New Zealand: Initial Findings*. Bulletin of the New Zealand Society for Earthquake Engineering, 43(4): 1 – 7.

Rattenbury, M.S., Townsend, D.B., Johnston, M.R. (compilers). (2006). *Geology of the Kaikoura area*. Institute of Geological & Nuclear Sciences 1:250 000 geological map 13. 1 sheet + 70p. Lower Hutt, New Zealand. GNS Science.

Reyners, M., & Cowan, H. (1993). *The transition from subduction to continental collision; crustal structure in the North Canterbury region, New Zealand*. Geophysical Journal International, 115(3): 1124–1136.

Roberts, G. P., Michetti, A. M., Cowie, P., & Morewood, N. C. (2002). *Fault slip-rate variations during crustal-scale strain localisation, central Italy.* Geophysical Research Letters, 29(8): 2–5.

Rother, H. (2006). *Late Pleistocene Glacial Geology of the Hope-Waiau Valley System in North Canterbury, New Zealand*. PhD Thesis, Department of Geology, University of Canterbury, Christchurch.

Rowan, A. V., Roberts, H. M., Jones, M. A., Duller, G. A. T., Covey-Crump, S. J & Brocklehurst, S. H. (2012). *Optically stimulated luminescence dating of glaciofluvial sediments on the Canterbury Plains, South Island, New Zealand*. Quaternary Geochronology, 8: 10 – 22.

Souque, C., Frison De Lamotte, D., Leturmy, P., Robion, P. (2003) *Duplex at the lateral tip of a thrust fault: the "La Cagalière" example (NE Pyrenees, France)*. Geodinamica Acta 16.2: 89-98.

Spearing, D.R. 1974: *Alluvial fan deposits*. Summary sheets of sedimentary deposits, Sheet I, Boulder Colorado. Geological Society of America.

Speight, R. (1926). *Varved glacial silts from the Rakaia Valley*. Records of the Canterbury Museum, 3: 55-81.

Stahl, T. (2014). *Active Tectonics and Geomorphology of the central South Island, New Zealand: Earthquake Hazards of Reverse Faults*. PhD Thesis, Department of Geology, University of Canterbury, Christchurch.

Steacy, S., Gerstenberger, M., Williams, C., Rhoades, D., & Christophersen, A. (2014). *A new hybrid Coulomb/statistical model for forecasting aftershock rates.* Geophysical Journal International, 196(2): 918–923.

Steacy, S., Jimenez, A., & Holden, C. (2013). *Stress triggering and the Canterbury earthquake sequence.* Geophysical Journal International, 196(1): 473–480.

Stirling, M., Gerstenberger, M., Litchfield, N., Mcverry, G., Smith, W., Pettinga, J., & Barnes, P. (2008). *Seismic hazard of the Canterbury region, New Zeland: New earthquake source model and methodology*. Bulletin of the New Zeland Society for Earthquake Engineering, 41(2): 51–67.

Stirling, M., Rhoades, D., & Berryman, K. (2002). *Comparison of earthquake scaling relations derived from data of the instrumental and preinstrumental era*. Bulletin of the Seismological Society of America, 92(2): 812–830.

Stirling, M. W., Mcverry, G. H., & Gerstenberger, M. (2012). *New National Seismic Hazard Model for New Zealand : Changes to Estimated Long-Term Hazard*. 2012 NZSEE, (048):1–5.

Townend, J., Villamor, P., & Quigley, M. (2012). *Introduction to the Canterbury earthquake sequence special issue*. New Zealand Journal of Geology and Geophysics, 55(3): 151–154.

Van Dissen, R. J., Berryman, K., Webb, T., Stirling, M., Villamor, P., Wood, P. R., Nathan, S., Nicol, A., Begg, J., Barrell, D., McVerry, G., Langridge, R. & Litchfield, N. (2003*). An interim classification of New Zealand's active faults for the mitigation of surface rupture hazard*. NZSEE, In proceedings, Pacific Conference on Earthquake Engineering: 1-8.

Villamor, P., Berryman, K., Webb, T., Stirling, M., McGinty, P., Downes, G., Harris, J., Litchfield, N. (2001). *Waikato seismic load - Task 2.1.* Revision of seismic source characterisation, GNS client report, 59.

Walcott, R. I. (1998). *Modes of oblique compression: Late Cenozoic tectonics of the South Island of New Zealand*. Reviews of Geophysics, 36(1): 1.

Wallace, L. M., Beavan, J., McCaffrey, R., Berryman, K., & Denys, P. (2007). *Balancing the plate motion budget in the South Island, New Zealand using GPS, geological and seismological data*. Geophysical Journal International, 168(1): 332–352.

Wallace, R. E. (1977). *Profiles and ages of young fault scarps, north-central Nevada*. Bulletin of the Geological Society of America, 81: 2875 – 2889.

Wang, N. (2015). *Luminescence Dating Technical Report*. Luminescence Dating Laboratory, School of Geography, Environment and Earth Sciences, Victoria University of Wellington, Wellington.

Wells, D. L., & Coppersmith, K. J. (1994). *New Empirical Relationships among Magnitude, Rupture Length, Rupture Width, Rupture Area, and Surface Displacement*. Bulletin of the Seismological Society of America, 84(4): 974–1002.

Wesnousky, S. G. (2006). *Predicting the endpoints of earthquake ruptures.* Nature, 444 (7117): 358–360.

Wesnousky, S. G. (2008). *Displacement and geometrical characteristics of earthquake surface ruptures: Issues and implications for seismic-hazard analysis and the process of earthquake rupture*. Bulletin of the Seismological Society of America, 98(4): 1609–1632.

Yang, X., Li, W., & Qin, Z. (2015). *Calculation of reverse-fault-related parameters using topographic profiles and fault bedding*. Geodesy and Geodynamics, 6(2): 106–112.

Yetton, M. D. (2000). *The probability and consequences of the next Alpine Fault earthquake, South Island, New Zealand.* PhD Thesis, Department of Geology, University of Canterbury, Christchurch.

Appendices

APPENDIX A

Appendix A - Luminescence Dating Field Methods

Samples were collected by driving 5 cm diameter and 25 cm long cylinder stainless-steel tubes into the sedimentary units selected for dating. Before sample extraction a representative section of the unit was chosen with sufficient fine grained material in order to get the most accurate ages and thoroughly cleaned, which involved taking approximately 5 cm off the surface. The tube itself was packed tightly with approximately 2 cm of newspaper and then sealed with thick duct tape to ensure no light contamination of the sample. Once prepared and the face cleaned the tube was driven in until flush with the unit surface. Much of the material surrounding the tube was removed before attempting to take out the sample. During removal care was taken to not disturb the sample excessively to ensure it remained as intact as possible. Duct tape was prepared and then applied directly to the end as the tube was taken from the hole, enough was applied to stop light contamination at this end also. Any space in this end of the tube that could cause mixing of the sample during transportation was packed full of newspaper and sealed once more. Once the sample was successfully taken and sealed it was placed in a large re-sealable bag and labelled carefully based on location in trench. Sediment samples were taken from within and directly around the OSL sample site for U, Th and K analysis if needed and labelled accordingly. OSL samples were taken using long tubes to ensure that once sent to the lab to be analysed there would be a large enough section in the middle of the sample to ensure no light contamination.

APPENDIX B

Appendix B - Luminescence Dating Technical Report

Report No. 3/15

Luminescence Dating Technical Report

Luminescence Dating Laboratory

School of Geography, Environment and Earth Sciences

Victoria University of Wellington

Wellington

New Zealand

Reported by: Ms. Ningsheng Wang
Date of Issue: 10-7-2015
Contact: Room 414
Cotton Building
Victoria University of Wellington
Ph: (04) 463 6127

CONTENTS

1. SUMMARY

Five samples (Field code: LV-EW-BW, LV-EW-C1, LV-SW-CWT, LV-SW-FD and LV-SW-BU) were submitted for luminescence dating by Ellyse Gore, University of Canterbury. The laboratory codes of the samples are from WLL1165 to WLL1169 respectively.

Due to the sample being fine material, the fine grain (4-11μm) preparation technique was used. The paleodose (the equivalent dose) of all samples was evaluated using the Multiple Aliquot Additive Dose method (MAAD) based on measurements of blue luminescence from the fine grain feldspar produced during infrared stimulation. The dose rate was determined on the basis of gamma spectrometry measurements.

2. EXPERIMENTAL WORK

A) Sample Preparation

Samples had their outer surfaces removed. "Fresh" sample material, that had outer surfaces removed earlier (unexposed light sample material), was treated in 10% HCl. This was carried out overnight until all carbonate was removed by the reaction. Following this treatment the sample was further reacted overnight with 10% H_2O_2 in order to remove organic matter. The next step involved 200ml CBD* solution being added to the sample for 12 hours to remove iron oxide coatings. Note, after every chemical treatment procedure distilled water was used to wash the sample several times. After chemical treatment, calgon solution (1g sodium hexametaphosphate per litre distilled water) was added to make thick slurry. This slurry was placed into an ultrasonic bath and mechanically agitated for an hour. The sample was then placed into a 1L measuring cylinder, filled with a certain amount of distilled water to separate out the 4-11μm grains according to Stokes' Law.

The 4-11μm grains were then rinsed with ethanol and acetone and a suspension of these grains were then deposited evenly onto 70 aluminium disks (diameter 9.8mm).

in air tight perspex containers, then stored for at least four weeks before the gamma spectrometer analysis. The storage time minimizes the loss of the short lived noble gas ^{222}Rn and allows ^{226}Ra to reach equilibrium with its daughters ^{214}Pb and ^{214}Bi.

A plastic cube was then filled with remaining scrapings in preparation for water content measuring.

*CBD solution: 71g sodium citrate, 8.5 g sodium bicarbonate, and 2g sodium dithionate per litre of distilled water.

B) Measurements

Luminescence age was determined by two factors: the equivalent dose (D_e) and the dose rate. It involves measurements of luminescence for determination of D_e and concentrations of ^{238}U, ^{232}Th, ^{40}K and water contents (used to determine of dose rate).

> Equivalent dose: obtained from the lab equivalents to the paleodose absorbed by samples during the burial time in the natural environment since their last exposure to the light.
> Dose rate: amount dose received by the sample each year.

B1. Determination of Equivalent Dose (De)

D_e for all of these samples were obtained by using the *Multiple Aliquot Additive Dose Method (MAAD).*

The test dose obtained from an initial test measurement was used for the MAAD. As luminescence vary between disks, all disks for MAAD need to be normalised before β irradiation. 0.1 second infrared measurements were taken before irradiation of all aliquots. Six groups (30 disks divided by five) were β irradiated up to five times of the test dose. Beta irradiation were done on the Riso TL-DA-15 ^{90}Sr/Y β irradiator, calibrated against ^{60}Co gamma source, SFU, Vancouver, Canada with about 3%

uncertainty. Three groups (three disks per group) were α irradiated up to three times of the test dose. The α irradiation was carried out on a ^{214}Am irradiator,

supplied and calibrated by ELSEC Littlemore, UK. The next step was that these 39 disks together with nine non-irradiated disks (total of 48 disks) were stored for four weeks to relax the crystal lattice after irradiation.

After storage, the 48 disks were preheated for five minutes at 230oC, then were measured using a Riso TL-DA-15 reader with infrared diodes at 880nm used to deliver a stimulated beam (30mW/cm2)at the room temperature for 100s. Blue luminescence centred about 410nm emission from feldspar was then detected by an EMI 9235QA photomultiplier fixed behind two filters consisting of a Schott BG-39 and Kopp 5-58.

Luminescence growth curve (β induced luminescence intensity versus added dose) was constructed by using the initial the 10 seconds of the shine down curves and subtracting the average of the last 20 seconds, along with the so called late light which was thought to be a mixture of background and hardly bleachable components. Extrapolation of this growth curve to the dose axis was obtained the equivalent dose De which was used as a paleodose. The shine plateau was checked to be flat after this manipulation.

Fading has been checked, n fading has been recorded from the fading test.

Measurement of a-value

A similar plot for the alpha irradiated disks allows for an estimation of α efficiency, a-value (a-value is measured by comparing the luminescence induced by alpha irradiation with that induced by beta or gamma irradiation). The a-value was for dose rate calculation.

B2: Determination of Dose Rate

Dose rate consisted of two parts.

(i) Dose rate from sample's burial environment

(ii) Dose rate from cosmic rays.

(i) Dose rate from burial environment

Dose rate from sample's burial environment was determined by radionuclide contents of ^{238}U, ^{232}Th and ^{40}K, a-value and water content.

Determination of Contents of U, Th and K by Gamma spectrometry

Gamma rays produced from sample material was counted for a minimum time of 24 hours by a high resolution and broad energy gamma spectrometer. The spectra were then analysed using GENIE2000 software. The contents of U, Th and K were obtained by comparison with standard samples. The dose rate calculation was based on the activity concentration of the nuclides ^{40}K, ^{208}TL, ^{212}Pb, ^{228}Ac, ^{214}Bi, ^{214}Pb, ^{226}Ra, using dose rate conversion factors published by Guérin, G., Mercier, N., Adamiec, G. 2011.

Measurement of Water Contents

Water content was measured as weight of water divided by dry weight of the sample taking into account a 25% uncertainty.

(ii) Dose rate from cosmic rays

Dose rate from cosmic rays were determined by the depth of sample below the surface along with its longitude, latitude and altitude, convention formula and factors published by Prescott, J.R. & Hutton, J.T. (1994).

3. RESULTS

Table 1 Cosmic dose rates

Table 2 Water contents, radionuclide contents

Table 3 a- Values, dose rates, equivalent doses and luminescence ages.

Table 1: Cosmic Dose Rates

Laboratory Code	Depth Below the Surface(m)	Cosmic Dose Rate (Gy/ka)	Field Code
WLL1165	3.33	0.1453±0.0073	LV-EW-BW
WLL1166	0.70	0.2065±0.0103	LV-EW-CI
WLL1167	0.60	0.2094±0.0105	LV-SW-CWT
WLL1168	1.09	0.1957±0.0098	LV-SW-FD
WLL1169	1.82	0.1771±0.0089	LV-SW-BU

Table 2: Water Contents, Radionuclide Contents

Laboratory Code	Water Content (%)	U(ppm) from 234Th	U(ppm) from 226Ra, 214Pb, 214 Bi	U(ppm) from 210Pb	Th(ppm) From 208Tl 212 Pb 228 Ac	K(%)	Field Code
WLL1165	17.0	2.80±0.22	2.86±0.14	3.11±0.19	8.76±0.11	1.84±0.04	LV-EW-BW
WLL1166	10.0	2.85±0.24	2.49±0.13	2.25±0.17	9.76±0.12	2.14±0.05	LV-EW-CI
WLL1167	9.3	3.01±0.27	2.69±0.15	2.54±0.20	10.56±0.14	2.39±0.05	LV-SW-CWT
WLL1168	9.9	3.10±0.25	2.51±0.13	2.35±0.17	10.37±0.13	2.38±0.05	LV-SW-FD
WLL1169	13.1	2.90±0.27	2.74±0.15	2.67±0.21	10.64±0.14	2.34±0.05	LV-SW-BU

Table 3: a-Values, Dose Rates, Equivalent Doses and Luminescence Ages

Laboratory Code	a-value	De(Gy)	Dose Rate(Gy/ka)	**Luminescence Age(ka)**	Field Code
WLL1165	0.09±0.01	21.24±0.65	3.79±0.19	**5.6±0.3**	LV-EW-BW
WLL1166	0.07±0.003	57.12±3.98	4.19±0.15	**13.6±1.1**	LV-EW-CI
WLL1167	0.07±0.01	97.12±4.35	4.63±0.13	**21.0±1.1**	LV-SW-CWT
WLL1168	0.06±0.003	96.62±7.14	4.37±0.15	**22.1±1.8**	LV-SW-FD
WLL1169	0.07±0.004	95.13±6.17	4.39±0.16	**21.7±1.6**	LV-SW-BU

4. REFERENCES

Guérin, G., Mercier, N., Adamiec, G. 2011: Dose- rate conversion factors: update. Ancient TL, Vol.29, No.1, 5-8.

Murray, A.S. & Wintle, A.G. 2000: Luminescence dating of quartz using an improved single aliquot regenerative dose protocol. Radiation Measurements 32, 57-73.

Prescott, J.R. & Hutton, and J.T. 1994: Cosmic ray contributions to dose rates for luminescence and ESR dating: Large depths and long-term time variations. Radiation Measurements. Vol.23,Nos.2/3, 497-500.

APPENDIX C

Appendix C – Luminescence Dating Technical Report Supplementary Table

Recalculated OSL ages based on water contents change. It can be observed from the ST3 that luminescence ages have shifted ~ 5% due to water contents change, except WLL1166.

Supplementary Table 3: a-Values, Equivalent Doses, Dose Rates and Luminescence Ages

Laboratory Code	a-value	D_e(Gy)	Dose Rate (Gy/ka)	Water Content (%)	**Luminescence Age(ka)**	Field Code
WLL1165	0.09±0.01	21.24±0.65	3.79±0.19 3.61±0.20 #	17.0 21.9# (saturated)	**5.6±0.3** **5.9±0.4#**	LV-EW-BW
WLL1166	0.07±0.003	57.12±3.98	4.19±0.15 3.57±0.22 #	10.0 26.4# (saturated)	**13.6±1.1** **16.0±1.5#**	LV-EW-CI
WLL1167	0.07±0.01	97.12±4.35	4.63±0.13 4.82±0.14 *	9.3 5.4 * (as received)	**21.0±1.1** **20.1±1.1***	LV-SW-CWT
WLL1168	0.06±0.003	96.62±7.14	4.37±0.15 4.57±0.09 *	9.9 5.9* (as received)	**22.1±1.8** **21.1±1.6***	LV-SW-FD
WLL1169	0.07±0.004	95.13±6.17	4.39±0.16 4.55±0.13 *	13.1 9.7* (as received)	**21.7±1.6** **20.9±1.5***	LV-SW-BU

Dose rates and luminescence ages were calculated used the saturated water contents.

*Dose rates and luminescence ages were evaluated used the water contents which were measured as received from the OSL samples (mass of water divide by mass of dry samples).